

A NUMERICAL EVALUATION OF THE DESIGN OF AN  
AUTOTHERMAL REFORMER FOR THE ONBOARD PRODUCTION  
OF HYDROGEN FROM ISO-OCTANE

by

SHAFQAT HUSSAIN

A thesis submitted to the  
Department of Mechanical and Materials Engineering  
in conformity with the requirement for  
the degree of Master of Science (Engineering)

Queen's University

Kingston, Ontario, Canada

March, 2009

Copyright © Shafqat Hussain, 2009

## ABSTRACT

A numerical study was carried out to improve the design of an autothermal reformer for the onboard production of hydrogen to be used in fuel-cell- powered auxiliary power units (APU) to provide heating and electricity in long haul trucks when they are at rest. The development of these auxiliary power units is based upon the use of power generated by solid oxide fuel cell (SOFC) system, instead of from a conventional gasoline engine. The present work was undertaken to improve the design of a prototype autothermal fuel reformer that had been developed by the Fuel Cell Research Centre (FCRC) at Queen's University to convert liquid hydrocarbon truck fuel to a hydrogen rich product gas. In this development work and in the previous work iso-octane ( $C_8H_{18}$ ) has been used as a surrogate fuel.

Using this surrogate of gasoline, the reformer was simulated using various inlet steam/carbon ( $H_2O/C$ ), oxygen/carbon ( $O/C$ ) molar ratios and gas-hourly-space-velocity (GHSV). In the reformer considered the reforming process is carried out in a compact tubular reactor with a centerline thermocouple tube using a 2% Pt-ZrCe based catalyst with a local porosity of 0.6. During the initial simulations, it was observed that near the start of the catalyst region there were large temperature gradients due to an exothermic partial oxidation reaction. In order to reduce the temperature gradients and facilitate heat transfer by conduction along the reformer, the central thermocouple tube was replaced with a central solid rod. The effects of variations in the thermal conductivity of central solid rod, of the reactor wall, of the catalyst bed, of the inert porous material near the inlet and the outlet of the catalyst bed, of the gas hourly space velocity, of the effectiveness factor of the chemical reaction mechanism on the performance of the reactor were

studied. The results so obtained were analyzed to determine potential design improvements that would increase the hydrogen output. The results were compared with the previous numerical and experimental results obtained in the previous studies of the reformer and found to be in good agreement with the general trends of the temperature profiles as well as the outlet molar concentrations of product species.

After the analysis and evaluation of all the results, it was found that by replacement of central thermocouple tube with central solid rod made of high conductivity material and by using material for inert porous region at the outlet that had a thermal conductivity equal to that of the catalyst bed led to more even temperature profiles within the catalyst region. It was also found that the hydrogen molar percentage output could be increased by approximately more than 25% and that the length of the reactor could be reduced by 20mm by incorporating these changes in the reformer design.

## ACKNOWLEDGMENTS

I wish to express my heartfelt gratitude to my supervisor, Dr. Patrick Oosthuizen who contributed to the development and conclusion of this project. His patience, support, guidance and enthusiasm to this research were invaluable. He provided me with enough freedom, personal and academic advice, and encouragement to complete this work.

I must single out the Auto 21 Network of Centers of Excellence and the Mechanical and Material Engineering Department at Queen's University who gave their approval and financial support, without which this research work would not have been possible.

It is also a pleasure to recognize the cooperation of my colleagues and friends in the Heat Transfer Lab in the Mechanical Engineering Department. Specially, I am deeply indebted to my colleague, a PhD student Abdulrahim Kalendar, for his extraordinary direction and help throughout this research work. This project would not have been finished in time without his continuous support.

I am also thankful to my friends who painstakingly read and edited my drafts. A special debt of gratitude is owed to Ellie in the writing center of Queen's University.

I would also like to warmly thank my family who was extremely supportive throughout this process, especially my parents, who always pray for my success in life.

Last, but not least, I thanks to my wife, Yasmine. Without her patience, love and unwavering support, I could not have completed this thesis.

## Table of Contents

<b>ABSTRACT</b> .....	<b>ii</b>
<b>ACKNOWLEDGEMENTS</b> .....	<b>iv</b>
<b>TABLE OF CONTENTS</b> .....	<b>v</b>
<b>LIST OF FIGURES</b> .....	<b>viii</b>
<b>LIST OF TABLES</b> .....	<b>xii</b>
<b>NOMENCLATURE</b> .....	<b>xiii</b>
<b>Acronyms</b> .....	<b>xiv</b>
<b>Greek Symbol</b> .....	<b>xv</b>
<b>CHAPTER 1 INTRODUCTION</b> .....	<b>1</b>
<b>1.1 Background</b> .....	<b>1</b>
<b>1.2 Reforming of hydrocarbons for production of hydrogen</b> .....	<b>3</b>
<b>1.3 Fuel Cells</b> .....	<b>7</b>
<b>1.4 Fuel-Cell-Powered Auxiliary Power Unit</b> .....	<b>10</b>
<b>1.5 Scope of Thesis</b> .....	<b>12</b>
<b>CHAPTER 2 LITERATURE REVIEW</b> .....	<b>13</b>
<b>2.1 Introduction</b> .....	<b>13</b>
<b>2.2 Reforming of Hydrocarbons</b> .....	<b>13</b>
<b>2.2.1 Steam reforming (SR) method</b> .....	<b>14</b>
<b>2.2.2 Partial oxidation reforming (POR) method</b> .....	<b>15</b>
<b>2.2.3 Auothermal reforming (ATR) method</b> .....	<b>15</b>
<b>2.3 Autothermal Reforming of Iso-octane (C<sub>8</sub>H<sub>18</sub>),         a Surrogate of Gasoline</b> .....	<b>17</b>

2.3.1 Reaction Kinetics and Catalysts for Autothermal Reforming of Iso-octane. -----	20
2.3.2 Catalysts for Autothermal Reforming -----	21
2.4 Autothermal Reforming with Surrogates and other Hydrocarbons-----	23
<b>CHAPTER 3 Previous Progress -----</b>	<b>27</b>
3.1 An Overview -----	27
3.1.1 First Generation Reformer Results and problems -----	30
3.1.2 Second Generation Reformer Results and Problems -----	38
<b>Chapter 4 Numerical and Computational Fluid Dynamics Modeling -----</b>	<b>46</b>
4.1 An Introduction -----	46
4.2 Mathematical Modeling -----	48
4.2.1 Conservation Equations -----	50
4.2.2 Chemical Reactions Mechanism and Kinetic Expressions -	54
4.2.31 Effectiveness Factor -----	57
4.3 Computational Fluid Dynamics (CFD) Modeling -----	58
4.3.1 Grid Generation -----	58
4.3.2 Solution Procedures -----	60
4.3.3 Solution Algorithm -----	62
<b>Chapter 5 Results and Discussion -----</b>	<b>66</b>
5.1 Introduction -----	66
5.2 Numerical Simulations by Using Sylvestre (2007) Operating Conditions (Phase-1) -----	68
5.3 Numerical Simulations by Using Shaw (2007) Experimental Operating Conditions (Phase-II) -----	77

<b>5.3.1 Effect of effectiveness factor upon the performance of the reactor</b> .....	<b>77</b>
<b>5.3.2 The Results Obtained Using Experimental Conditions</b> .....	<b>79</b>
<b>5.3.3 Effect of Main Input Variables on Results</b> .....	<b>82</b>
<b>5.3.4 Temperatures Distributions</b> .....	<b>84</b>
<b>5.4 Comparison of Modeling Predictions to Experimental Results</b> .....	<b>86</b>
<b>5.4.1 Comparison of the Outlet Composition</b> .....	<b>86</b>
<b>5.4.2 Comparison of Temperature Profiles</b> .....	<b>88</b>
<b>5.5 Numerical Evaluation of possible improvements in the reformer design (Phase –III)</b> .....	<b>89</b>
<b>5.5.1 Numerical Simulations with central solid rod and without inert porous zone at the outlet of the reformer</b> .....	<b>89</b>
<b>5.5.2. Final Design of the Autothermal Reformer Suggested</b> .....	<b>93</b>
<b>5.5.3 Numerical Simulations with new design</b> .....	<b>94</b>
<b>Chapter 6 Conclusions and Recommendations</b> .....	<b>98</b>
<b>6.1 Conclusions</b> .....	<b>98</b>
<b>6.2 Recommendations for Future Work</b> .....	<b>101</b>
<b>References</b> .....	<b>102</b>
<b>Appendix A</b> .....	<b>107</b>
<b>Appendix B</b> .....	<b>116</b>
<b>Appendix C</b> .....	<b>121</b>
<b>Appendix D</b> .....	<b>124</b>

## List of Figures

<b>Figure 1.1:</b> Fuel reformer schematic -----	4
<b>Figure 1.2:</b> Hydrogen Pathways, ( <a href="http://www.ch2bc.org/index2a.htm">http://www.ch2bc.org/index2a.htm</a> ) -----	6
<b>Figure 1.3:</b> Comparison of the relative amount of carbon dioxide production from different fuels for one unit of energy. -----	7
<b>Figure 1.4:</b> Scheme of Fuel Cell -----	8
<b>Figure 1.5:</b> Schematic of fuel cell-powered APU system -----	10
<b>Figure 2.1:</b> Iso-octane conversion and product distribution as a function of O/C ratio (experimental conditions: 680°C 1.3 vol,% iso-octane, H <sub>2</sub> O/C=1.5) -----	17
<b>Figure 2.2:</b> Iso-octane conversion and product distribution as a function of O/C ratio (experimental conditions: 680°C, 1.3vol,%iso-octane, H <sub>2</sub> O/C=1.5, GHSV=150,000h <sup>-1</sup> ) -----	18
<b>Figure 2.3</b> Iso-octane conversion rate for transition metals doped in ceria base at different temperatures -----	21
<b>Figure 2.4:</b> Comparison of H <sub>2</sub> , CO, CO <sub>2</sub> , and CH <sub>4</sub> yields for different catalyst from Mawdsle (2004) (yields produced from <450 ppb sulfur gasoline at 700°C) -----	22
<b>Figure 2.5:</b> Comparison of product distribution for gasoline and C <sub>8</sub> H <sub>18</sub> (H <sub>2</sub> O/C=1.25, O <sub>2</sub> /C=0.5, GHSV=5000h <sup>-1</sup> ) -----	24
<b>Figure 2.6:</b> Comparison of product distribution for diesel and C <sub>16</sub> H <sub>34</sub> (H <sub>2</sub> O/C =1.25, O <sub>2</sub> /C = 0.5, GHSV =5000h <sup>-1</sup> ) -----	24
<b>Figure 3.1:</b> Drawing of the ATR designed and developed by Middleton (2004) -----	28
<b>Figure 3.2:</b> Cross sectional view of the ATR designed by Middleton (2004) with catalyst regions and thermocouple locations -----	28
<b>Figure 3.3:</b> Temperature contour plot (degree Kelvin) of the first ATR from a model created by McIntyre(2005) (Note: contour plot is an axisymmetric, two-dimensional representation of the ATR -----	32
<b>Figure 3.4:</b> Schematic of the new design of the auto-thermal reformer -----	34
<b>Figure 3.5:</b> Picture of the new autothermal reformer with wall thermocouples -----	37
<b>Figure 3.6:</b> A representation of the two-dimensional, axis-symmetric model created by Sylvester (2007) -----	39
<b>Figure 3.7:</b> Temperature profile for base case (Sylvestre 2007) at GHSV 30000h <sup>-1</sup> -----	40
<b>Figure 3.8:</b> Temperature distribution along centreline of reformer for varying catalyst thermal conductivity at GHSV 30000h <sup>-1</sup> -----	41

<b>Figure 3.9:</b> Predicted mole fractions along reformer bed for base case at GHSV = 30000h <sup>-1</sup> -----	41
<b>Figure 3.10</b> Approximate positions for the permanent wall thermocouples and centerline temperature reading locations along the ATR bed -----	42
<b>Figure 3.11</b> Experimental temperature profiles along the wall of the reformer, Shaw (2008). -----	43
<b>Figure 3.12</b> Experimental temperature profiles along the centerline of the reformer, Shaw (2008) --	44
<b>Figure 4.1:</b> Magnified view of mesh topology for the inlet region of the geometry -----	59
<b>Figure 4.2:</b> Outline of the solution algorithm adopted in FLUENT software -----	62
<b>Figure 4.3:</b> Overview of Segregated Solver Approach -----	64
<b>Figure 5.1:</b> Compact autothermal reformer, Length = 180 mm, Outer radius = 4.75 mm, Inner radius = 3.75mm -----	69
<b>Figure 5.2:</b> Profiles of mole fractions of product species within the reformer in the catalyst bed (GHSV =30,000h <sup>-1</sup> , H <sub>2</sub> O:C = 2, O:C = 1, Effectiveness factor = 0.001) -----	71
<b>Figure 5.3:</b> Temperature distribution within the reformer. (GHSV =30,000h <sup>-1</sup> , H <sub>2</sub> O:C = 2, O:C = 1, Effectiveness factor = 0.001) -----	72
<b>Figure 5.4:</b> Temperature profile along the centreline of the reformer. -----	72
<b>Figure 5.5:</b> Profiles of mole fractions of Hydrogen in the catalyst bed (GHSV =30,000 h <sup>-1</sup> , S:C=1, O:C=1.3, Effectiveness factor =0.001) -----	74
<b>Figure 5.6:</b> Centerline temperatures profiles along the length of the reformer -----	74
<b>Figure 5.7:</b> Reformer simulated without inert porous region at the outlet of the catalyst bed, Length = 150 mm, Radius = 4.75 mm -----	75
<b>Figure 5.8:</b> Mole fraction of Hydrogen profile without central thermocouple tube and inert porous region at outlet of the reformer(GHSV =30,000 h <sup>-1</sup> , S:C=2, O:C=1 Effectiveness factor =0.001) -----	75
<b>Figure 5.9:</b> Temperature distribution within the reformer -----	76
<b>Figure 5.10:</b> Temperature profile along the centreline of the reformer -----	76
<b>Figure 5.11:</b> Reformer used in experimental study by Shaw (2008), length = 180 mm, outer radius = 4.75 mm, with hollow central tube of length =140mm and outer radius = 1.6mm and inner radius =1.05mm -----	77
<b>Figure 5.12:</b> Comparison of molar percentage of hydrogen at different values of effectiveness factors with experimental molar percentage of hydrogen determined by Shaw (2008) -----	78
<b>Figure 5.13:</b> Profiles of mole fractions of reformate compositions within the reformer in the catalyst bed, at GHSV =20,000 h <sup>-1</sup> , S:C=2, O:C=1, effectiveness factor =0.0032 -----	80

<b>Figure 5.14:</b> Mole fractions of hydrogen distribution in the catalyst bed of the reformer (GHSV=20,000 h <sup>-1</sup> , S:C = 2, O:C = 1) -----	80
<b>Figure 5.15:</b> Temperature distribution along the axial length of the reformer (GHSV=20,000 h <sup>-1</sup> , S:C = 2, O:C = 1). -----	80
<b>Figure 5.16:</b> Temperature profile along the centreline of the reformer. (GHSV =20,000 h <sup>-1</sup> , S:C = 2, O:C = 1) -----	81
<b>Figure 5.17:</b> Temperature profile along the outer wall of the reformer (GHSV =20,000 h <sup>-1</sup> , S:C = 2, O:C = 1) -----	81
<b>Figure 5.18:</b> Temperatures profile along the thermocouple tube wall of the reformer (GHSV=20,000 h <sup>-1</sup> , S:C = 2, O:C = 1) -----	82
<b>Figure 5.19:</b> Average dry molar percentage of outlet gases vs. O/C obtained in present numerical results -----	83
<b>Figure 5.20:</b> Average dry molar percentage of outlet gases vs. H <sub>2</sub> O/C obtained in present numerical results -----	83
<b>Figure 5.21:</b> Profiles of numerical and experimental reformate composition at outlet of the reformer at different O/C and H <sub>2</sub> O/C molar ratios. -----	87
<b>Figure 5.22:</b> Comparison of numerical and experimental reformate composition at the outlet of the reformer at different O/C and H <sub>2</sub> O/C molar ratios. -----	87
<b>Figure 5.23:</b> Comparison of numerical and experimental peak and lowest temperatures along the centerline of the reformer, GHSV = 20,000h <sup>-1</sup> , S:C = 2, O:C =1. -----	88
<b>Figure 5.24:</b> Reformer with central solid rod and without inert porous region at the outlet, Length =150 mm, Radius = 4.75 mm, with central rod of length =130 mm and radius = 1.6mm. -----	90
<b>Figure 5.25:</b> Reformer temperature distribution (GVSH = 20,000 h <sup>-1</sup> , H <sub>2</sub> O:C =2, O:C =1) -----	91
<b>Figure 5.26:</b> Temperature profile along the wall of the reformer, (GVSH=20,000 h <sup>-1</sup> , S:C=2, O:C=1) -----	91
<b>Figure 5.27:</b> Temperature profile along the centerline of the reformer (GVSH=20,000 h <sup>-1</sup> , S:C=2, O:C=1) -----	91
<b>Figure 5.28:</b> Comparison of numerical and experimental reformate composition at various O/C and H <sub>2</sub> O/C molar ratios and effectiveness factor = 0.001 -----	92
<b>Figure 5.29:</b> Reformer with central solid rod of length =130mm and radius = 1.6mm, inert porous region at inlet of length 30mm and inert porous region at outlet of the catalyst bed of length 10mm. -----	94
<b>Figure 5.30:</b> Reformer hydrogen distribution (GHSV=20,000 h <sup>-1</sup> , S:C = 2, O:C = 1) -----	95
<b>Figure 5.31:</b> Reformer temperature distribution (GHSV=20,000 h <sup>-1</sup> , S:C = 2, O:C = 1) -----	95

**Figure 5.32:** Temperature profile along the centerline of the reformer  
(GHSV=20,000 h<sup>-1</sup>, S:C = 2, O:C = 1) ----- 96

**Figure 5.33:** Comparison of numerical and experimental hydrogen  
molar percent at different O/C and H<sub>2</sub>O/C molar ratios,  
GHSV = 20,000h<sup>-1</sup> ----- 96

## List of Tables

<b>Table 1.1:</b> The fuel requirements for the principal types of fuel cells -----	8
<b>Table 2.1:</b> Approximate results adapted from Moon et al.(2001) for auto-thermal reforming of iso-octane -----	19
<b>Table 3.1:</b> Dimensions of the concentric cylinder design by Middleton (2004) -----	29
<b>Table 3.2:</b> Experimental results from the first generation design of an autothermal reformer for the iso-octane -----	31
<b>Table 3.3:</b> Major components of the new design along with important dimensions -----	35
<b>Table 3.4:</b> Experimental results for the second generation design of an auto-thermal reformer for the iso-octane at GHSV 20000h <sup>-1</sup> by Shaw (2008) -----	43
<b>Table 4.1:</b> Values of the pre-exponential factors determined from experimental data and the kinetic parameters used from the literature -----	56
<b>Table 5.1:</b> Results of mesh sensitivity analysis -----	70
<b>Table 5.2</b> Summary of Results by using Sylvestre’s operating conditions -----	71
<b>Table 5.3:</b> Numerical results from the model of the ATR at inlet temperature = 500 °C , TC of tube and wall = 17.5 ~31.5 W/mk and GHSV =20000h <sup>-1</sup> and effectiveness factor = 0.0032 -----	78
<b>Table 5.4:</b> Selected results from the model of the ATR at inlet temperature = 500°C, TC of tube and wall = 17.5 ~31.5 W/mk and GHSV =20000h <sup>-1</sup> -----	79
<b>Table 5.5:</b> Peak and Lowest temperatures in the catalyst bed -----	79
<b>Table 5.6:</b> Numerical and experimental results of the ATR obtained by present simulations and by Shaw (2008) at outlet of the reformer (inlet temperature equal to 500 °C, and GHSV =20000h <sup>-1</sup> ) -----	86
<b>Table 5.7:</b> Selected results from the model of the ATR at inlet temperature = 500 °C, TC of rod and wall = 17.5 ~31.5 W/mk and GHSV =20000h <sup>-1</sup> and effectiveness factor = 0.001 -----	90
<b>Table 5.8:</b> Numerical results from the model of the ATR ( inlet temperature = 500°C, TC of rod =100 W/m.K, TC of wall =17.5 ~31.5 W/mk, GHSV =20000h <sup>-1</sup> and effectiveness factor = 0.0032) --	94
<b>Table 5.9:</b> Peak and Lowest temperatures in the catalyst bed -----	95

## Nomenclature

$A$	Arrhenius pre-exponential constant (units vary depending on reaction)
$C_p$	gas phase heat capacity (kJ/kg·K)
$d_p$	diameter of catalyst particle (m)
$D_{eff}$	effective diffusion coefficient (m <sup>2</sup> /s)
$D_k$	knudson diffusion coefficient (m <sup>2</sup> /s)
$D_m$	bulk diffusion coefficient (m <sup>2</sup> /s)
$E$	Arrhenius activation energy (kJ/mol)
$F_x$	axial momentum source term (m/s <sup>2</sup> )
$F_r$	radial momentum source term (m/s <sup>2</sup> )
$h$	enthalpy (kJ/mol)
$h_i^o$	standard enthalpy of formation of species $i$ (kJ/mol)
$J$	diffusion flux (kg/m·s)
$K$	thermal conductivity (W/m·K)
$K_b$	Boltzmann constant (kg·m <sup>2</sup> /s <sup>2</sup> -k)
$K_f$	fluid thermal conductivity (W/m·K)
$K_s$	solid thermal conductivity (W/m·K)
$k_{eff}$	effective thermal conductivity (W/m·K)
$k_{r,n}$	reaction rate constant for reaction $n$ (units vary depending on reaction)
$K_i$	adsorption coefficient of species $i$ (bar <sup>-1</sup> )
$K_n$	equilibrium constant of reaction $n$ (units vary depending on reaction)
$L$	axial reactor length (m)
$L_d$	characteristic length (m)

$M_i$	molar mass of species $i$ (kg/mol)
$P_i$	partial pressure of species $i$ (bar)
$\Delta_p$	pressure change (bar)
$P_e$	Peclet number (dimensionless)
$P_r$	Prandtl number (dimensionless)
$r_i$	rate of production of species $i$ by chemical reaction (mol/m <sup>3</sup> ·s)
$r$	radial direction coordinate (m)
$Re$	Reynolds number (dimensionless)
$R$	universal gas constant (KJ/mol·K)
$S$	general source term (units vary depending on governing equation)
$S_\phi$	general source term for flow variable (units vary depending on governing equation)
$t$	tortuosity (dimensionless)
$T$	absolute temperature (K)
$T_{ref}$	reference temperature (K)
$u$	axial direction velocity component (m/s)
$U_s$	superficial velocity (m/s)
$v$	radial direction velocity component (m/s)
$x$	axial direction coordinate (m)
$Y_i$	mass fraction of species $i$ in mixture (dimensionless)

## Greek Symbols

$\alpha$	thermal diffusivity ( $\text{m}^2/\text{s}$ )
$\beta$	relaxation factor (dimensionless)
$\eta$	catalyst effectiveness factor (dimensionless)
$\sigma$	diameter of gas molecule (m)
$\phi$	general flow variable (units vary depending on variable)
$\phi_f$	face value of general flow variable (units vary depending on variable)
$\phi_f$	arithmetic mean of general flow variable face value (units vary depending on variable)
$\varphi$	packed bed porosity (dimensionless)
$\theta$	kinetic concentration function for catalytic and gas-phase reactions (units vary depending on reaction)
$\rho$	fluid density ( $\text{kg}/\text{m}^3$ )
$\mu$	fluid kinematic viscosity ( $\text{kg}/\text{m}\cdot\text{s}$ )

# Chapter 1

## Introduction

### 1.1 Background

The development of an efficient autothermal reformer is considered for the onboard production of hydrogen from liquid hydrocarbon fuels for application of fuel-cell-powered auxiliary power units (APU) in long haul trucks when they are at rest. This is an area of study which is gaining attention because of economic and environmental benefits that can arise from the use of such a system. The development of such a unit requires detailed kinetic information about the chemical reaction mechanism of the reforming process and of the heat transfer inside the reformer. The present research work deals with the development of such an autothermal reformer.

Since 2004, the Fuel Cell Research Centre (FCRC) at RMC/Queen's University Kingston has undertaken work that aims to develop a small-scale compact autothermal reformer to produce onboard hydrogen rich-product gas to power a solid oxide fuel cell (SOFC) unit. This device would be used in an auxiliary power unit in long haul trucks. This unit would be used when the truck is at rest to eliminate the need for idling at rest stops when electrical power is still in demand. The use of such an APU will reduce overall fuel consumption, reduce emissions and result in longer engine life. The present numerical study is a continuation of the previous studies carried out at FCRC to develop such an autothermal reformer. Following previous work the conversion of iso-octane ( $C_8H_{18}$ ), a surrogate of gasoline, to hydrogen rich gas stream to be used as a fuel in the fuel cell-powered auxiliary power unit will be conducted.

Initially a concentric cylinder bench-scale autothermal reformer was designed and constructed as a prototype reactor by Middleton (2004) at the Fuel Cell Research Centre. The objectives of the design were to construct a prototype reactor that could facilitate heat transfer throughout the reactor while meeting plug flow criteria, that was robust in design, and would produce high hydrogen output. Caners (2005) completed an experimental study of the first prototype at the Fuel Cell Research Centre and obtained a wide range of results giving the temperature profiles inside the reactor and the overall performance characteristics of the reactor under various operating conditions. A one-dimensional computer model of this prototype reactor was prepared by Li (2004) at Queen's University, this model serving as the basis for the development of a more sophisticated two-dimensional model. McIntyre(2005) prepared a two-dimensional computer model and defined more accurate physical properties of the reactor. A reaction mechanism prepared by Pacheco et al (2003) to describe the chemical reaction mechanism of autothermal reforming of iso-octane over platinum on ceria oxide based catalyst was adopted by McIntyre (2005) in his modeling work. McIntyre (2005) found from his numerical results that most of the steam reforming reaction completed before the end of the first catalyst bed indicating that concentric cylinder design is not a good option for an autothermal reforming process.

As a result, a single-cylinder configuration design was prepared and constructed by personnel at the Fuel Cell Research Centre. Sylvestre (2007) performed a numerical study of this new design and found that higher temperature gradients exist at the start of the catalyst bed and temperature distribution within the reformer is not even. Shaw (2008) carried out experimental study of this new design, compared his experimental

results with Sylvestre's (2007) numerical predictions, noted certain discrepancies between the numerical and experimental results and recommended improvements in the design to get more even distribution of temperature profiles in the catalyst bed of the reformer. The present study was undertaken to analyze the numerical and experimental results obtained by Sylvestre (2007) and Shaw (2008) to match the numerical results with experimental data obtained by Shaw (2007). The purpose was to improve the design of the reformer to reduce temperature gradients in the catalyst bed and increase hydrogen output. Previous numerical and experimental studies to develop an autothermal reformer by personnel at Fuel Cell Research Centre are discussed in detail in chapter 3.

## 1.2 **Reforming of hydrocarbons for production of hydrogen**

Reforming is a technical term which is used to describe the chemical conversion of hydrocarbon fuel into a gaseous hydrogen rich fuel stream, usually in the presence of a catalyst. There are three reforming methods which are most commonly used namely steam reforming, partial oxidation reforming and autothermal reforming. Each of these methods has its own advantages and disadvantages depending on the application. For the present research work, autothermal reforming has been utilized. Autothermal reforming is a combination of catalytic steam reforming and partial oxidation of the fuel that takes place in varying proportion depending upon the amount of hydrogen required and the desired exit temperature. These methods are discussed in detail in chapter 2.

The conversion of hydrocarbons to hydrogen is a potential source of hydrogen production and supply to onboard fuel-cell-powered auxiliary power units. Hydrogen required for such applications can be generated onboard with a fuel processor module. The module consists of a reformer where the fuel is primarily converted to hydrogen rich gas stream. With some fuel cell system one or more CO clean-up units are then used depending on the amount of CO that is allowable at inlet of the fuel cell system. The first part of this unit comprises the shift reactor where the CO concentration is reduced to 1-2%. The primary reaction in this reactor is the Water Gas Shift reaction (WGS). The exit of the shift reactor then enters the Preferential Oxidation (PROX) reactor where CO present in a hydrogen rich stream is preferentially oxidized and the CO concentration is reduced to 10-15ppm depending on the fuel cell requirement. A schematic of a typical fuel processor system is illustrated in Figure 1.1.

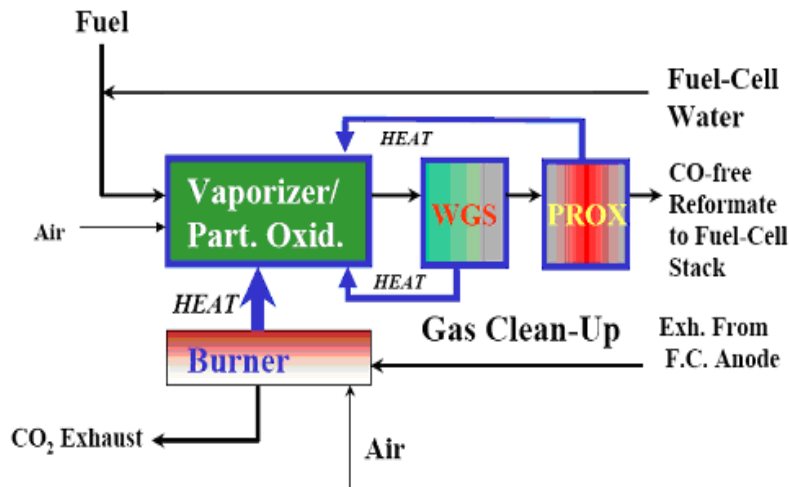


Figure 1.1: Fuel reformer schematic.

For fuel-cell-powered auxiliary power unit applications, some extra demands are placed on the design of the fuel reformer. Onboard fuel reformers for mobile applications are required to be:

- Compact both in weight and volume.
- Capable of starting up quickly.
- Able to follow demands rapidly and operate efficiently over a wide range of operating conditions.
- Capable of delivering low-CO content gas to the fuel cell stack.
- Emit very low levels of pollutants.

One of the major obstacles to the production of hydrogen from most commonly used fuels, gasoline and diesel, is the presence of sulfur content and other additives suitable for engines. Sulfur is poisonous to the catalyst activity in fuel cell applications. Fuel cell suppliers recommend that sulfur content should be less than 1 part per million by weight in the feed gas. The removal of sulfur during onboard autothermal reforming process is not an economically good option but to remove sulfur in fuel refineries is considered feasible. That is why iso-octane ( $C_8H_{18}$ ), a surrogate of gasoline, has been selected in the present and previous studies performed by FCRC group for the reforming process of hydrogen production in a compact autothermal reformer.

Fuel cell types that have been developed so far employ hydrogen ( $H_2$ ) as the preferred fuel because of its high reactivity for the electrochemical anode reaction and oxidation of hydrogen produces water, which is environmentally more suitable than  $CO_2$ . Unfortunately, large quantities of hydrogen not naturally available as a gaseous fuel and

for practical fuel cell systems it usually has to be generated by fuel processing from whatever fuel source is locally available. This has led researchers around the world to explore alternative fuel sources and means to produce hydrogen. Presently other pathways available for the production of hydrogen are depicted in Figure 1.2.

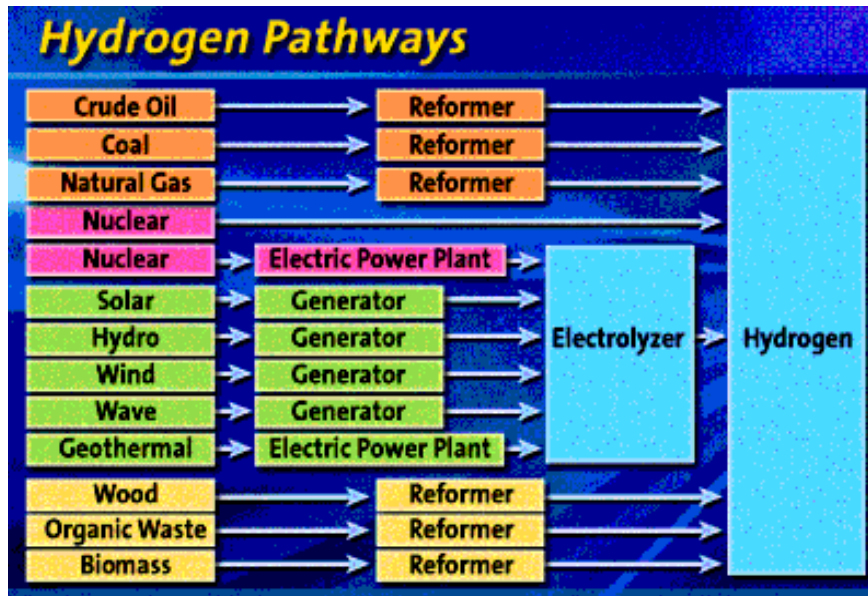


Figure 1.2: Hydrogen Pathways, (<http://www.ch2bc.org/index2a.htm>)

For mobile applications, the most promising option for environmentally benign operation is to use hydrogen as the energy carrier source and to adopt fuel cells as the clean and efficient means of energy conversion and power generation. Figure 1.3 shows the relative amount of carbon dioxide produced by various fuels for one unit of energy consumed.

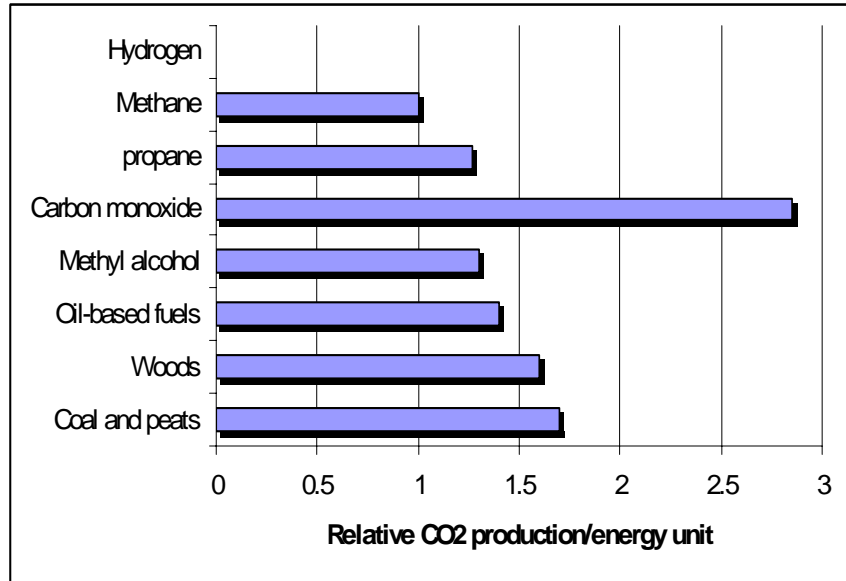


Figure 1.3: Comparison of the relative amount of carbon dioxide production from different fuels for one unit of energy (Xianguo, 2006).

It is seen that hydrogen does not produce any carbon dioxide. Until the hydrogen infrastructure is developed and hydrogen storage problems are solved, fossil fuel-based reformers are a good option for the onboard production of hydrogen to exploit the existing fuel infrastructure for mobile applications of the fuel cell technology.

### 1.3 Fuel Cells

Different types of fuel cells are under development according to the nature of their applications. The main fuel cells include Phosphoric Acid Fuel Cell (PAFC), Molten Carbonate Fuel Cell (MCFC), Solid Oxide Fuel Cell (SOFC), Proton Exchange Membrane Fuel Cell (PEMFC) and Direct Methanol Fuel Cell (DMFC). Some of these cells show promise for use in industrial power generation such as MCFC and SOFC and other cells may be useful for small portable applications such as PEMFC. Figure 1.4 illustrates the schematic of a standard Fuel Cell.

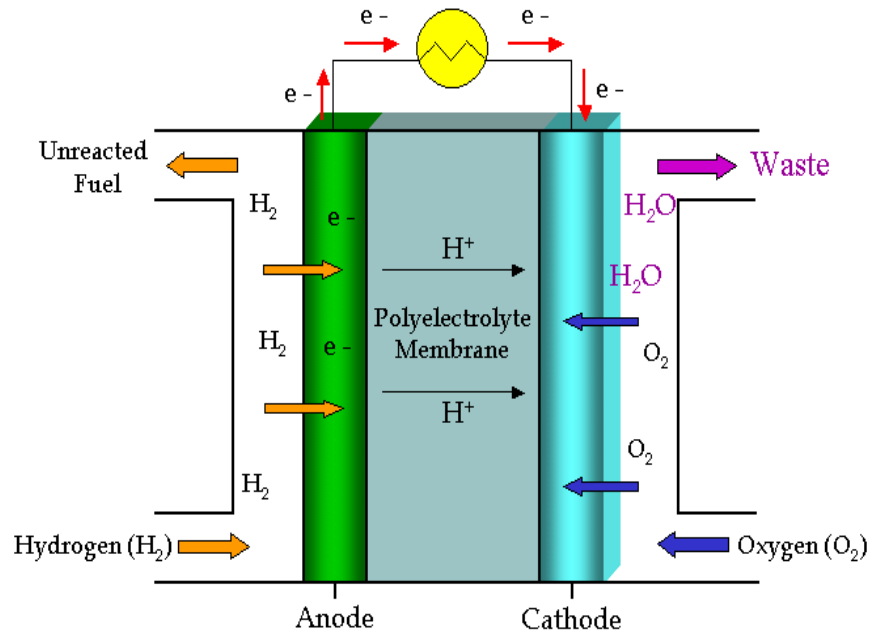


Figure 1.4: Scheme of Fuel Cell (Monica, 2006)

Each type of fuel cell has some particular fuel requirements summarized in the Table 1.1(Monica, 2006).

Table 1.1: The fuel requirements for the principal types of fuel cells

Gas species	PEMFC	AFC	PAFC	MCFC	SOFC
H <sub>2</sub>	Fuel	Fuel	Fuel	Fuel	Fuel
CO	Poison (>10 ppm)	Poison	Poison (>0.5%)	Fuel	Fuel
CH <sub>4</sub>	Diluent	Diluent	Diluent	Diluent	Diluent
CO <sub>2</sub>	Diluent	Poison	Diluent	Diluent	Diluent
&H <sub>2</sub> O (as H <sub>2</sub> S) COS)	Few studies,	Unknown	Poison (>50 ppm)	Poison (>50 ppm)	Poison (>1.0 ppm)

The auxiliary power unit for trucks considered in the present study is based on the use of solid oxide fuel cell where CO can be utilized as a fuel and there is a no need to reduce the amount of CO to low level present in the hydrogen rich gas stream of the reformer's output.

Fuel cell technology, also known as energy conversion technology, has the potential of clean and efficient power generation. Through Bacon's pioneering work in the 1950s, fuel cells were successfully developed for the American manned space program. This success led to substantial development programs in America and Japan in the 1970s and the 1980s. During recent years, the energy crisis in the world has again stimulated new and expanding interest in the development of fuel cell technology. With the growth of world population, the consumption of energy has increased to a large extent. The excessive energy consumption has a significant adverse impact on the environment, resulting in increased health risks to all life forms and the threat of global climate change. Fuel cells, the energy conversion technology, with operation on hydrogen ( $H_2$ ) to produce electric power on demand, have the potential to meet the extraordinary effects of energy consumption. Fuel cells are environmentally friendly devices for energy conversion and power generation, and are one of the most promising candidates as a zero-emission power source. Hence, the fuel cell technology is often regarded as one of the advanced energy technologies of the future.

#### 1.4. Fuel-Cell-Powered Auxiliary Power Unit

Fuel-cell-powered auxiliary power unit is a device on a vehicle whose purpose is to provide energy for functions other than propulsion. The schematic view of application of fuel cell powered APU system in mobile applications is illustrated in the following Figure 1.5.



Figure 1.5: Schematic of fuel cell-powered APU system

The application of onboard fuel-cell-powered-auxiliary power unit in a long haul truck while at rest can reduce the fuel consumption and general wear and tear on the engine resulting in longer engine life. It can generate enough electric power to meet all electric needs of the truck while at rest. The transport truck needs power for heating, ventilation and air conditioning in the cabin areas as well as powering all other electrical systems including lighting, refrigerators, radios and televisions. Generally these extra demands are met by electricity supplied by the engine through alternator assembly. When engines are idling to meet the electric demands of truck at rest, they consume more fuel and produce significant amounts of green house gas (GHG) emissions causing adverse impact on the environment.

Argonne National Laboratories (2007a) reported that over 500,000 trucks driving in North America on a daily basis consume approximately 3 billion gallons of fuel during idling times and estimates of emissions from overnight idling over one year are about 180,000 tons of NO<sub>x</sub>, 5,000 tons of particulate matter, and 7.6 million tons of CO<sub>2</sub>. The use of fuel-cell-powered auxiliary power unit in trucks can serve as the additional source of power to produce clean and more efficient power without polluting the climate and can meet electric demands of the truck at rest.

Fuel-cell-powered auxiliary power unit offers potential advantages in overall energy efficiency, emissions and costs. Many heavy-duty vehicles idle regularly to power the cabin's climate control and electric accessories. Some passenger vehicles also idle for long durations to power lights and communications systems. Other vehicles that operate tools and machinery may idle their engines for extended periods. Key parameters in determining where and how fuel-cell-powered auxiliary power unit might be attractive include operational characteristics of the auxiliary power (total power requirement, time of use, etc.).

## **2. Scope of Thesis**

Present study is a continuation of the numerical work completed by Sylvestre (2007), which describes a 2-dimensional, axis-symmetric, single cylindrical auto-thermal reformer and is based on the chemical reaction mechanism developed by Pacheco et al (2003). The objectives for the present work are to:

- Use the numerical model to carry out improvements in the reformer design, determine the value of the effectiveness factor of the catalyst bed, reduce the temperature gradients in the catalyst bed of the reformer and increase the hydrogen output.
- Undertake a comparison between the numerical results with the experimental data obtained by Shaw (2008) using the experimental operating conditions.
- Perform numerical simulations to carry out further possible improvements in the design of the reformer to increase its overall performance.

## **Chapter 2**

### **Literature Review**

#### **2.1 Introduction**

The lack of an infrastructure for producing and distributing hydrogen fuel for fuel cells applications is the major obstacle to commercialization of fuel cell technology in the transportation industry. As a result, research efforts at different levels are in progress to develop onboard fuel processing technology for reforming of available fossil fuels to generate hydrogen onboard. In recent years, onboard autothermal reforming of liquid fuels is being considered the most attractive for fuel-cell-powered auxiliary power unit applications in heavy-duty trucks when at rest for emission control and economic benefits.

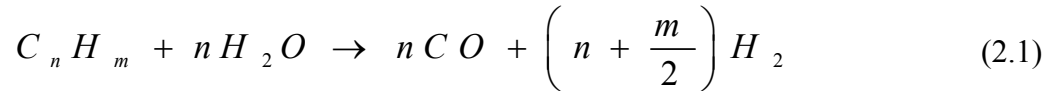
In this chapter, literature review is presented to describe the available methods for reforming of hydrocarbon fuels, catalysts available for reforming process, chemical reaction mechanism for autothermal reforming, reformer operating conditions and application of autothermal reformer in fuel-cell-powered auxiliary power units.

#### **2.2 Reforming of Hydrocarbons**

The methods most commonly used for conversion of hydrocarbon fuels to hydrogen include steam reforming (SR), partial oxidation (PO), and autothermal reforming (ATR). Each of these methods has its own advantages and disadvantages depending on the application. These are discussed here briefly.

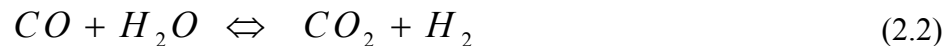
### 2.2.1 Steam reforming (SR) Method

This method is generally used in industrial applications for the production of hydrogen at large scale. It involves the reaction of steam ( $H_2O$ ) with hydrocarbon fuel ( $C_nH_m$ ) in the presence of a catalyst to produce hydrogen ( $H_2$ ) and carbon monoxide ( $CO$ ) as described by the equation (2.1). (Sylvester, 2007)



Steam reforming is an endothermic process and it needs preheating. Some of the fuel must be burned and heat produced be transferred to the reformer via heat exchanger. Steam reforming requires heat to make the reaction progress which results in a relatively lower overall efficiency of the system. Higher temperatures are required, around  $700^\circ C$ , for increased hydrogen yield (Larminie and Dicks, 2003). This method shows the highest hydrogen production efficiency but the requirement of a large energy input due to endothermic nature of the reaction is considered to be its major drawback.

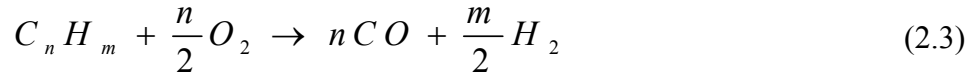
Another chemical reaction which occurs during steam reforming of hydrocarbons is the water-gas-shift reaction in which carbon monoxide reacts with water to form carbon dioxide and hydrogen as described by the equation (2.4).



This reaction is slightly exothermic and is a part of steam reforming of hydrocarbons. It is an equilibrium reaction which means that the reaction will continue in either direction until equilibrium is achieved. This reaction is useful because it utilizes the undesirable carbon monoxide product gas of the steam reforming reaction to produce additional hydrogen. (Sylvestre, 2007)

### 2.2.2 Partial oxidation reforming (POR) Method

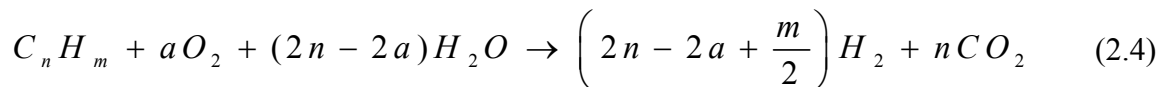
Partial oxidation reforming method involves the reaction of oxygen (O<sub>2</sub>) with fuel to produce H<sub>2</sub> and CO when oxygen-to-fuel ratio is less than that required for total combustion i.e. complete conversion of fuel to CO<sub>2</sub> and H<sub>2</sub>O and is described by the equation (2.2).(Sylvestre,2007)



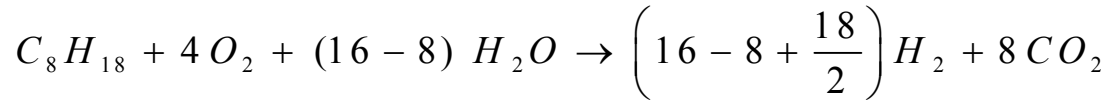
Partial oxidation is an exothermic process which eliminates the need for preheating as compared with the steam reforming process and is considered comparatively a more simple system. But it produces less hydrogen per mole of fuel feed than the steam reforming reaction as seen in equations (2.1) and (2.3). Furthermore, since providing pure oxygen for the reforming process is not a viable option, air is usually used as an oxygen source and therefore it dilutes hydrogen rich gas stream with inert nitrogen, resulting in a lower overall reformer efficiency. The reaction rates are much higher for the partial oxidation than for the steam reforming but the hydrogen yield per carbon in a fuel is lower.

### 2.2.3 Autothermal reforming (ATR) Method

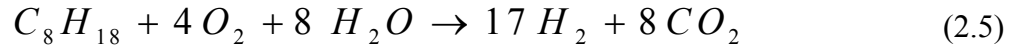
Autothermal reforming involves the reaction of oxygen, steam and fuel over a catalytically active region to produce H<sub>2</sub> and CO<sub>2</sub>. It can be viewed as a combination of partial oxidation and steam reforming process. In the ideal situation, the overall autothermal process is described by the following chemical reaction: (Sylvestre,2007)



For the autothermal reforming of iso-octane, the general equation (2.4) for  $n=8$ ,  $m=18$ , and  $a=4$  can be written as follows:



On simplification, the equation will be:



The exothermic reaction of partial oxidation forms  $H_2$  and  $CO$  as products while providing heat for the endothermic steam reforming reaction. The autothermal reforming provides hydrogen-rich gas and can overcome the limitations of steam reforming since the heat required for the endothermic reactions is generated within the catalyst bed, a property that allows for more rapid response to changing power demands and faster startup. The lower operating temperature of catalytic autothermal reforming has several advantages including less complicated reactor design, wider choice of materials for construction and lower fuel requirements during startup over the higher operating temperature of partial oxidation or steam reforming for fuel-cell-powered auxiliary power unit applications. (Rajesh, 2004). The choice of the reaction process for onboard reforming depends on the operating characteristics. The steam reforming process is heat transfer limited and does not respond rapidly to changes in the power demand. When power demand rapidly decreases, the catalyst can overheat, causing sintering, which in turn results in loss of activity. As a result, the autothermal reforming process is considered to be a better option for hydrocarbon conversion to hydrogen-rich gas. (Ersoz, 2003). The important parameters for autothermal reforming process are temperature, pressure, oxygen to carbon ratio (O/C) and steam to carbon ( $H_2O/C$ ) ratio. These parameters are

selected carefully to avoid formation of coke on catalyst and minimize methane production.

### 2.3 Autothermal Reforming of Iso-octane ( $C_8H_{18}$ ), a Surrogate of Gasoline.

In this section the most relevant papers concerned with the use of iso-octane reforming within the scope of autothermal reforming are reviewed. Villigas (2006) performed an experimental study on the reforming of iso-octane as a surrogate of gasoline over a Pt catalyst on a ceria-zirconia mixed oxide support using the experimental conditions of a similar nature and scale used in the present research work. The author obtained the results using a mass Gas Hourly Space Velocity (GHSV) of  $150,000h^{-1}$ . GHSV ( $h^{-1}$ ) is generally defined in literature as the ratio of the volume flow rate of all inlet species in cc/h divided by the catalyst volume in cc and is always calculated at STP. Results of this study for varying the O/C ratio are shown in

Figure 2.1

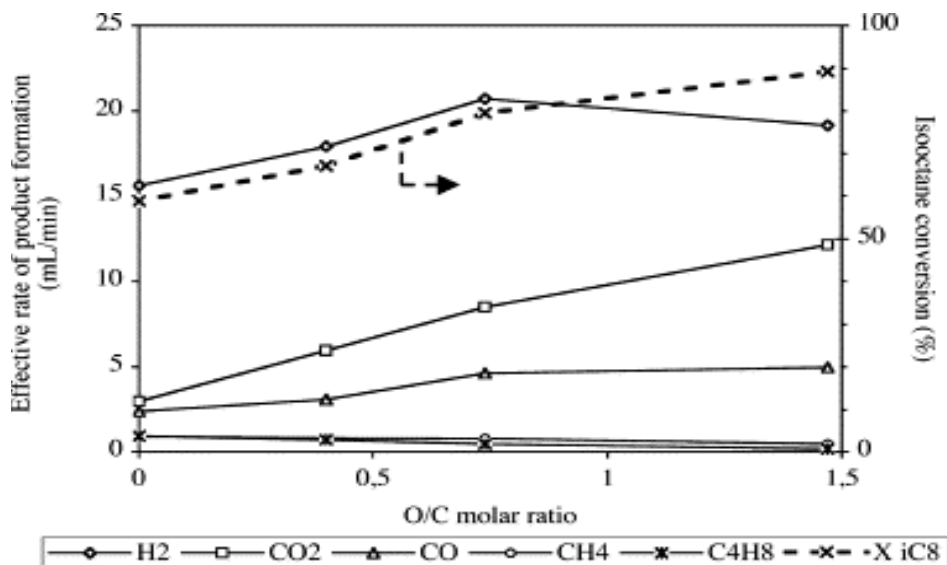


Figure 2.1: Iso-octane conversion and product distribution as a function of O/C ratio (experimental conditions:  $680^{\circ}C$  1.3 vol,% iso-octane,  $H_2O/C=1.5$ )(Villigas,2006)

It should be noted that throughout this thesis, the O/C refers to atomic oxygen to atomic carbon ratio and not to O<sub>2</sub>/C ratio which is often reported in literature and confused with O/C. Villegas noted that with the increase of O/C ratio, conversion increases from 60% to 90%. The hydrogen production increases to a maximum with increasing O/C up to 0.75, and then decreases. The effects of varying the H<sub>2</sub>O/C ratio were also studied and the results obtained are shown in Figure 2.2. Villegas (2006) found that with higher H<sub>2</sub>O/C ratios the hydrogen production increased significantly and the fuel conversion was not greatly affected. The author attributed this to higher water-gas-shift reaction rates.

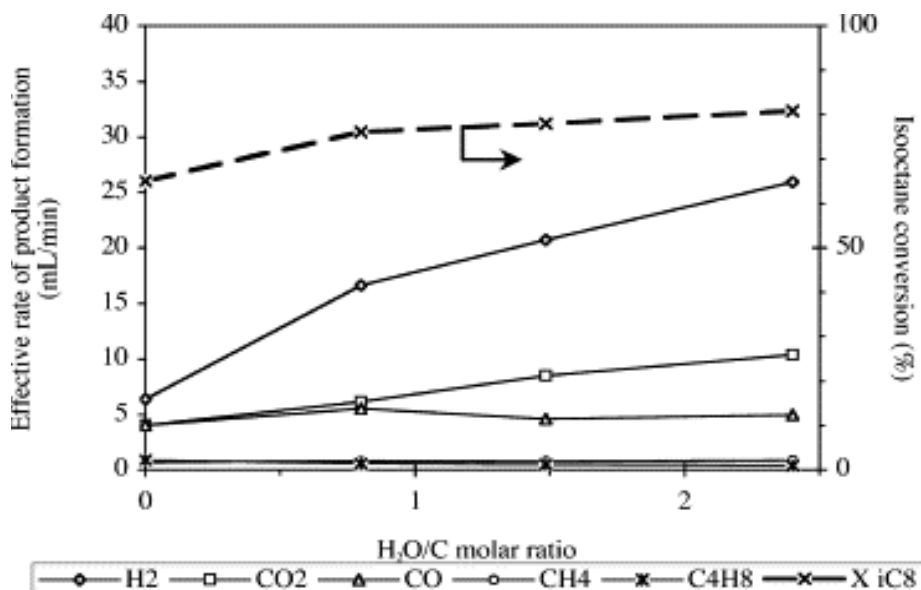


Figure 2.2: Iso-octane conversion and product distribution as a function of O/C ratio (experimental conditions: 680°C, 1.3vol,%iso-octane, H<sub>2</sub>O/C=1.5, GHSV=150,000h<sup>-1</sup>)(Villegas,2006)

Moon et al. (2001) performed an experimental analysis of the autothermal reforming of iso-octane using a very similar reactor as well as operating conditions utilized in the reactor investigated in the present work. The catalyst used was one gram of naphtha reforming catalyst. A summary of results obtained by Moon et al (2001) is given in Table 2.1.

Table 2.1: Approximate results adapted from Moon et al. (2001) for autothermal reforming of iso-octane.

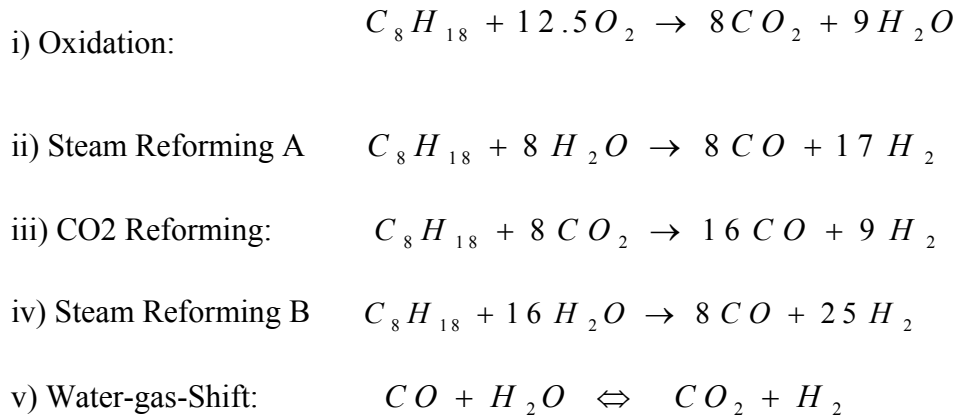
H <sub>2</sub> O/C	O/C	H <sub>2</sub> Molar %	CO <sub>2</sub> Molar %	CH <sub>4</sub> Molar %	CO Molar %
0.5	1.0	53.7	21.0	14.0	29.0
1.0	1.0	60.0	21.0	4.0	21.0
1.5	1.0	62.0	21.0	1.0	17.5
2.0	1.0	64.0	24.0	0.5	11.0
3.0	0.5	67.7	14.7	2.5	15.0
3.0	1.0	64.7	24.0	0.5	11.5
3.0	1.5	57.0	30.0	1.0	11.5
3.0	2.0	49.9	41.9	2.0	8.0

Moon (2001) noted that by increasing O/C ratio, from 0.5 to 2.0, the hydrogen molar production progressively decreased from 67.7% to 49.9% while a rise in the CO<sub>2</sub> concentration from 14.7 % to 41.9% was observed. When the H<sub>2</sub>O/C ratio was increased from 0.5 to 3.0, hydrogen concentration increased from 53.7% to 64.7%, while CO production decreased from 29% to 11%.

Moon (2001) also studied the effects of the variation of GHSV on the production of hydrogen. It was noted that when the GHSV was varied from 4,000h<sup>-1</sup> to 17,000h<sup>-1</sup>, the hydrogen concentration remained consistent. When the space velocities were increased to above 17,000h<sup>-1</sup> the production of hydrogen decreased. The optimum operating conditions were determined to be an O/C ratio of 1.0, a H<sub>2</sub>O/C ratio of 3.0 and a reactor temperature of 700°C.

### 2.3.1 Reaction Kinetics and Catalysts for Autothermal Reforming of Iso-octane.

The chemical reaction mechanism of autothermal reforming of iso-octane consists of several chemical reaction steps depending upon the molecular weight of several hydrocarbons. A chemical reaction mechanism was developed by Pacheco et al. (2003) for reforming of iso-octane based on the studies carried out by Xu, Froment (1989) and Jin et al. (2000) for methane reforming. Pacheco et al. (2003) described the primary reactions of autothermal reforming of iso-octane as follows:



Pacheco et al (2003) developed rate expressions for each reaction and determined new kinetic reaction constants by performing several tests at different inlet temperatures and gas-hourly-space velocities. This reaction mechanism describes the primary reactions that occur during autothermal reforming of iso-octane but do not include the formation of lighter hydrocarbons, like CH<sub>4</sub>, that have been shown to be present in the product gas stream of autothermal reformers by Roychoudhury et al. (2005).

Villegas et al. (2005) worked on the autothermal reforming of iso-octane but did not develop the kinetic data. At present, no reaction kinetic data has been reported in the literature that can completely describe all the step reactions of autothermal reforming of hydrocarbons for computer simulations. For this reason, the reactions mechanism

described by Pacheco et al. (2003) was adopted by both McIntyre (2005) and Sylvester (2007) in the modeling work of the reformer under study. The present numerical study to improve the design of the autothermal reformer is also based on the Pacheco et al (2003) reactions mechanism.

### 2.3.2 Catalysts for Autothermal Reforming

Krumpelt et al.(2002) performed catalyst testing of different transition metals doped on a ceria base for autothermal reforming of iso-octane and reported that all metals tested showed iso-octane conversions of more than 95 % at 600°C, a gas-hourly-space-velocity of  $3000\text{h}^{-1}$ ,  $\text{O}/\text{C} = 0.46$ , and  $\text{H}_2\text{O}/\text{C} = 1.14$  as shown in the Figure 2.3:

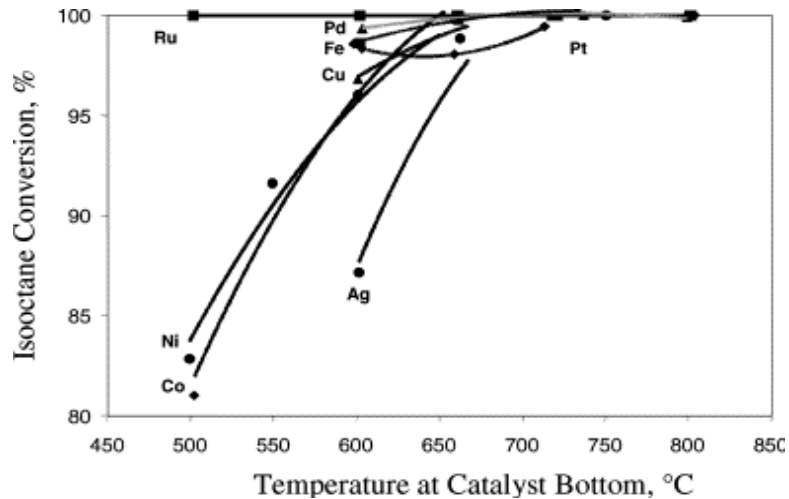


Figure 2.3: Iso-octane conversion rate for transition metals doped on ceria base at different temperatures (conditions:  $\text{O}/\text{C} = 0.46$ ,  $\text{H}_2\text{O}/\text{C} = 1.14$ ,  $\text{GHSV} = 3000\text{h}^{-1}$ )

Mawdsle (2004) tested different monolith catalysts, including Rh, Rh-Pt, and Pt in autothermal reforming of sulfur-free gasoline. It was found that monoliths coated with Rh

or Rh-Pt catalyst produced reformates with a higher hydrogen concentration than the monolith coated with only pt as shown by the results given in Figure 2.4.

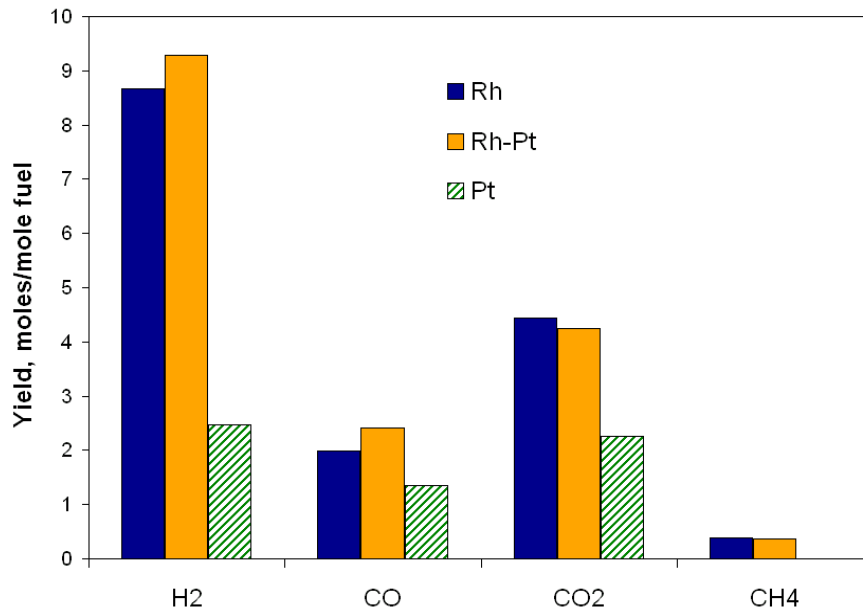


Figure 2.4: Comparison of H<sub>2</sub>, CO, CO<sub>2</sub>, and CH<sub>4</sub> yields for different catalyst from Mawdsle (2004) (yields produced from <450 ppb sulfur gasoline at 700°C)

Tiemersma and Roychoudhury(2005) reported that Rh-Pt and Pt performed very well over a broad range of temperatures and are mostly used in autothermal reformers. Gudlavalleti et al.,(2007) investigated the catalyst deactivation due to sintering, coking and poisoning in the autothermal reforming of desulfurized methane both numerically and experimentally.

## 2.4 Autothermal Reforming with Surrogates and other Hydrocarbons

The general characteristics of autothermal reforming of various hydrocarbons are all similar in nature, and are relevant to the current research. Since an autothermal reforming of a surrogate fuel for gasoline (iso-octane) is studied in the present research work, a comparison of the results of fuels and their surrogates can be useful. The more widely available commercial fuels such as gasoline, diesel and natural gas are not homogeneous and contain a mixture of alkanes, alkenes and aromatic hydrocarbons which need pre-reforming treatment before autothermal reforming process is carried out. In addition, commercial fuels contain sulfur compounds that can cause catalyst deactivation (Murata, 2007). A lot of research is going on to develop integrated onboard autothermal fuel reformers for gasoline and diesel fuels and their surrogate fuels ( $C_8H_{18}$ ,  $C_{16}H_{34}$ ).

Kang and Bae (2006) conducted a comparative study of gasoline ( $C_7H_{13.9}O_{0.1}$ ) and diesel ( $C_{11.6}H_{19.5}$ ) versus their surrogate fuels ( $C_8H_{18}$  and  $C_{16}H_{34}$ ) for autothermal reforming and found the differences in the product gas concentrations. The packed bed type reactor consisted of a 0.5 weight percent pt catalyst with comparable pellet size to the catalyst utilized in the present work. Experiments were conducted at a space velocity of  $5000h^{-1}$ . The results obtained for gasoline and diesel, and their surrogates with varying inlet temperatures are as shown in the Figures 2.5 and 2.6.

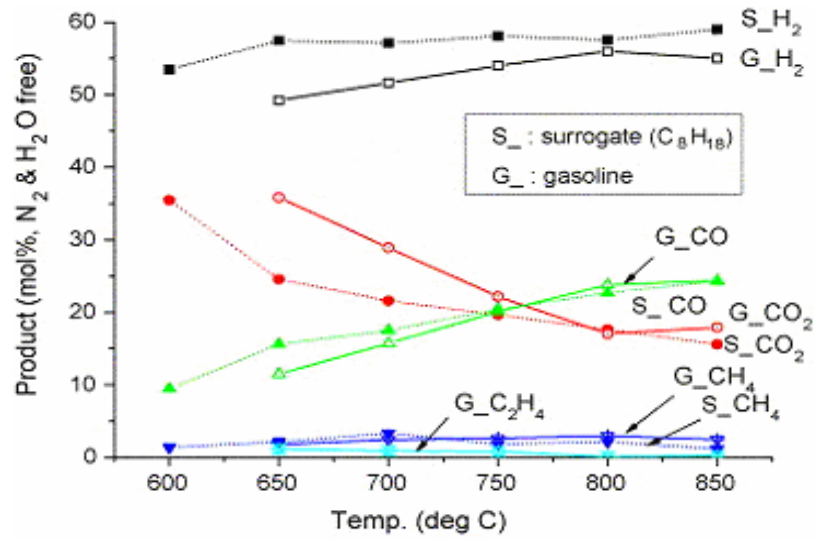


Figure 2.5: Comparison of product distribution for gasoline and C<sub>8</sub>H<sub>18</sub> (H<sub>2</sub>O/C=1.25, O/C=0.5, GHSV=5000h<sup>-1</sup>) (Kang and Bae, 2006)

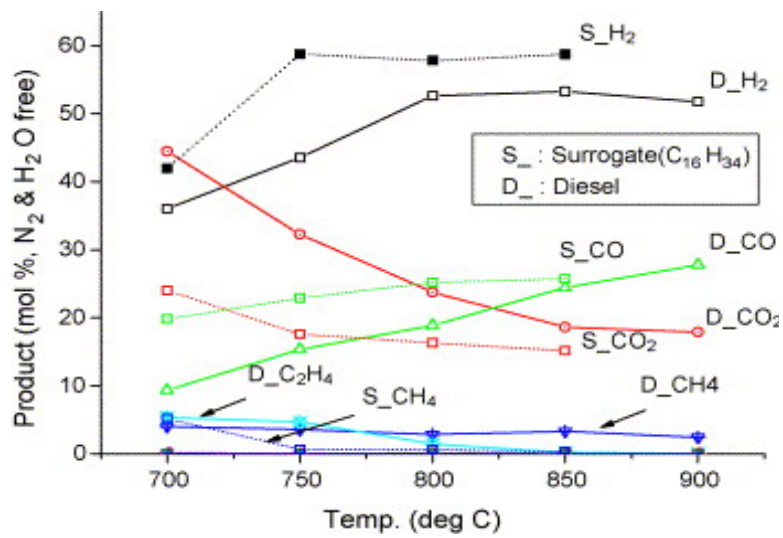


Figure 2.6: Comparison of product distribution for diesel and C<sub>16</sub>H<sub>34</sub> (H<sub>2</sub>O/C = 1.25, O/C = 0.5, GHSV = 5000h<sup>-1</sup>) (Kang and Bae, 2006)

The authors noted that at higher temperatures there was a good agreement between the reformat composition for gasoline and iso-octane. Ahmed and Krumpelt (2001) determined the maximum theoretical efficiencies of different hydrocarbons and found that heavier hydrocarbons have lower overall efficiencies due to lower hydrogen to carbon ratios.

Moon et al. (2001) investigated the autothermal reforming of iso-octane and found that the reactions at higher gas hourly space velocity (GHSV) resulted in lower H<sub>2</sub> yield. This is attributed to the fact that the gas hourly space velocity is inversely related to the residence time of a reactant gas at an active catalyst site. With a longer residence time, more reactant gas is able to convert to product gas due to longer exposure to the catalyst zone.

Aicher et al investigated the autothermal reforming of propane at working conditions of T= 800°C, C<sub>3</sub>H<sub>8</sub>/O<sub>2</sub> = 2.0 and H<sub>2</sub>O/C =1.5 over nickel-based catalysts. When the reaction was performed at GHSV of 57,000h<sup>-1</sup>, ethylene was present in products. It was reported that when complex fuels like gasoline or diesel are used as feedstock, reaction temperatures higher than 850°C are necessary to achieve complete fuel conversion over nickel-based reforming catalysts. The main obstacles to H<sub>2</sub> production from the gasoline ATR over nickel-based reforming catalysts are catalyst deactivation by coke deposition and the slip of higher hydrocarbons into the down-stream processing units. Pre-reforming has been successfully integrated in the process of naphtha or natural gas steam reforming for H<sub>2</sub> production. However, its integration into the process of H<sub>2</sub> production from gasoline ATR indicates that gasoline could be efficiently converted into H<sub>2</sub> over nickel-based reforming catalyst. The products from pre-reformer

could be heated to temperatures up to 800°C without coke deposition risk. Higher hydrocarbons present in reformat from the ATR reactor could be eliminated in the integrated process. The combined characteristics of the integrated process make it potentially applicable to small-scale onboard H<sub>2</sub> production unit using the worldwide gasoline infrastructure

## Chapter 3

### Previous Progress

#### 3.1 Overview

Queen's/RMC Fuel Cell Research Centre (FCRC) group has developed a compact autothermal reformer for onboard production of hydrogen from iso-octane for fuel-cell-powered auxiliary power unit applications. The type of fuel cell considered for this application is the micro-tubular solid-oxide fuel cell (SOFC) due to its fast startup time and small, durable design. The present numerical study is a continuation of the research efforts carried out by the Fuel Cell Research Centre group to develop an autothermal reformer.

An overview of the development and progress of an autothermal reformer design prepared by the Fuel Cell Research Centre and results obtained in the previous studies is presented because it had a great influence on the present study. The first prototype of a concentric cylinder bench-scale autothermal reformer for the onboard conversion of iso-octane to hydrogen was designed and manufactured by the Queen's/RMC Fuel Cell Research Group in 2004. A schematic diagram of the catalyst regions and cross-sectional view of concentric cylinder design are shown in Figure 3.1. Its specifications were prepared by Middleton (2004) which are given in Table 3.1.

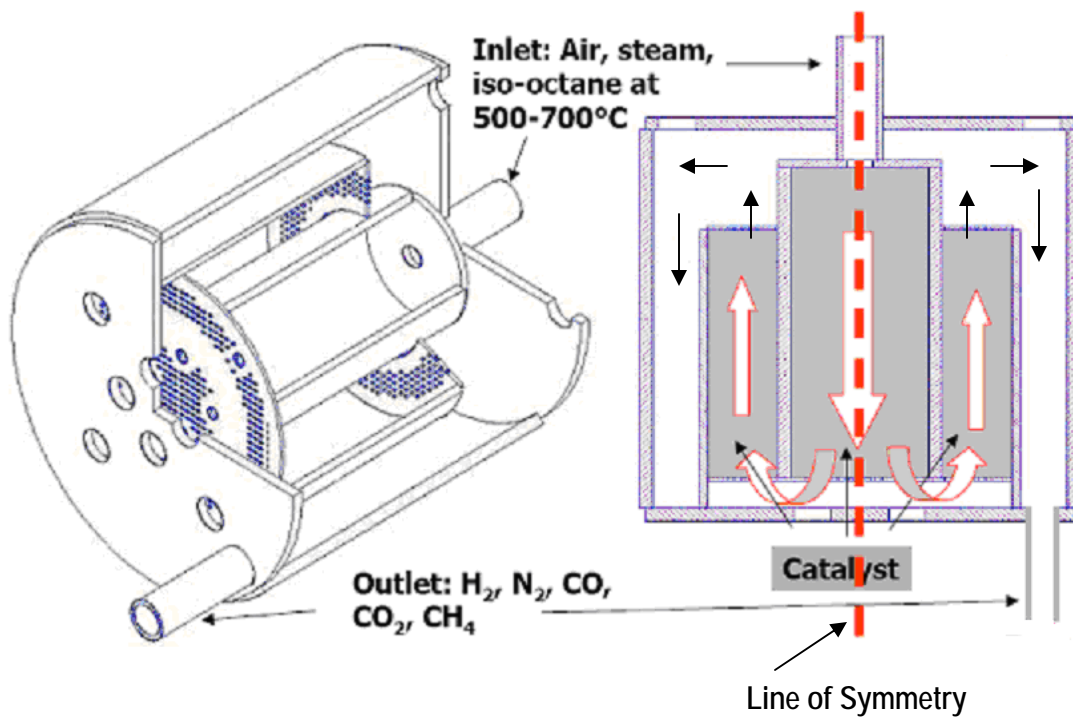


Figure 3.1: Drawing of the ATR designed and developed by Middleton (2004)

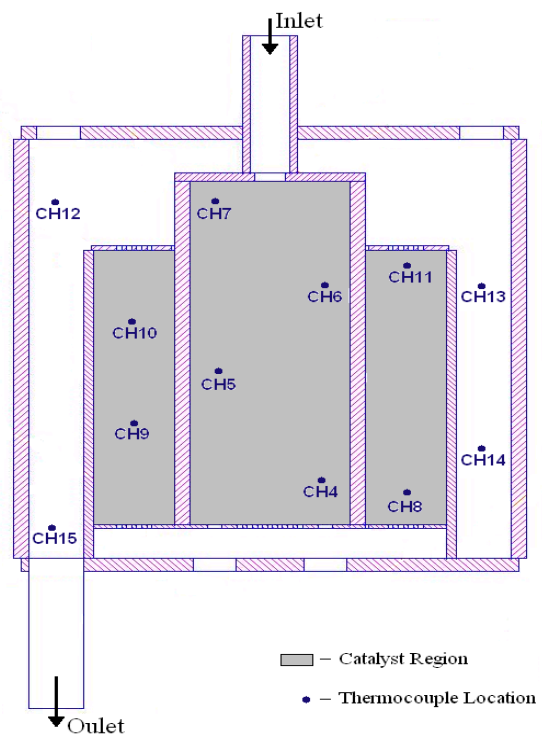


Figure 3.2: Cross sectional view of the ATR designed by Middleton (2004) with catalyst regions and thermocouple locations.

Table 3.1: Dimensions of the concentric cylinder design prepared by Middleton (2004)

Region	Length (mm)	Inner Diameter (mm)	Outer Diameter (mm)
Inlet Pipe	51	13	17
Outlet Pipe	51	13	17
Primary Cylinder	127	51	60
Secondary Cylinder	114	111	114
Outer Cylinder	156	152	162

The first reformer design was prepared with the purpose to meet the basic requirements and characteristics including resistance to corrosion, thermal cycling, hydrogen embrittlement, and adequate heat supply to drive the steam reforming reaction, minimal heat loss to the environment and to keep plug flow. This design utilized three concentric cylinders to promote heat transfer from the primary (or innermost) cylinder, where the partial oxidation reaction occurred, to the secondary (or intermediate) cylinder where steam reforming is expected. Only the two innermost cylinders contained catalyst where the reactions occur. Third cylinder was used to increase heat transfer to the steam reforming reaction. Materials that could withstand large temperatures changes, hydrogen embrittlement and corrosion were selected. The commercially available catalyst Pt/CeO<sub>2</sub> (1%Pt) impregnated on standard gamma-alumina ( $\gamma$ -Al<sub>2</sub>O<sub>3</sub>) substrate particles with an average diameter of 5mm was used. The criteria for plug flow conditions were adapted

from a paper by Mears (1971) and can be seen Equations (3.1) and (3.2) to determine reformer's dimensions.

$$\frac{\textit{Minimum wall to wall distance}}{\textit{Catalyst pellet diameter}} \geq 10 \quad (3.1)$$

$$\frac{\textit{Reactor length (total gas path length)}}{\textit{Catalyst pellet diameter}} \geq 30 \quad (3.2)$$

### **3.1.1 First Generation Reformer Results and problems:**

Caners (2005) conducted an experimental study of the first prototype of the autothermal reformer utilizing three concentric cylinders, at different inlet operating conditions by varying the inlet temperature, oxygen-to-fuel (O/C) molar ratio, steam-to-fuel (H<sub>2</sub>O/C) molar ratio and the flow rate of iso-octane. The results obtained by Caners (2005) are given in Table 3.2. It was found that the basic parameters such as oxygen-to-fuel ratio (O/C), steam-to-fuel ratio (H<sub>2</sub>O/C), the inlet stream temperature, the operating pressure, and gas-hourly-space velocity play a key role in determining the performance of the reactor and selected carefully to get higher hydrogen output. It was reported that fuel conversion percentages and dry hydrogen percentages ranged from 69% to 97% and 26% to 62% respectively.

Table 3.2: Experimental results from the first generation design of an autothermal reformer for the conversion of iso-octane.

Experimental Number	H <sub>2</sub> O/C Ratio	O/C Ratio	Iso-octane Flow Rate (ml/min)	H <sub>2</sub> Molar %	CO Molar %	CH <sub>4</sub> Molar %	H <sub>2</sub> Yield %
1	1	0.8	0.5	23.16	0.89	9.44	32.67
2	1	0.8	2.0	35.30	7.66	4.09	61.30
3	2	0.8	2.0	41.63	3.66	1.12	52.00
4	2	0.8	1.25	33.07	1.85	2.73	35.07
5	3	0.8	2.0	42.78	2.63	0.58	41.33
6	3	0.8	0.5	22.87	0.32	6.56	15.87
7	1	1.1	0.5	8.67	1.14	4.89	30.43
8	1	1.1	1.25	27.00	5.66	3.68	52.08
9	2	1.1	1.25	34.37	3.63	1.53	50.17
10	2	1.1	2.0	34.58	5.76	0.71	51.02
11	1	1.4	2.0	25.03	9.41	0.02	56.53
12	2	1.4	0.5	23.18	1.62	2.23	34.39
13	2	1.4	1.25	29.44	3.98	0.58	47.66
14	3	1.4	1.25	30.20	2.95	0.21	37.20
15	3	1.4	2.0	29.12	4.50	0.00	35.49
16	3	1.4	0.5	23.78	0.89	1.39	25.50

First 1-dimensional model of the concentric cylinder autothermal was prepared by Li (2004) at Queen's University. The results obtained by using this model were found to agree with the observed trends in the reactor behavior. A two-dimensional numerical study was carried out by McIntyre (2005) to improve the model of the reformer. For chemical reaction mechanism in the autothermal reforming of iso-octane, a chemical reaction mechanism described by Pacheco et al. (2003) was adopted by McIntyre in his modeling work. The temperature profiles obtained by McIntyre are shown in Figure 3.2.

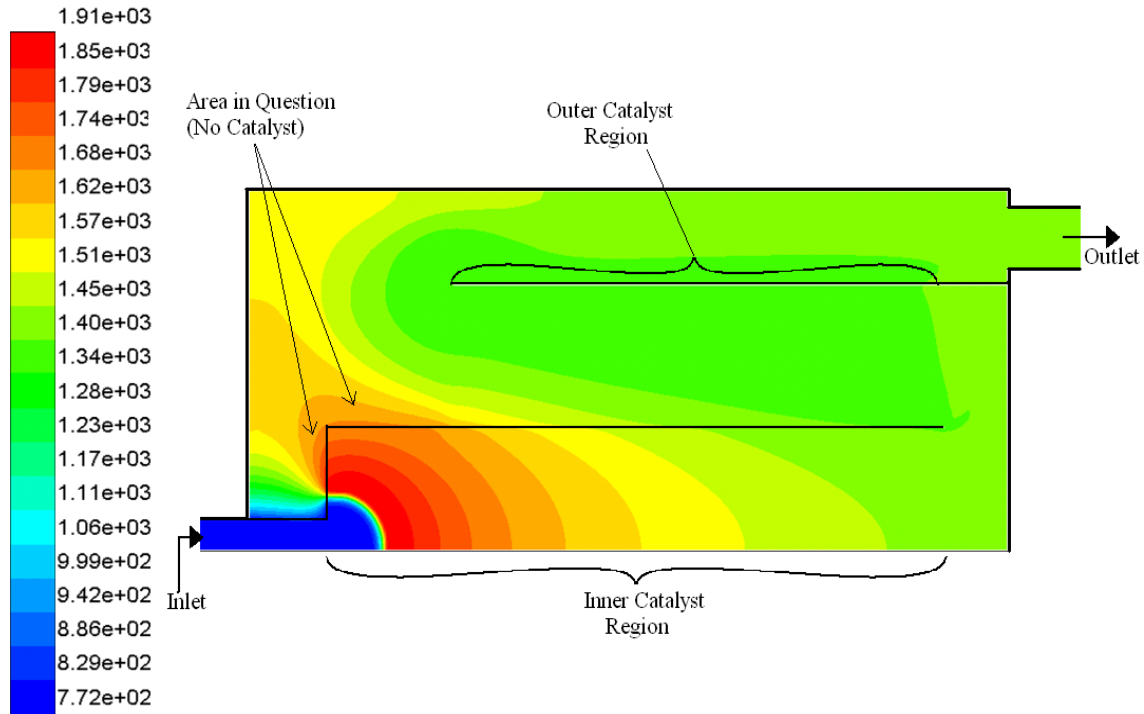


Figure 3.3: Temperature contour plot (degree Kelvin) of the first ATR from a model created by McIntyre (2005) (Note: contour plot is an axisymmetric, two-dimensional representation of the ATR)

Large temperature gradients at the beginning of the catalyst region were observed by the author indicating that large heat release by the exothermic oxidation reaction was not conducting effectively throughout the bed as desired. A lot of heat generated from the partial oxidation reaction was lost to areas in the reformer without catalyst. This can be easily seen in the Figure 3.2 in the section labeled “Area in Question” that the heat losses to the catalyst free zones are significant. McIntyre (2005) compared the numerical results with experimental data obtained by Canner (2005) and noted that most of the steam reforming reaction had gone to completion before the end of the first catalyst bed, indicating that concentric cylinders design of the reformer was not a good option. From these numerical and experimental studies, it was realized that size of the reactor should

be reduced and the thermal conductivity of the bed should be increased. Based upon the suggested improvements in the design of the first prototype of the reformer, a set of new distinctive characteristics were identified such as:

- A simplified design and a more detailed temperature profile measurement arrangement along the catalyst bed.
- Sufficient heat supply to drive the steam reforming process.
- Minimal external heat loss through the walls of the reactor.
- Ability to easily adjust reformer size and catalyst bed length.

Keeping in mind these desired characteristics for the new design, a second prototype of compact autothermal reformer was designed and manufactured by FCRC utilizing single cylinder configuration as shown in the Figure 3.3.

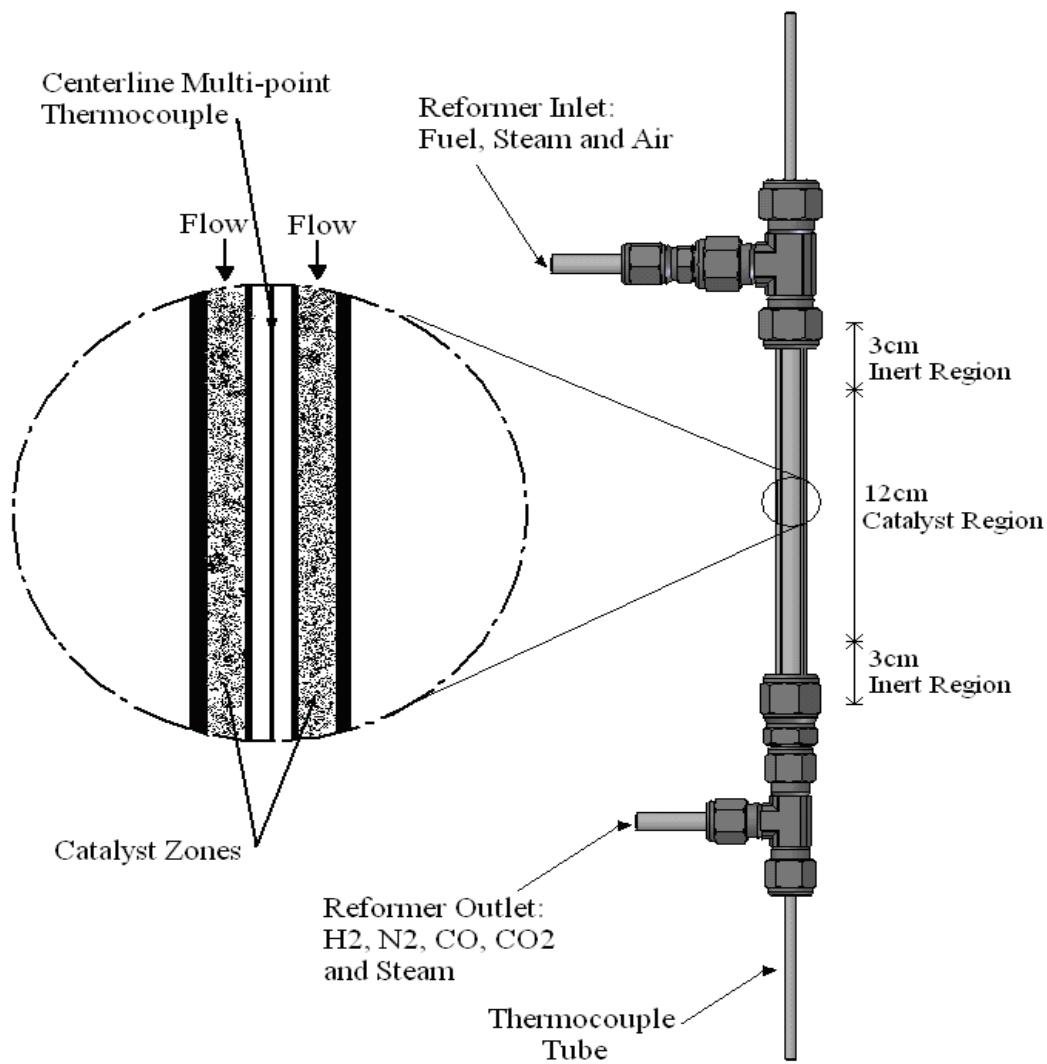


Figure 3.4: Schematic of the new design of the autothermal reformer.(Sylvestre,2007)

All major components of the new design along with important dimensions are listed in Table 3.3 and reactor drawings are given in appendix D.

Table 3.3: Major components of the new design along with important dimensions (Sylvestre, 2007)

Components	Length (cm)	Inner Diameter (cm)	Outer Diameter (cm)	Source	Additional Information
Reactor tube	18	0.75	0.95	Fuel cell Technologies	Four grooves milled on outside wall
Centerline tube	90	0.21	0.32	Micro Group Inc	Thin-walled tubing
Centerline thermocouple	30.5	N/A	0.16	Armate Controls Ltdk	3 points k-type
Wall thermocouples	10	N/A	N/A	Watlow	6 points, k-type with 90° bends
Fittings	N/A	N/A	N/A	Swagelok and Conex	Breakable 'Lava' seals
Catalyst Screens	N/A	0.32	0.96	Cleveland Wire Cloth	100 mesh screens, cut to size in-house

In order to maintain plug flow in the reactor tube to prevent recirculation and channeling in the catalyst bed and to achieve uniform velocity profile, an inert porous region 3 cm in length was added at both ends of catalyst bed. Silicon carbide (SiC) was used as the inert solid porous material because of its good heat transfer properties. Platinum on ceria (2% Pt) was used as a catalyst for high temperature reforming reactions with its average pellets diameter approximately 0.29mm allowing for a smaller and more simplified reformer design and higher bed conductivity. A small 0.32 cm outer diameter thermocouple centerline hollow tube made of inconel-600 was inserted along the entire length of the bed to facilitate centerline temperature measurements. The SiC and catalyst pellets of same diameter were held in place by using 100 and 60 mesh screens made of

inconel-600 material. Both screens were held in place by trapping them between the 0.95cm reactor tube made of Inconel-625 and Swagelok fittings. All tubing and Swagelok connections were made from Inconel-600 due to high temperatures reached in the reformer. To seal the centerline tube in place, high temperature breakable seals were used to allow for new catalysts to be put into reactor easily and to allow changes to reformer parameters such as catalyst length or reactor diameter. In order to measure the temperature profile along the catalyst bed, wall thermocouples were attached to the outside of the reactor by wrapping them in flexible, high temperature Ni-Chromium wire as shown in Figure 3.4. To increase the contact surface between surface wall and thermocouples, four grooves were milled into the reactor wall with the same radius as that of the thermocouple and are shown in Appendix D.

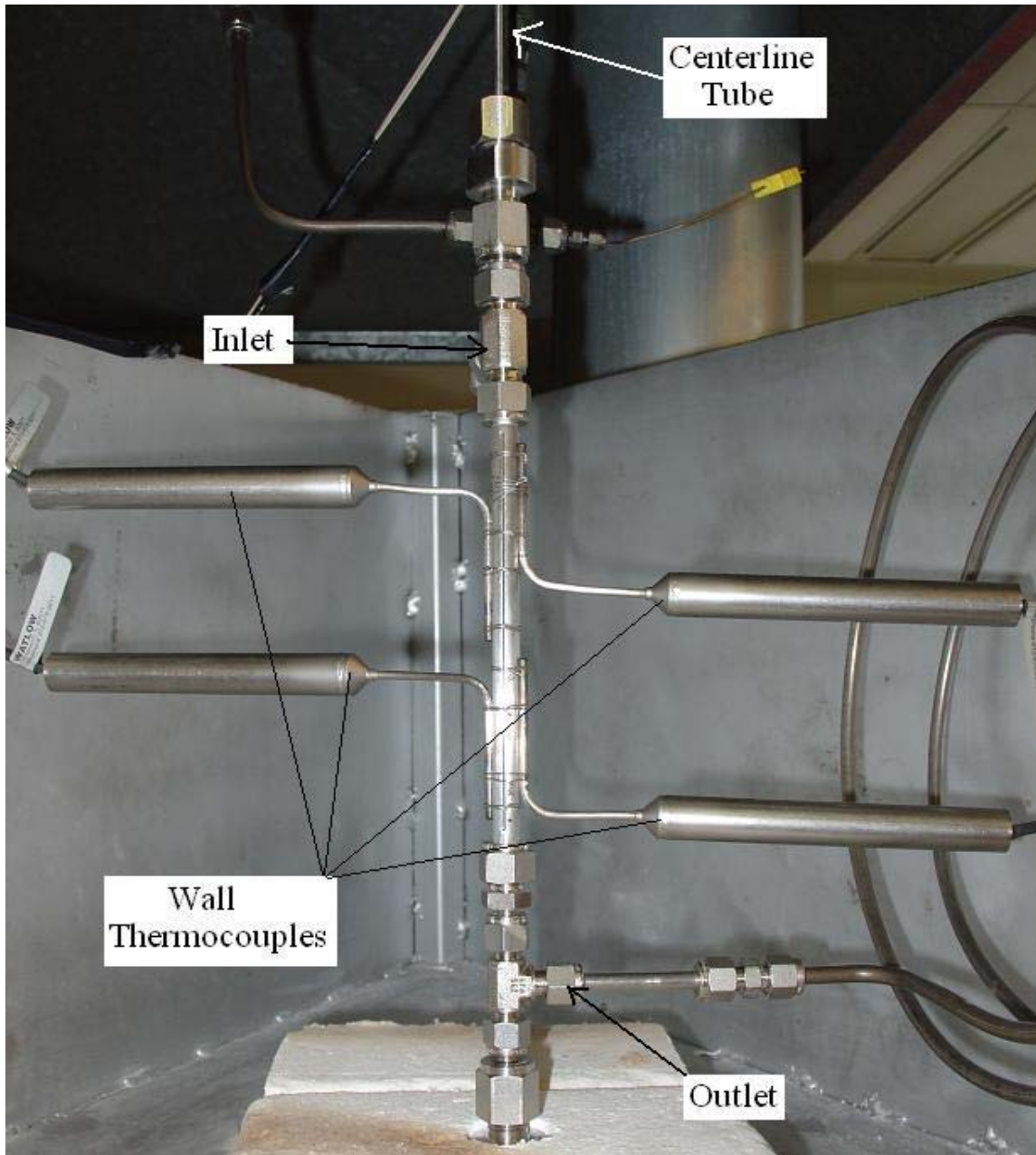


Figure 3.5: Picture of the new autothermal reformer with wall thermocouples. (Shaw, 2008)

### 3.1.2 Second Generation Reformer Results and Problems

A numerical study of the new design of the reformer was undertaken by Sylvestre (2007) and the results were obtained by using a 2-dimensional, axis-symmetric computational fluid dynamics model and Pacheco et al (2003) reaction mechanism. The conservation of mass, momentum, energy and species transport equations in cylindrical coordinates were solved. The assumptions used by Sylvestre (2007) in his numerical model are as follows:

- The flow is axis-symmetric, laminar and steady.
- A pseudo-homogenous flow condition is imposed on the porous regions.
- Bed porosity is constant in the axial and radial bed directions.
- Molecular diffusion is assumed to be negligible relative to the bulk motion/momentum of the fluid.
- Thermal radiation is not considered
- Outer walls of the reformer are heavily insulated and are assumed to be adiabatic.
- Gases are assumed to be incompressible and obey the ideal gas law.
- The effect of viscous heating is negligible.
- Catalyst deactivation has been neglected.
- Kinetic and pressure terms in the energy equations are negligible.
- Production of lighter hydrocarbons such as methane ( $\text{CH}_4$ ) through chemical decomposition has been ignored.

The basis of the Sylvester' model is shown in Figure 3.5.

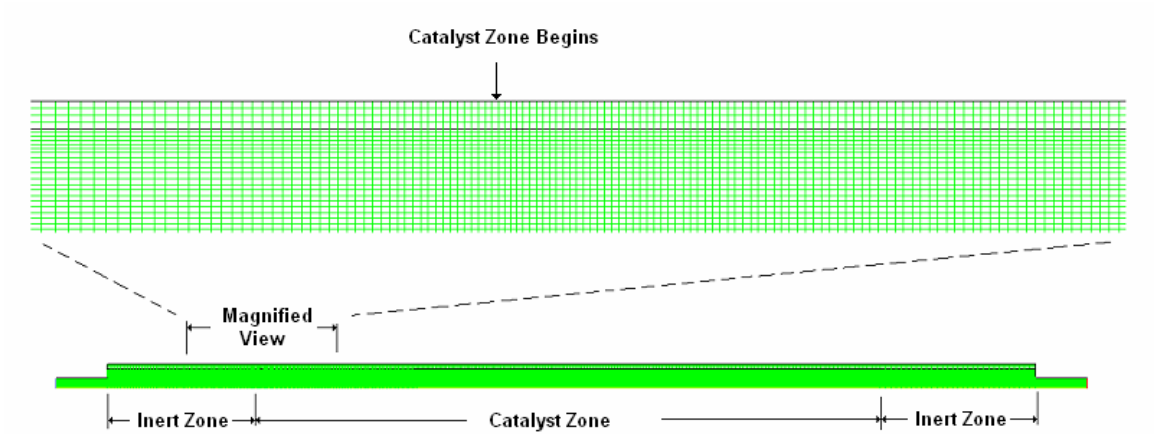


Figure 3.6: A representation of the two-dimensional, axis-symmetric model created by Sylvester (2007)

Sylvestre (2007) investigated the effects of axial heat conduction by varying the wall and catalyst thermal conductivity, inlet flow characteristics, porosity of catalyst and inert porous regions on the outlet species concentrations. He also studied the effects of various air-to-fuel and steam-to-fuel inlet stream ratios, inlet temperatures and effectiveness factor of the reaction mechanism on the performance of the reformer. He calculated fuel conversion percentage and dry hydrogen yield at different gas-hourly-space-velocities. Sylvestre (2007) found from his numerical work that the dry hydrogen yield of the base case was 9.2% and the fuel conversion efficiency 40.6%. It was observed that by increasing the wall and catalyst thermal conductivity, a more evenly distributed temperature distribution could be achieved along the catalyst bed resulting in higher chemical reactivity and thus higher hydrogen yield. It was noted that the variations of the inlet temperatures had a small influence on the performance of the reformer and a  $H_2O/C$  molar ratio of 3.0 and  $O/C$  molar ratio between 1.0 and 1.15 yielded higher fuel

conversion percent and more hydrogen yield. These results also indicated that an increase in the gas-hourly-space-velocity value resulted in a decrease in the performance of the reformer. It was also noted that by improving the effectiveness factor, product species concentrations at outlet of the reformer could be increased. The temperature profiles and molar fractions of product species along the catalyst bed as exhibited in numerical results obtained by Sylvestre (2007) are shown in Figures 3.6 to 3.8.

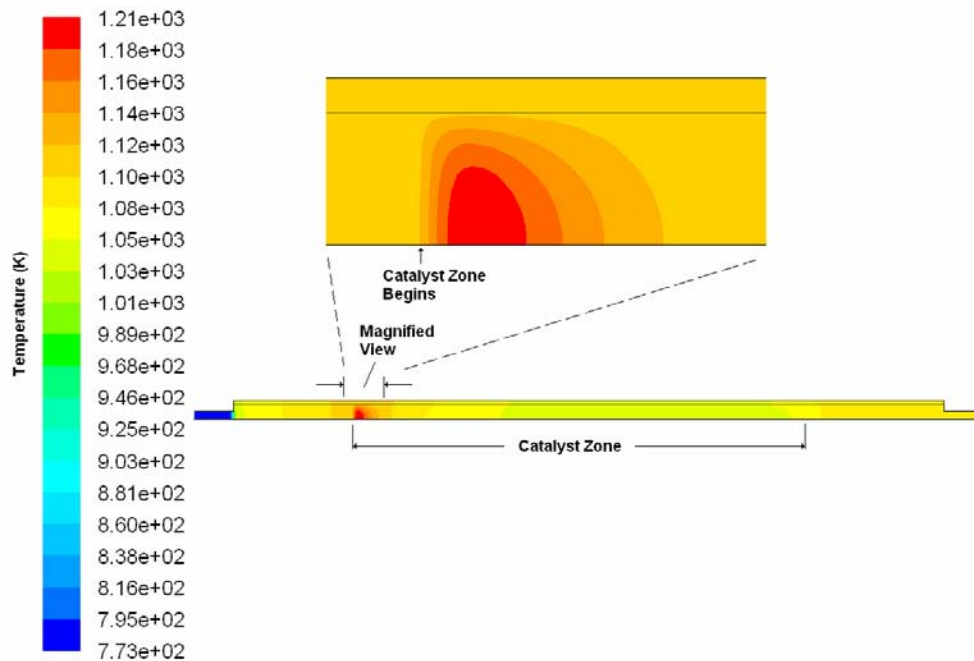


Figure 3.7: Temperature profile for base case (Sylvestre 2007) at GHSV  $30000\text{h}^{-1}$

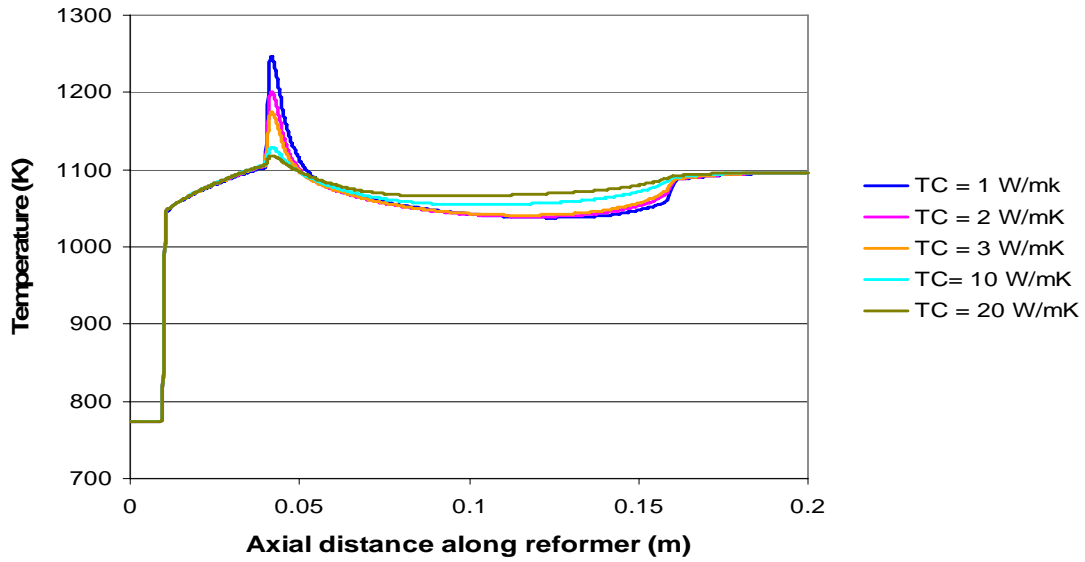


Figure 3.8: Temperature distribution along centreline of reformer for varying catalyst thermal conductivity at GHSV  $30000\text{h}^{-1}$ .

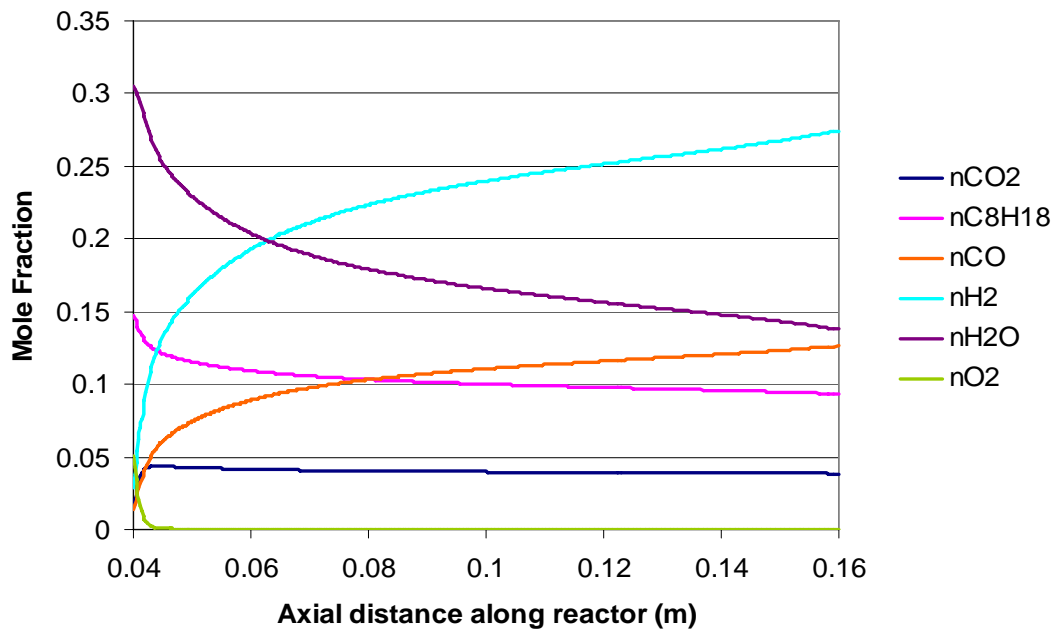


Figure 3.9: Predicted mole fractions along reformer bed for base case at GHSV  $30000\text{h}^{-1}$ .

Shaw (2008) carried out an experimental study of the second prototype of the reformer developed by FCRC group. The approximate positions for the permanent wall thermocouples and centerline temperature reading locations along the ATR bed are shown in Figure 3.9. The results obtained by Shaw (2007) are given in the Table 3.4 and Appendix-C.

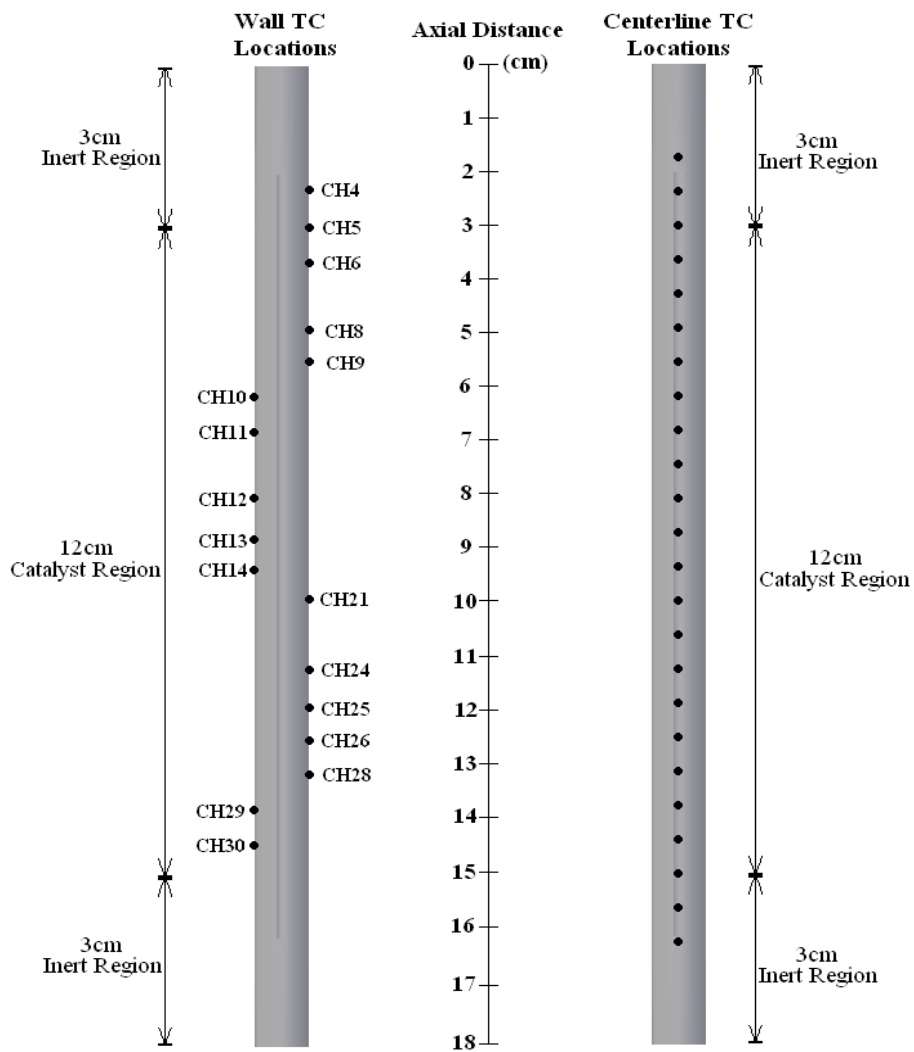


Figure 3.10: Positions for the permanent wall thermocouples and centerline temperature reading locations along the ATR bed.

Table 3.4: Experimental results for the second prototype of an autothermal reformer at  $\text{GHSV } 20000\text{h}^{-1}$  obtained by Shaw (2008)

Trial Number	O/C	H <sub>2</sub> O/C	Iso-octane Flow Rate (ml/min)	Air Flow Rate (SLPM)	H <sub>2</sub> Molar %	CO Molar %	CO <sub>2</sub> Molar %	CH <sub>4</sub> Molar %
1	0.7	1	0.52	1.02	25.2	6.7	12.1	2.5
2	0.7	2	0.38	0.75	27.7	4.6	14.4	2.7
3	0.7	3	0.30	0.60	28.6	2.4	14.9	2.9
4	1	1	0.42	1.16	28.6	7.4	10	1
5	1	2	0.32	0.90	32.1	4.8	12	1.2
6	1	3	0.27	0.74	32.4	2.8	12.9	1.4
7	1.3	1	0.35	1.26	20.4	7.9	9.1	0.1
8	1.3	2	0.28	1.02	22.2	5.1	11.5	0.1
9	1.3	3	0.23	0.85	22	3	12.7	0.3

Temperature measurements performed by Shaw (2008) using the thermocouples at different locations along the outer wall of the reformer and along the centerline thermocouple tube for nine experimental runs and at various O/C and H<sub>2</sub>O/C molar ratios are shown in the Figures 3.10 and 3.11

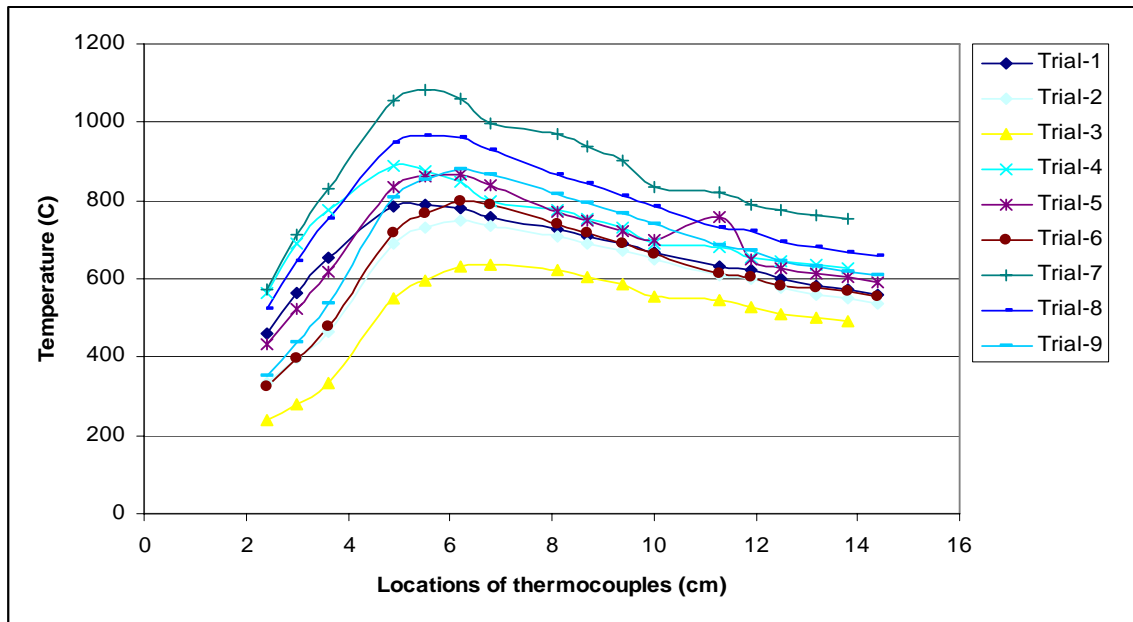


Figure 3.11: Experimental temperature profiles along the wall of the reformer, Shaw (2008).

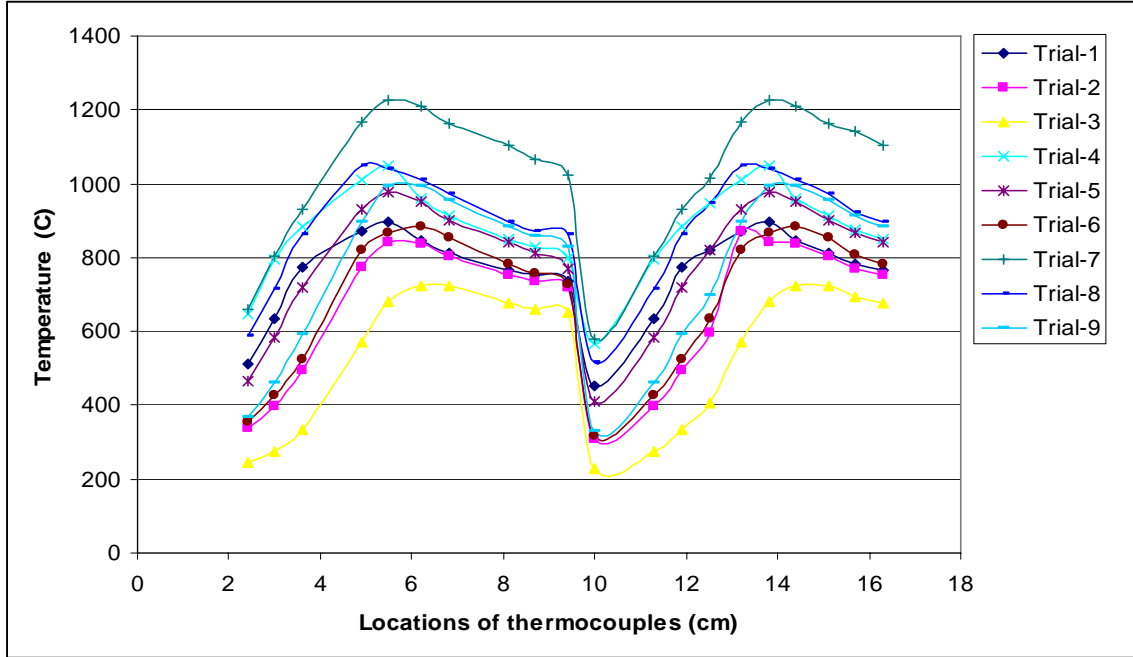


Figure 3.12: Experimental temperature profiles along the wall of the centerline thermocouple tube of the reformer, Shaw (2008).

Shaw (2008) found from his experimental results that the highest molar percent of hydrogen was obtained for an O/C ratio of 1.0 and an H<sub>2</sub>O/C ratio of 2.0. The performance characteristics used for the reformer were the lower heating value, the percent hydrogen yield and the fuel conversion percentage and were found to have maximum values of 46%, 47.6% and 67.7% respectively. The performance characteristics as used by Shaw 2008) are defined in the equations (3.3), (3.4) and (3.5).

The lower heating value percentage:

$$\eta_{LHV} = \frac{\left( n_{H_2} \Delta h_{LHV.H_2} \right)_{out}}{\left( n_{C_8H_{18}} \Delta h_{LHV.C_8H_{18}} \right)_{in}} \times 100\% \quad (3.3)$$

The percent hydrogen yield:

$$\begin{aligned}
 \text{For } H_2O / C = 1 : \quad Y &= \frac{n_{H_2out}}{17 \times n_{C_8H_{18}in}} \times 100\% \\
 \text{For } H_2O / C = 2 \text{ or } 3 : \quad Y &= \frac{n_{H_2out}}{25 \times n_{C_8H_{18}in}} \times 100\% \quad (3.4)
 \end{aligned}$$

The fuel conversion percentage:

$$\begin{aligned}
 x_{fuel} &= 1 - \frac{(n_{C_8H_{18}})_{out}}{(n_{C_8H_{18}})_{in}} \times 100\% \\
 x_{fuel} &= 1 - \frac{(n_{CO} + n_{CO_2} + n_{CH_4})_{out}}{(n_{C_8H_{18}})_{in}} \times 100\% \quad (3.5)
 \end{aligned}$$

It was also observed that the outlet temperatures have a direct relationship to the outlet molar species concentrations. The experimental results were compared with the numerical results obtained by Sylvestre (2007). Certain discrepancies were noted between the model and the experimental data and further improvements in the design of the reformer were recommended for future work.

## Chapter 4

### Computational Fluid Dynamics Modeling

#### 4.1 Introduction

In this chapter, the Computational Fluid Dynamics (CFD) model including the assumptions and the governing equations, on which the generalized model framework for an autothermal reformer is based, is discussed. Subsequently the model is applied to the reformer and the results obtained are validated against experimental data. Finally, the parametric study is carried out to explore the power of the modeling framework to improve the reformer design.

The present numerical study is an extension of the numerical work performed by Sylvestre (2007) for predicting concentration profiles of various species and temperature profiles in the autothermal reformer for fuel processing. This model incorporates Pacheco et al (2003) chemical reaction mechanism to describe the chemical kinetics of an autothermal reforming process for the production of species as a function of concentration and temperature. The modeling framework is built within the computational fluid dynamics software package, FLUENT, environment to take advantage of available numerical schemes and optimization algorithms.

As mentioned earlier iso-octane ( $C_8H_{18}$ ), a surrogate of gasoline, was selected as a fuel for modeling and simulation work. The model described in the subsequent sections can be adapted to different fuels by changing the relevant properties and reaction rates. Once the fuel was selected, the next objective was to study the various parameters that affect the performance of the autothermal reformer. Experimental studies to determine

the effect of such parameters on the reformer design would lead to a large number of requirements in cost and time. As a result, it is more appropriate to model the reformer and perform parametric studies for design improvements. Relatively few models of fuel processing have been reported in the literature and simplifying assumptions about the relevant mass and heat transfer taking place in the reactor are usually made. The objective of the present study is to adopt a generalized reactor model which considers both mass transfer and reaction rate schemes to predict the performance of the reformer when used for APU applications. Present model has the following features:

- Incorporates bulk mass transfer and catalytic surface reactions.
- Involves reaction rate schemes.
- Includes parameters such as the thermal conductivity of reactor wall, of centerline thermocouple tube, of catalyst bed and inert porous material, the catalyst porosity, the main input variables such as oxygen to carbon and steam to carbon ratios, the effectiveness factor of the catalyst bed and the chemical reaction mechanism as described by Pacheco et al (2003).

## 4.2 Mathematical Modeling

In this section, the two-dimensional model that includes both bulk mass transfer and phenomenological reaction rate expressions is described. The principal assumptions and characteristics underlying this model are as follows:

- The flow is axis-symmetric, laminar and steady.
- Bed porosity is constant in the axial and radial directions.
- The outer walls of the reformer are heavily insulated and are assumed to be adiabatic.
- The effect of viscous heating is negligible.
- Catalyst deactivation has been neglected.
- Production of lighter hydrocarbons such as methane ( $\text{CH}_4$ ) through chemical decomposition has been ignored.
- Gases are assumed to be incompressible and obey the ideal gas law.
- Thermal radiation is not considered
- A pseudo-homogenous flow condition is imposed on the porous regions.

A pseudo-homogenous assumption was made to simplify the modeling which means that mass of the catalyst is uniformly distributed throughout the packed bed, chemical reaction occur everywhere along the catalyst bed and flow is then assumed to only have gas phase present. The flow is considered incompressible which means that there is no change in the density with position. Therefore the bulk gas density is assumed to be constant. This is a reasonable assumption because the flow velocity in the reactor is very low with Reynolds number between 70 and 1000, and a pressure drop across the

reactor is approximately 4kpa. The density of individual gases will change as a result of temperature change and are calculated using the ideal gas law to conserve mass and a constant bulk density.

A computational model to predict catalyst deactivation is beyond the scope of this project. Viscous heating effects are considered negligible in comparison to thermal energy generation. Heat transfer due to thermal radiation is not considered to occur inside the bed or to the ambient. Inside the porous region of the reformer, the presence of the inert and catalytically active pellets reduce the radiation mean beam length and, as a result radiative heat transfer is negligible in comparison to the conductive and convective heat transfer occurring inside the reactor. Production of lighter hydrocarbons such as methane ( $\text{CH}_4$ ) through chemical decomposition has been ignored because the reaction mechanism as described by Pacheco et al. (2003) used in the present and previous numerical studies does not include the formation of methane.

### 4.2.1 Conservation Equations

Two-dimensional conservation of mass, momentum, energy and gas phase species equations in cylindrical coordinates in the  $x$  and  $r$  directions are given below:

The conservation of mass equation is:

$$\frac{\partial}{\partial x}(\rho u) + \frac{\partial}{\partial r}(\rho v) + \frac{\rho v}{r} = 0 \quad (4.1)$$

The equation (4.1) is an out growth of applying conservation of mass to the differential  $dx.dr.1$  control volume. The left-hand side represents the net outflow (outflow minus inflow) of mass in the  $x$ -and  $r$ -directions, the sum of which must be zero for steady flow.

The conservation of momentum equations are:

$$\begin{aligned} \frac{1}{r} \frac{\partial}{\partial x}(\rho uu) + \frac{1}{r} \frac{\partial}{\partial r}(r \rho uv) = & -\frac{\partial p}{\partial x} + \frac{1}{r} \frac{\partial}{\partial x} \left[ r \mu \left( 2 \frac{\partial u}{\partial x} - \frac{2}{3} \left( \frac{\partial u}{\partial x} + \frac{\partial v}{\partial r} + \frac{v}{r} \right) \right) \right] \\ & + \frac{1}{r} \frac{\partial}{\partial r} \left[ r \mu \left( \frac{\partial u}{\partial r} + \frac{\partial v}{\partial x} \right) \right] + F_x \end{aligned} \quad (4.2)$$

$$\begin{aligned} \frac{1}{r} \frac{\partial}{\partial x}(\rho uv) + \frac{1}{r} \frac{\partial}{\partial r}(r \rho vv) = & -\frac{\partial p}{\partial r} + \frac{1}{r} \frac{\partial}{\partial r} \left[ r \mu \left( 2 \frac{\partial v}{\partial x} - \frac{2}{3} \left( \frac{\partial u}{\partial x} + \frac{\partial v}{\partial r} + \frac{v}{r} \right) \right) \right] \\ & + \frac{1}{r} \frac{\partial}{\partial x} \left[ r \mu \left( \frac{\partial u}{\partial r} + \frac{\partial v}{\partial x} \right) \right] - 2\mu \frac{u}{r^2} + \frac{2}{3} \frac{\mu}{r} \left( \frac{\partial u}{\partial x} + \frac{\partial v}{\partial r} + \frac{v}{r} \right) + F_r \end{aligned} \quad (4.3)$$

The equations (4.2) and (4.3) result from application of Newton's second law of motion in the x and r directions to the differential control volume in the fluid. The left-hand side represents the net rate at which momentum leaves the control volume due to fluid motion across its boundaries. The first term on the right-hand side represents the net pressure force, whereas second and third terms represent the net force due to viscous shear stresses.

The terms  $F_x$  and  $F_r$  are momentum sink terms and represent the effects of pressure decrease due to the flow through a porous media. These terms are derived from the well known Ergun's law that describes the pressure decrease per unit length in the porous media (Ergun, 1952) as seen by the relation (4.4).

$$\frac{\Delta P}{L} = \frac{150(1-\phi)^2}{\phi^3 d_p^2} \mu u + \frac{3.5(1-\phi)}{\phi^3 d_p} u^2 \quad (4.4)$$

Where  $d_p$  represents particle size, and  $\phi$  represents porosity. Assuming a porosity value equal to 0.6 as stated by the catalyst manufacturer and average catalyst particle size equal to 0.3mm, the terms  $F_x$  and  $F_r$  can be written as follows:

$$F_x = 1.234 \times 10^9 \mu u + 21605 u^2 \quad (4.5)$$

$$F_r = 1.234 \times 10^9 \mu v + 21605 v^2 \quad (4.6)$$

The energy equation for steady state conditions and with negligible kinetic and potential energy changes and viscous heating effects can be written as follows:

$$u \frac{\partial T}{\partial x} + v \frac{\partial T}{\partial r} = \left( \frac{k}{\rho c_p} \right) \left[ \frac{\partial^2 T}{\partial x^2} + \frac{1}{r} \frac{\partial}{\partial r} \left( r \frac{\partial T}{\partial r} \right) \right] + \dot{q} \quad (4.7)$$

Where  $T$  is temperature,  $c_p$  is the specific heat at constant pressure,  $k$  is thermal conductivity. The equation (4.7) results from application of conservation of energy to a differential control volume in the flowing fluid. Terms on the left-hand side account for the net rate at which thermal energy leaves the control volume due to bulk fluid motion (advection). The first term on the right hand side accounts for the net inflow of thermal energy due to conduction. The second term on the right hand side is the net volumetric rate of thermal energy generation from chemical reactions.

In the inlet and outlet regions, only the gas phase is present and the overall thermal conductivity is calculated by a mass-weighted-mixing law utilizing the known thermal conductivities and masses of the species in the mixture. For the inert and catalytically active porous regions, an effective thermal conductivity,  $k_{eff}$ , can be defined to account for both the fluid and solid conductivities. This is obtained by multiplying the porosity value with the fluid thermal conductivity and adding it to the remaining solid volume multiplied by the solid thermal conductivity as given by the equation 4.9. This method is used by the CFD code of FLUENT by default.

$$k_{eff} = \varphi k_f + (1 - \varphi) k_s \quad (4.9)$$

The species transport equation used in the present model is:

$$u \frac{\partial C_i}{\partial x} + v \frac{\partial C_i}{\partial r} = D \left( \frac{\partial^2 C_i}{\partial x^2} + \frac{1}{r} \frac{\partial}{\partial r} \left( \frac{\partial C_i}{\partial r} \right) \right) + r_i \quad (4.10)$$

Where  $C_i$  is the molar concentration of species  $i$ ,  $D$  is the diffusion coefficient, and  $r_i$  is the molar rate of production or consumption of species  $i$ . The terms on the left of the equation (4.10) represents the bulk mass transfer while the first term on the right

represents the net inflow due to diffusion. The rate of production or consumption of each species  $r_i$  is calculated using Pacheco et al (2003) equations which describe the complex set of chemical reactions required to describe the reforming process of iso-octane. These equations are described in the next section.

An effective species diffusion term, denoted by  $D_{eff}$ , is derived from the dimensionless number called the Peclet number (Pe) which is described by the equation 4.11:

$$P_e = \frac{VL_d}{\alpha} \quad (4.11)$$

Where  $V$  = velocity

$L_d$  = characteristic length

$\alpha$  = thermal diffusivity

For the present case, the equation (4.11) is modified as follows:

$$D_{eff} = \frac{U_s d_p}{P_e} \quad (4.12)$$

Where the thermal diffusivity term  $\alpha$  is replaced with the effective diffusion term,  $D_{eff}$ , and the characteristic length  $L_d$  is replaced with the catalyst particle diameter,  $d_p$ . The physical velocity in the porous media is calculated using the equation for the superficial velocity (4.13).

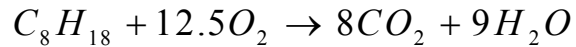
$$U_s = \phi \sqrt{u^2 - v^2} \quad (4.13)$$

The Peclet Number for mass transfer in packed beds is reported to be between 4 and 12. A mean value of 8 has been used for the present work. The resulting effective species diffusion term,  $D_{eff}$ , is applied to all of the chemical species present in the reformer. Through the appearance of  $u$  and  $v$  in equations (4.7) and (4.10), the temperature and species concentration are coupled to the velocity field.

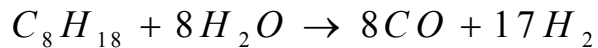
#### 4.2.2 Chemical Reactions Mechanism and Kinetic Expressions

Pacheco et al. (2003) proposed the reaction mechanism and kinetic expressions for the reforming of iso-octane based on the studies of methane steam reforming conducted by Xu and Froment (1989) and of methane partial oxidation by Jin et al.(2000). The reaction mechanism described by Pacheco et al (2003) consists of the following five reactions:

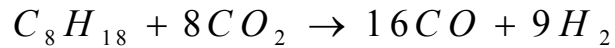
i) Oxidation:



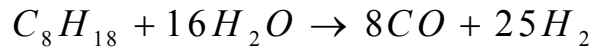
ii) Steam Reforming A:



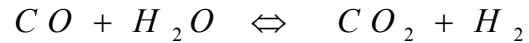
iii) Carbon Dioxide Reforming:



iv) Steam Reforming B:



v) Water-Gas-Shift:



For these reactions a set of rate expressions for the change in concentration of iso-octane was described by Pacheco et al (2003) as follows:

$$r_{oxidation} = K_{r1} P_{iC_8H_{18}} P_{O_2}$$

$$r_{steam\ reforming\ A} = \frac{K_{r2}}{P_{H_2}^{2.5}} \left( P_{iC_8H_{18}} P_{H_2O}^2 - \frac{P_{H_2}^3 P_{CO_2}}{K_2 \left( 1 + K_{CO} P_{CO} + K_{H_2} P_{H_2} + K_{iC_8H_{18}} P_{iC_8H_{18}} + K_{H_2O} (P_{CO} / P_{H_2}) \right)^2} \right)$$

$$r_{carbon\ reforming} = K_{r3} P_{iC_8H_{18}} P_{CO_2} \left( 1 - \frac{P_{CO}^2 P_{H_2}^2}{K_3 P_{iC_8H_{18}} P_{CO_2}} \right)$$

$$r_{steam\ reforming\ B} = \frac{K_{r4}}{P_{H_2}^{3.5}} \left( P_{iC_8H_{18}} P_{H_2O}^2 - \frac{P_{H_2}^4 P_{CO_2}}{K_4 \left( 1 + K_{CO} P_{CO} + K_{H_2} P_{H_2} + K_{iC_8H_{18}} P_{iC_8H_{18}} + K_{H_2O} (P_{CO} / P_{H_2}) \right)^2} \right)$$

$$r_{water-gas-shift} = \frac{K_{r5}}{P_{H_2}} \left( P_{CO} P_{H_2O} - \frac{P_{H_2} P_{CO_2}}{K_5 \left( 1 + K_{CO} P_{CO} + K_{H_2} P_{H_2} + K_{iC_8H_{18}} P_{iC_8H_{18}} + K_{H_2O} (P_{CO} / P_{H_2}) \right)^2} \right)$$

Where

$K_{r,n}$  = the reaction rate constant of reaction  $n$

$P_i$  = the partial pressure of species  $i$

$K_n$  = the equilibrium constant of reaction  $n$

$K_i$  = the adsorption constant for species  $i$

The rate of production of any species depends upon the reaction mechanism that applies to the reforming of iso-octane under consideration. The general form to describe a reaction rate is given by equation (4.14)

$$-r_i = k_r \cdot \theta \quad (4.14)$$

The reaction rate equation is a function of both temperature and concentration.  $k_r$  is the specific reaction rate constant which is dependent on temperature and  $\theta$  is a concentration function based on species concentrations or inherently on their partial pressure. The value  $k_r$  is expressed by an Arrhenius type function given by equation (4.15)

$$k_r = A e^{-\frac{E}{RT}} \quad (4.15)$$

For any Arrhenius type reaction there will be an associated pre-exponential factor  $A$ , and an activation energy  $E$  that can be determined from experimental results. The concentration function  $\theta$  needs to be defined for each of the reactions involved in the chemical process. Pacheco et al (2003) found through experimental work that six parameters have a significant effect on the performance of the reformer, those being the five pre-exponential factors for the Arrhenius rate constants  $k_1$  through  $k_5$  and the dissociative adsorption constant for water vapor at the catalyst active sites,  $k_{H_2O}$ . The values of these parameters determined from the experimental results obtained by Pacheco et al (2003) are listed in Table 4.1

Table 4.1: Values of the pre-exponential factors determined from experimental data and the kinetic parameters used from the literature (Pacheco, 2003)

Parameters	Pre-exponential Factor, A	Activation Energy, E(KJ/mol)	Enthalpy of Adsorption (KJ/mol)
$K_1(\text{mol}/(\text{g}_{cat} \text{ s bar}^2))$	$2.85 \times 10^8$	166.0	--
$K_2(\text{mol bar}^{0.5}/(\text{g}_{cat} \text{ s}))$	$2.61 \times 10^9$	240.1	--
$K_3(\text{mol}/(\text{g}_{cat} \text{ s bar}^2))$	$2.78 \times 10^{-5}$	23.7	--
$K_4(\text{mol bar}^{0.5}/(\text{g}_{cat} \text{ s}))$	$1.52 \times 10^7$	240.9	--
$K_5(\text{mol}/(\text{g}_{cat} \text{ s bar}))$	$1.55 \times 10^1$	67.1	--
$K_{H_2O}(\text{dimensionless})$	$1.57 \times 10^4$	--	88.7

### 4.2.3 Effectiveness Factor

The effectiveness factor has been popularly used for estimating the efficiency of catalytic particles when a catalytic reactor is designed. Nevertheless, in packed or fluidized beds, catalytic particles are subject to the interactions from their immediate neighbors. The main consideration in a catalytic design is to maximize the number of available catalyst sites for reactions to occur. Catalyst particles are porous in nature, allowing gases to access all active sites, a phenomenon known as intra-particle diffusion. The rate of reaction depends upon the ability of reactant gases to reach the active catalyst sites. The term effectiveness factor,  $\eta$ , is defined to account for the diffusion limitations and is the ratio of actual overall reaction rate and the rate existing if the entire catalyst surface is exposed to the bulk concentration. It can be evaluated for each reaction in a chemical reaction mechanism but it requires knowledge of a number of parameters and information about the catalyst pellet which is difficult to measure and estimate.

Pacheco et al (2003) conducted a study on a platinum/ceria-oxide based catalyst and reported that the effectiveness factors for the reactions ranged from 0.0003 to 0.002 at the start of the catalyst bed. In the present simulations, different values of effectiveness factor in the range 0.001 to 0.01 were adopted and results obtained were compared with the experimental data. It was found that 0.0032 is the suitable value for the effectiveness factor to be used for the reformer under study to match with experimental results.

### **4.3 Computational Fluid Dynamics (CFD) Modeling**

Computational fluid dynamics is the analysis of systems involving fluid flow, heat transfer and associated phenomenon such as chemical reactions by means of computer-based simulation. The technique is very powerful and spans a wide range of industrial and non-industrial application areas. Computational fluid dynamics modeling was utilized in the present project to implement the mathematical model described above for the purpose of modeling and simulation of transport phenomena, heat transfer and chemical reactions within the autothermal reformer. To achieve this goal, the CFD software package, FLUENT 6.2.16 was used. The program GAMBIT 2.2.30 (pre-processor) was utilized to prepare the geometry of the reformer and to define the domain of discretized cells to create mesh of the geometry. A 2-dimensional, axis-symmetric, steady state flow was assumed to exist in the reformer and the presence of the Inconel mesh screens to contain the inert and catalyst pellets were ignored.

#### **4.3.1 Grid Generation**

For the grid generation, a structured mesh was created to account for the expected high gradients in species concentrations and temperatures in the start of catalyst bed due to high reaction rates and almost zero towards the end of the catalyst region. Boundary conditions were then applied to the geometry to characterize inlet and outlet regions, the presence of walls, the centerline thermocouple tube, the axis of symmetry, the fluid and solid zones, etc. The mesh that was created as a result of these considerations is shown in Figure 4.1.

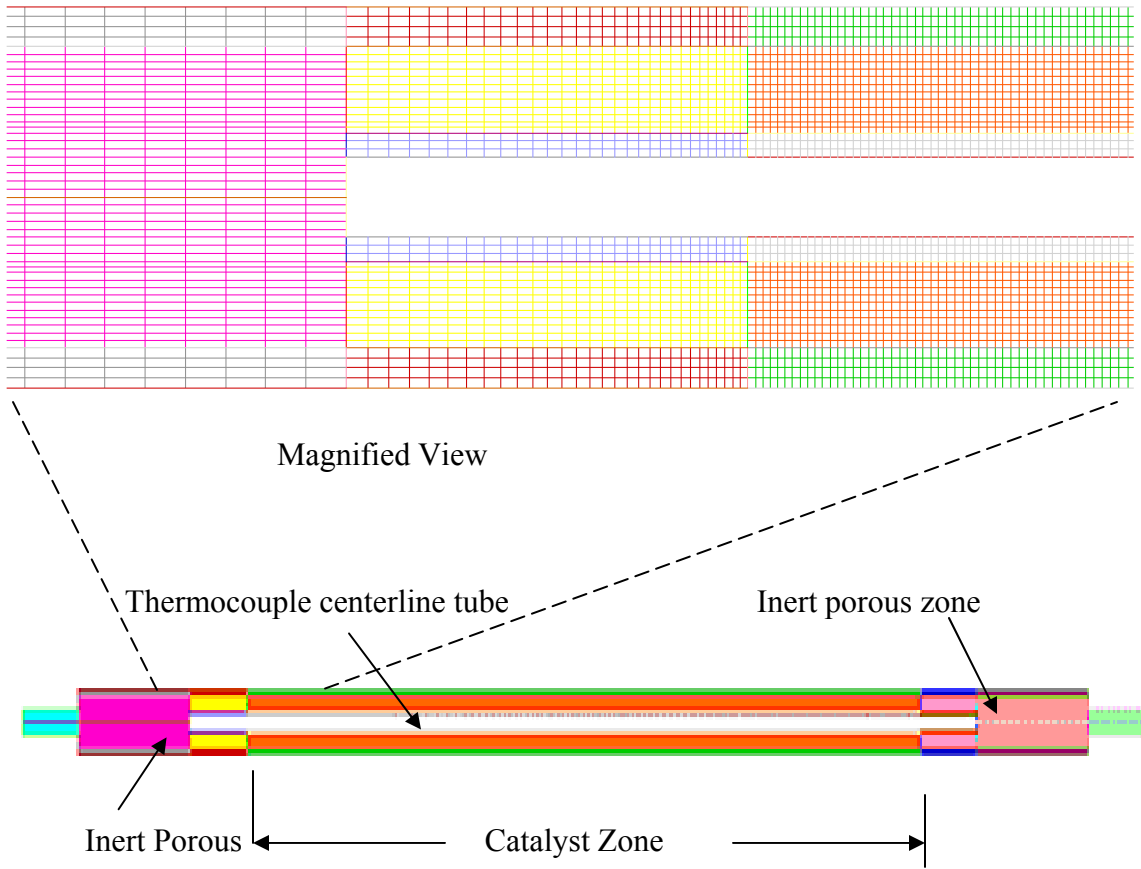


Figure 4.1: Magnified view of mesh topology for the inlet region of the geometry.

### 4.3.2 Solution Procedures

FLUENT software applies a finite volume based numerical scheme. One benefit of the finite volume method is that it allows an unstructured mesh to be used due to its integral formulation approach. It divides the domain of the problem to be solved numerically into discrete control volumes over which the transport equations of mass, momentum, energy and molecular species in conservative form are solved. Around each node of the geometry, a control volume is defined in such a way that no one should be overlapped. The governing equations are solved over each control volume giving a set of algebraic equations involving the values of all the dependent unknown flow variables such as the velocity, pressure, temperature and any other scalar variables at specific grid points.

FLUENT adopts an interpolation scheme between neighboring grid points to calculate a cell face value on the plane where the control volumes meet each other. Numerical solution techniques use many interpolation schemes for determining the cell face values. FLUENT uses a central-differencing scheme to calculate the diffusion flux terms and other available schemes such as upwind-differencing scheme to solve the convective flux terms in the governing equations depending upon the nature of the problem. In the central-differencing scheme, the cell face value of the flow variable is determined from the centroid values of neighbouring cells upwind and downwind of the face, while in upwind-differencing scheme, the cell face values are calculated from grid points upwind of the face only. The process of assigning the value of the upwind grid point to the cell face value is called first order-upwind-differencing scheme, while the second-order-upwind-differencing scheme accounts for a flow variable gradient over a

given displacement and adds this value to the grid point before calculating the cell face value. In order to improve accuracy usually a second-order-differencing scheme is preferred. Sylvestre (2007) found that the second-order-upwind-differencing scheme is more appropriate for the present problem, so the same was adopted for the present numerical work. The first iteration begins with the initial guess to the solution and results of this iteration are compared with the previous values to the next set of values for the next iteration. This process is continued until the solution is converged according to the residual factor defined.

### 4.3.3 Solution Algorithm

The outline of the general solution algorithm adopted in FLUENT software is as shown in the Figure 4.2. The solution algorithm is selected depending upon the nature of problem to be solved. In segregated solver, the governing equations are solved in a sequential manner while in coupled solver, the equations are solved simultaneously.

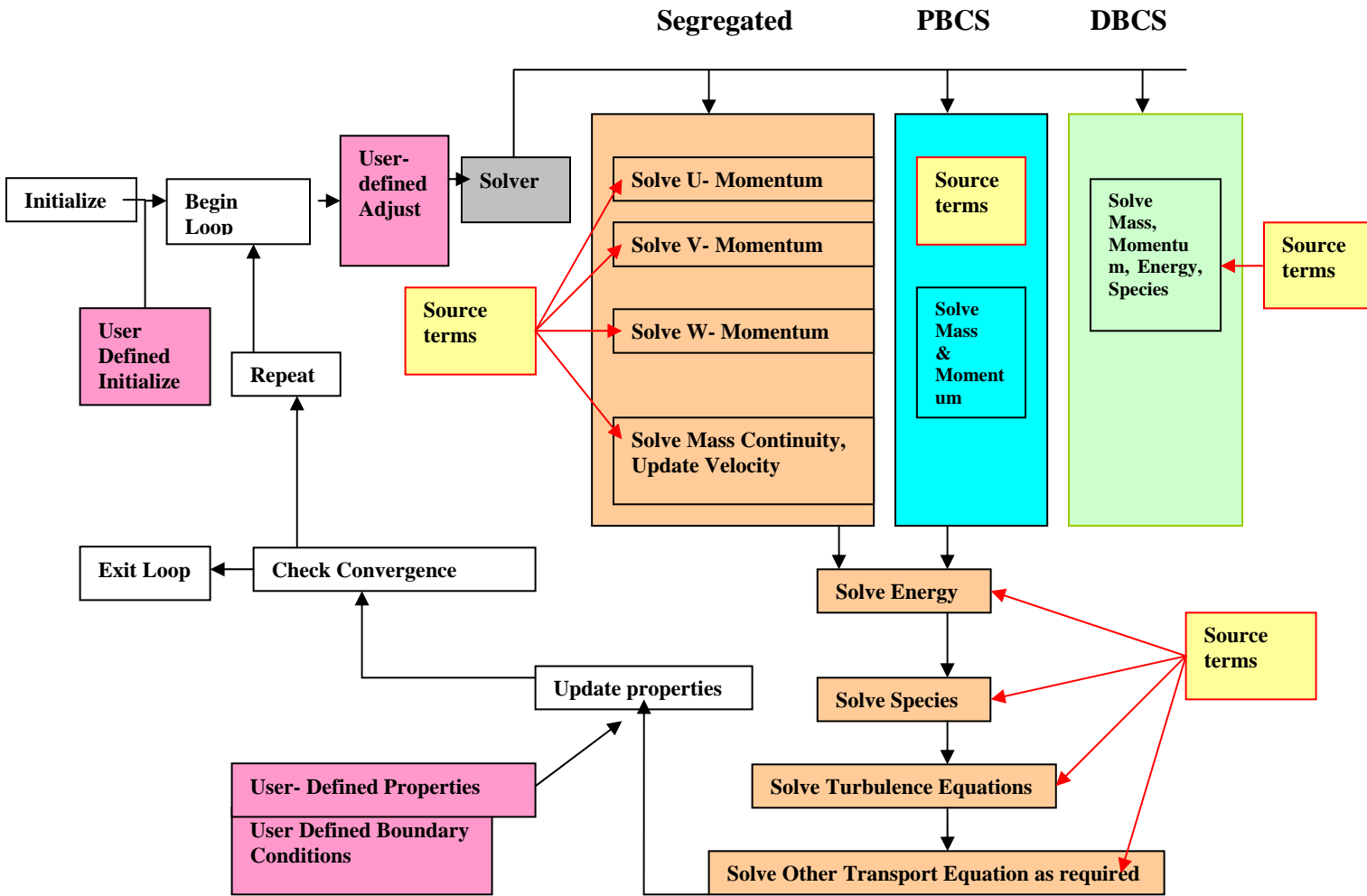


Figure 4.2: Outline of the general solution algorithm adopted in FLUENT software (Fluent).

The pressure-based segregated solution scheme was utilized for the present problem. An overview of the segregated solver approach is shown in Figure 4.3 and the sequence of each iterative step followed is as under:

- All fluid properties such as density, specific heat, viscosity, etc., are updated
- Each individual momentum equation is solved using the previously updated pressure and fluxes.
- A pressure correction is obtained using the previously updated velocity and mass fluxes.
- Mass fluxes, velocity and pressure are updated using the obtained pressure correction.
- Conservation equations are solved for energy and species terms.
- Source terms are obtained for the generation/depletion of energy and species due to chemical reactions.
- Convergence is checked to determine if more iteration required.

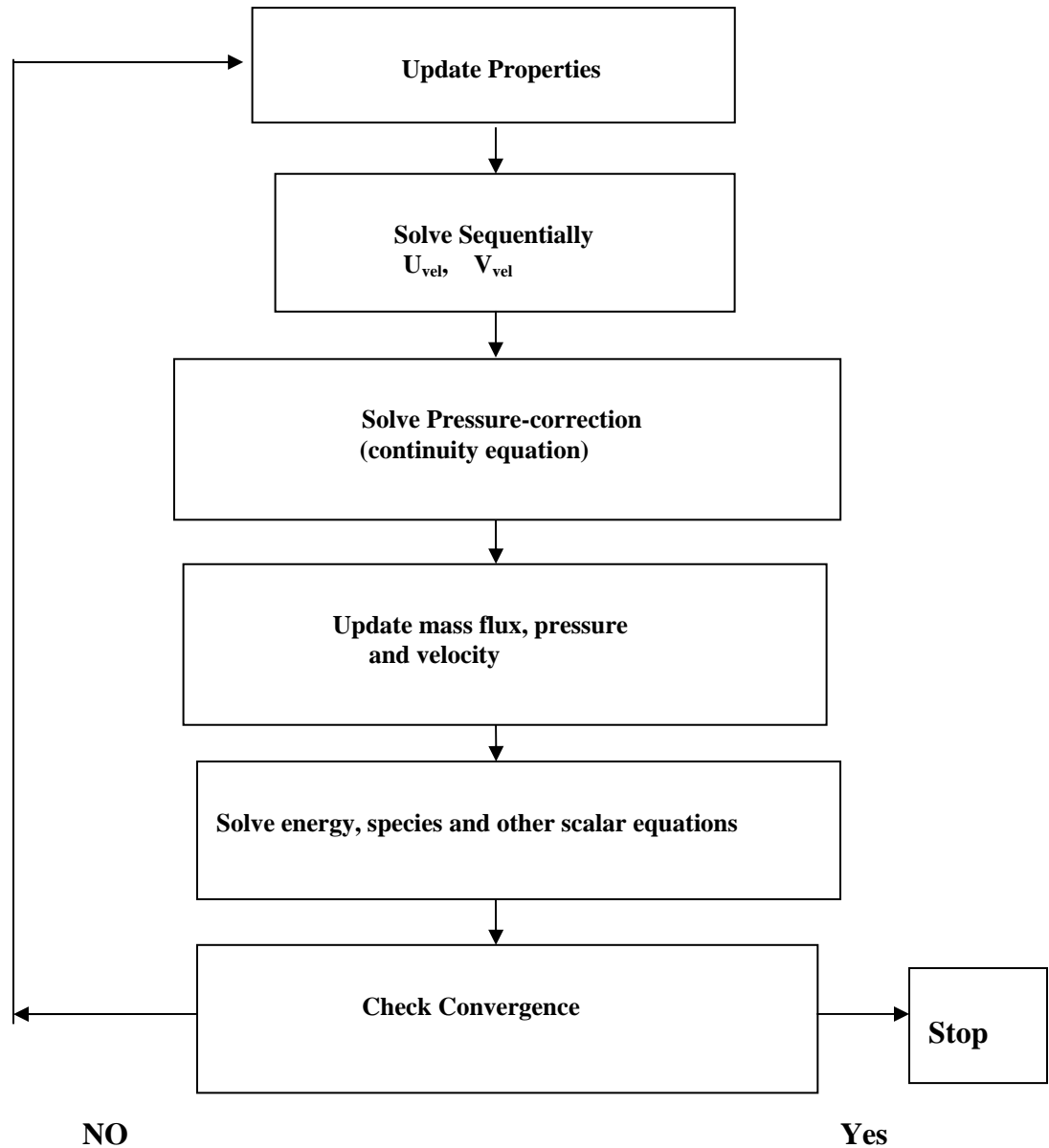


Figure 4.3: Overview of Segregated Solver Approach

The momentum equations are solved by fixing the pressure values. The iterative process returns the pressure values between cells along the reformer. To rectify the error, FLUENT uses a pressure correction interpolation scheme. Two interpolation schemes are incorporated in FLUENT, known as Standard and PRESTO (PREssure Staggering Option). For porous media problems, the PRESTO is always recommended to determine

the average pressure drop (Fluent, 2005). The SIMPLE pressure-velocity solution algorithm is utilized in FLUENT to provide relationship between the pressure and velocity for correction to conserve mass and momentum. Once the solution is obtained, the property dependent variables are updated. To stabilize the solution, relaxation factors are used in the iterative process to dampen the magnitude of change of field variables. The equation (4.16) is used to define a new variable by adding the previous value of the field variable with the change in the field variable multiplied by a dampening factor.

$$\phi_{updated} = \phi_{old} + \beta \Delta \phi \quad (4.16)$$

Where

$\beta$  = Relaxation factor

$\Delta \phi$  = change in field variable

Relaxations factors normally in the range 0.05 to 0.9 are used.

In order to implement the complex chemical reactions mechanism developed by Paceco et al (2003) into “user-defined functions” of FLUENT, a computer code was developed by Sylvestre (2007) in C++ and compiled by FLUENT to become accessible as a user-defined function and is listed in Appendix-B. The same was utilized in present simulations but the value of the effectiveness factor was changed to 0.0032 to match the numerical results with experimental data. To start the iterative process of the solution algorithm, an initial guess to the solution is provided for the flow variables in the domain. In the present case temperature, velocity and species concentrations were given initial values. The summary of the user input necessary to define the CFD model as outlined by Sylvester (2007) is shown in appendix-A.

## Chapter 5

### Results and Discussion

#### 5.1 Introduction

The results obtained using the CFD model of an autothermal reformer are discussed in this chapter. The FLUENT built-in post processor was utilized to calculate mass-averaged conditions at the reformer outlet and to draw graphs and contour plots illustrating the results. The numerical predictions so determined were validated by comparing with the previous numerical and experimental work completed on the reformer by Sylvestre (2007) and Shaw (2008) as well as against other relevant results published in the literature. After the analysis and evaluation of all the results, certain improvements in the design of the reformer have been suggested.

The present study was completed in three phases. In the first phase of the project, the results reported by Sylvester (2007) were analyzed in terms of the assumptions made in obtaining the numerical solution and based on this evaluation attention was focused to improve the design of the reformer. Initially it was assumed for simplicity reasons that there was no centerline thermocouple tube inside the autothermal reformer. Simulations were performed and determined the effect of varying the thermal conductivity of the reformer wall and catalyst bed, of varying the inlet conditions and of the effectiveness factor of the chemical reaction mechanism on the reactor performance.

In the second phase, a case was selected to represent the autothermal reformer with a centerline thermocouple tube as used in an experimental study undertaken by Shaw (2008) and simulations were performed using the experimental operating conditions. The experimental work completed by shaw (2008) determined the operating inlet temperature, the gas-hourly space velocity, and the inlet species concentration ratios. This was regarded as the base case and the results obtained using various values of thermal conductivity, inlet conditions and effectiveness factor. The base case parameters were selected as follows:

- The inlet temperature was 773K or 500°C.
- The GHSV was 20,000h<sup>-1</sup> at the entrance to the catalyst bed.
- The inert porous zones and catalyst zones had local porosity of 0.6
- The inlet molar ratios of oxygen and iso-octane (O<sub>2</sub>:C<sub>8</sub>H<sub>18</sub>) were 0.7, 1.0, and 1.3.
- The inlet molar ratios of steam and iso-octane (H<sub>2</sub>O:C<sub>8</sub>H<sub>18</sub>) were 1.0, 2.0 and 3.0.
- The inlet air stream consisted of 21% oxygen and 79% nitrogen on a molar basis.
- Different values of effectiveness factor in the range 0.001 to 0.1 (as reported in the literature for the entire catalyst bed) were used to try to match with the experimental results obtained by Shaw (2008).

In the third phase of the project, attention was focused for possible improvements in the reformer design to reduce temperature gradients in the catalyst bed of the reformer and to achieve the maximum hydrogen output. For this purpose, a series of simulations were performed with varying reactor dimensions (length and diameter) using solid rods of different dimensions and at different locations inside the reactor and under various operating conditions.

All three phases of the work are explained in more detail in the subsequent sections.

## **5.2 Numerical Simulations Using Sylvestre (2007) Operating Conditions (Phase-1)**

In the first phase, the numerical simulations were performed using the operating conditions as described by Sylvestre (2007) in his numerical work. A solution was obtained for these conditions. This solution gave the molar concentration of product species, the temperatures profiles, the conversion rate of fuel and the dry hydrogen yield (without steam and un-reacted fuel). The conversion rate of fuel was determined using equation (5.1) as described by Sylvestre, 2007.

$$\% \text{ conversion } C_8H_{18} = 1 - \frac{(mol / sec)_{C_8H_{18}}^{outlet}}{(mol / sec)_{C_8H_{18}}^{inlet}} \times 100 \quad (5.1)$$

The conversion rate of fuel is expressed as the ratio of the fuel molar flow rate at the inlet minus the ratio of the fuel molar flow at the outlet to the molar flow rate at the inlet

expressed as percentage. The hydrogen yield was calculated using the equation (5.2), (Sylvestre, 2007).

$$\text{dry-hydrogen-yield} = \frac{(\text{mol/sec}_{H_2})_{\text{outlet}} / [1 - (\text{mol/sec}_{H_2O})_{\text{outlet}} - (\text{mole/sec}_{C_8H_{18}})_{\text{outlet}}]}{25.(\text{mole/sec}_{C_8H_{18}})_{\text{inlet}}} \times 100 \quad (5.2)$$

The hydrogen yield is defined as the ratio of the molar flow rate of hydrogen at the outlet in the absence of steam and fuel over the maximum hydrogen molar rate possible if one mole of fuel is converted.

The autothermal reformer was simulated without centerline thermocouple tube as shown in Figure 5.1.

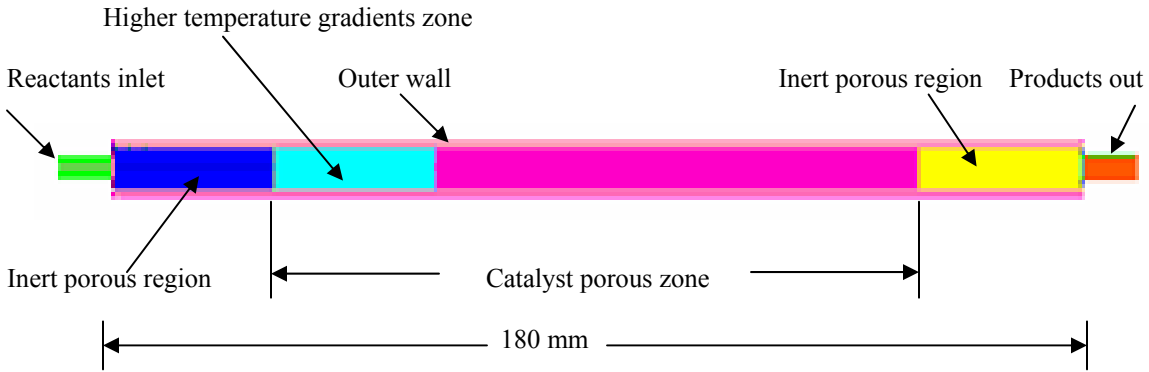


Figure 5.1: Compact autothermal reformer, Length = 180 mm, Outer radius = 4.75 mm, Inner radius = 3.75mm

A grid sensitivity analysis was carried out which indicated that the selected grid size gave results that were grid independent. The grid independence tests involving several trials with different axial and radial grid spacing were performed for each case to determine when an effectively grid independent results can be obtained. The species outlet mole

fractions for each trial as well as the maximum reactor temperature obtained in these trials are given below in Table 5.1.

Table 5.1: Results of mesh sensitivity analysis

Trial	No of Cells	Mole fraction of species at outlet				Max Temp (K)
		H <sub>2</sub>	CO	CO <sub>2</sub>	C <sub>8</sub> H <sub>18</sub>	
1	7966	0.260	0.119	0.0432	0.096	1170
2	9723	0.270	0.124	0.0434	0.0941	1180
3	12850	0.271	0.124	0.0434	0.0939	1180
4	16346	0.272	0.125	0.0434	0.0937	1180

By examining the changes in outlet species concentrations, it was found that a grid with 12850 cells was accurate enough to account for the simulation of the reformer without any noticeable change in the solution with an increased number of cells.

A summary of the numerical results obtained is given in Table 5.2 and Figures 5.2 to 5.4

Table 5.2: Summary of the numerical results obtained by using operating conditions as described by Sylvestre (2007)

Parameters	Results from present study	Sylvestre's Results
Conversion of fuel (%)	39.80	40.5
Dry hydrogen yield (%)	9.08	8.9
Mole fraction of C <sub>8</sub> H <sub>18</sub> at outlet	0.0939	0.0932
Mole fraction of O <sub>2</sub> at outlet	$2.08 \times 10^{-10}$	$1.4 \times 10^{-10}$
Mole fraction of CO <sub>2</sub> at outlet	0.0434	0.0437
Mole fraction of CO at outlet	0.124	0.1264
Mole fraction of N <sub>2</sub> at outlet	0.331	0.3296
Mole fraction of H <sub>2</sub> at outlet	0.271	0.2746
Mole fraction of H <sub>2</sub> O at outlet	0.141	0.1375
Pressure drop along bed (kpa)	3.5	3.5

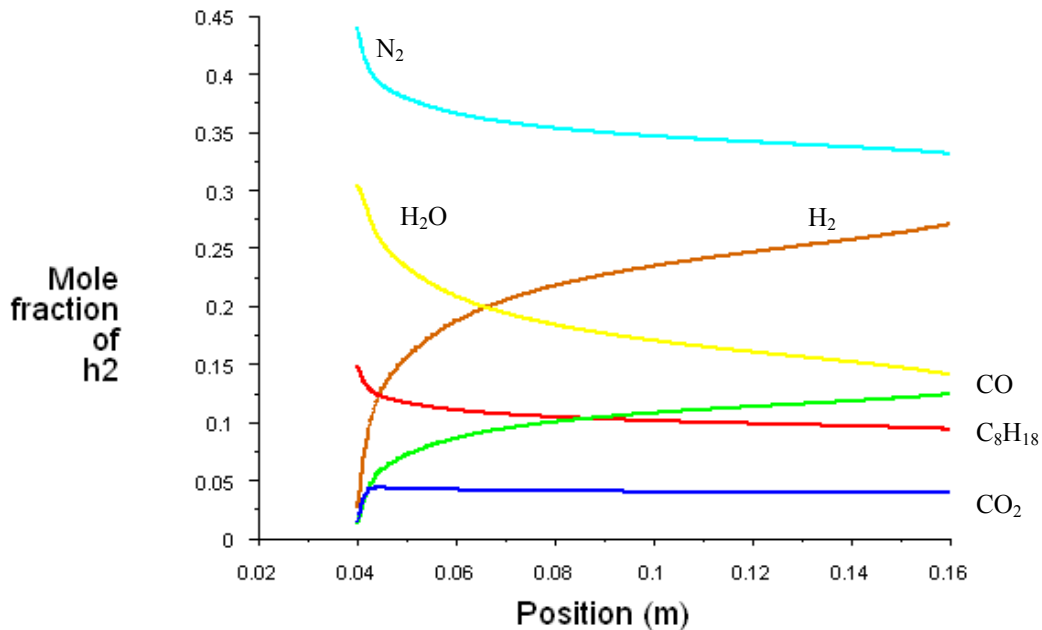


Figure 5.2: Profiles of mole fractions of product species in the catalyst bed of the reformer ( $GHSV = 30,000 h^{-1}$ ,  $H_2O:C = 2$ ,  $O:C = 1$ , Effectiveness factor = 0.001)

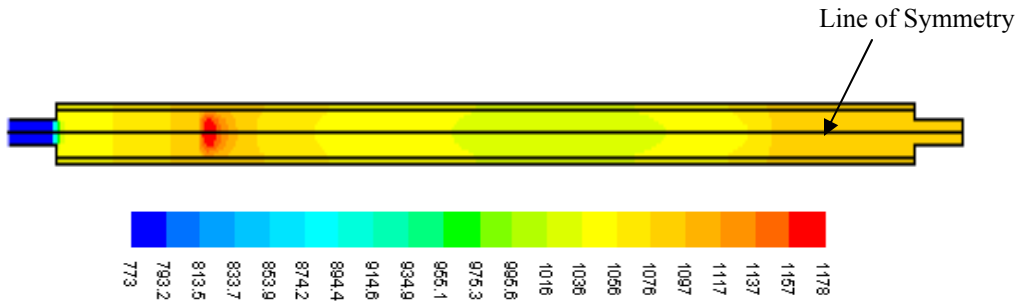


Figure 5.3: Temperature distribution within the reformer.  
 (GHSV =  $30,000\text{h}^{-1}$ ,  $\text{H}_2\text{O}:\text{C} = 2$ ,  $\text{O}:\text{C} = 1$ , Effectiveness factor = 0.001)

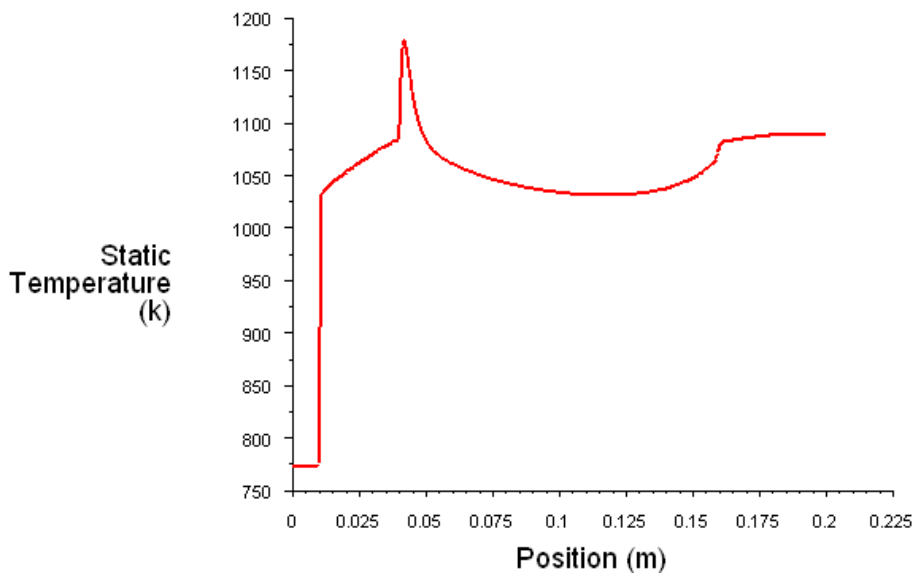


Figure 5.4: Temperature profile along the centreline of the reformer.

The results so obtained were compared with Sylvestre's (2007) numerical results as shown in Table 5.2 and, except for the molar fraction of  $\text{O}_2$  at outlet, were found to be in good agreement. The mole fraction of  $\text{N}_2$  decreases along the catalyst bed even the  $\text{N}_2$  is not participating in the chemical reactions as is seen in the Figure 5.2. This is attributed to the fact that as the reforming process proceeds along the catalyst bed of the reformer, the total number of moles of products increases as a result the mole fraction of  $\text{N}_2$  decreases.

From previous numerical and experimental results reported by Sylvestre (2007) and Shaw (2008) described in chapter three and present results shown above in Figures 5.3 and 5.4, it is seen that the temperature profile along the centreline of the reformer is not uniform and large temperature gradients exist within the catalyst bed which can affect the life of the catalyst bed and the overall performance of the reformer. At the start of the catalyst bed the temperature increases very sharply due to the heat released by the exothermic partial oxidation reaction and then decreases towards the centre of the bed because of heat absorbed by the endothermic steam reforming reaction. After the centre of the catalyst bed, the temperature again starts rising towards the outlet of the bed causing non-uniform temperature gradients. One of the aims of the design of the reformer was to have heat conducted along the outer tube from the region near the inlet where the high exothermic partial oxidation reaction was occurring to the lower temperature region near the exit where the endothermic steam reforming reaction was occurring. An examination of the numerical results indicated that a relatively small amount of heat was in fact being conducted down the tube and that the relatively high thermal conductivity inert porous media at the reformer exit was transferring heat away from the steam reforming reaction section to the exit section. For this reason a modified reformer design was considered. It was found that the inert porous material, Silicon Carbide (SiC), 30mm in length used before and after the catalyst bed to achieve plug flow, has much higher thermal conductivity value than that of the catalyst bed being equal to 200 W/m.K while that of the catalyst bed material is 2 W/m.K. Therefore more simulations were performed by using the thermal conductivity value equal to 2 W/m.K for both the catalyst bed and

the inert porous material at outlet of the bed to see its effect on the reformer performance and the temperature profiles. The results so obtained are shown in Figures 5.5 and 5.6.

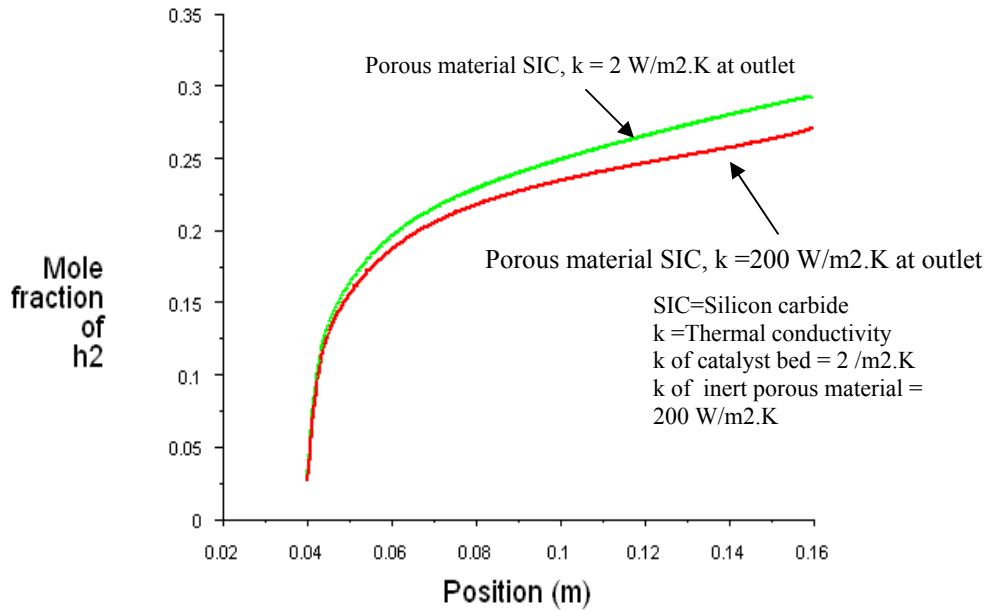


Figure 5.5: Profiles of mole fractions of Hydrogen in the catalyst bed (GHSV = 30,000 h<sup>-1</sup>, S:C = 1, O:C = 1.3, Effectiveness factor =0.001)

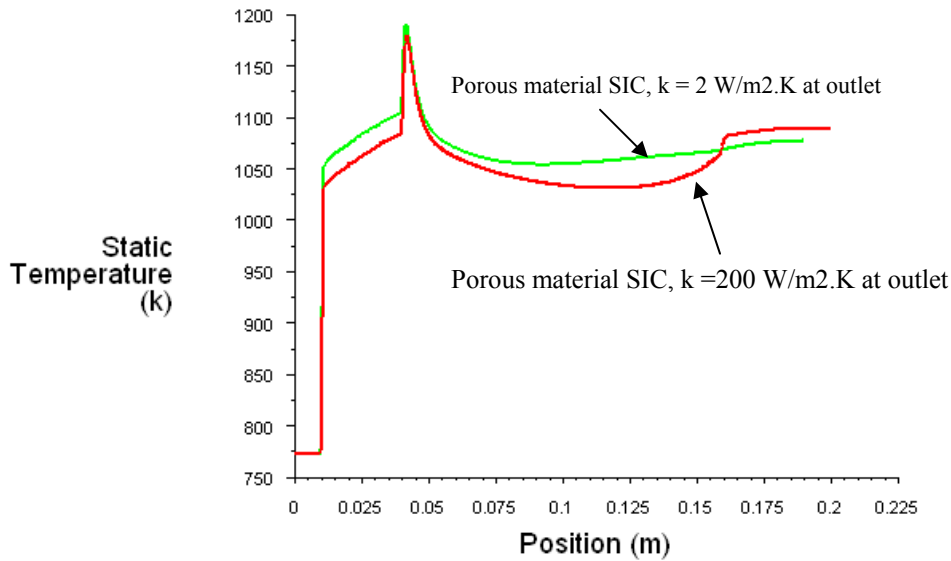


Figure 5.6: Centerline temperatures profiles along the length of the reformer

From the results obtained, it will be seen that by reducing the value of thermal conductivity of outlet inert porous material, the mole fraction of hydrogen is increased from 0.27 to 0.30 and that the centerline temperature profile becomes more uniform.

The effect of outlet inert porous region on the performance of the autothermal reformer was further investigated by removing it from the reformer, thus reducing the length of the reformer by 30mm and the reformer was re-simulated without outlet porous region as shown in Figure 5.7.

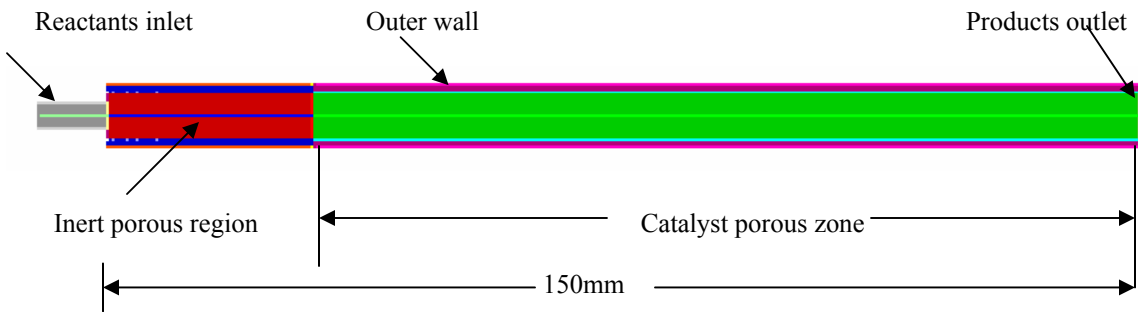


Figure 5.7: Reformer simulated without inert porous region at the outlet of the catalyst bed, Length = 150 mm, Radius = 4.75 mm

Numerical results obtained for the reformer simulated without the inert porous region at the outlet of the catalyst bed are shown in Figures 5.8 to 5.10

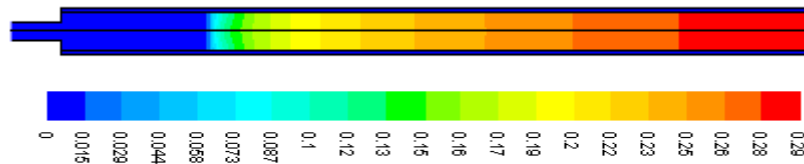


Figure 5.8: Mole fraction of hydrogen contours in the catalyst bed of the reformer without central thermocouple tube and inert porous region at outlet of the reformer (GHSV = 30,000 h<sup>-1</sup>, S:C=2,O:C =1, Effectiveness factor = 0.001)

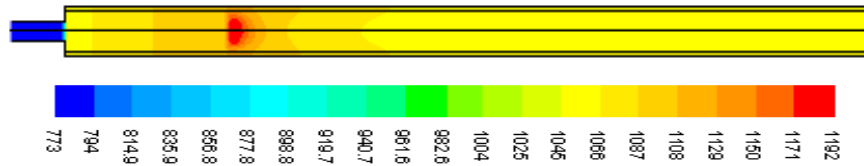


Figure 5.9: Temperature distribution within the reformer

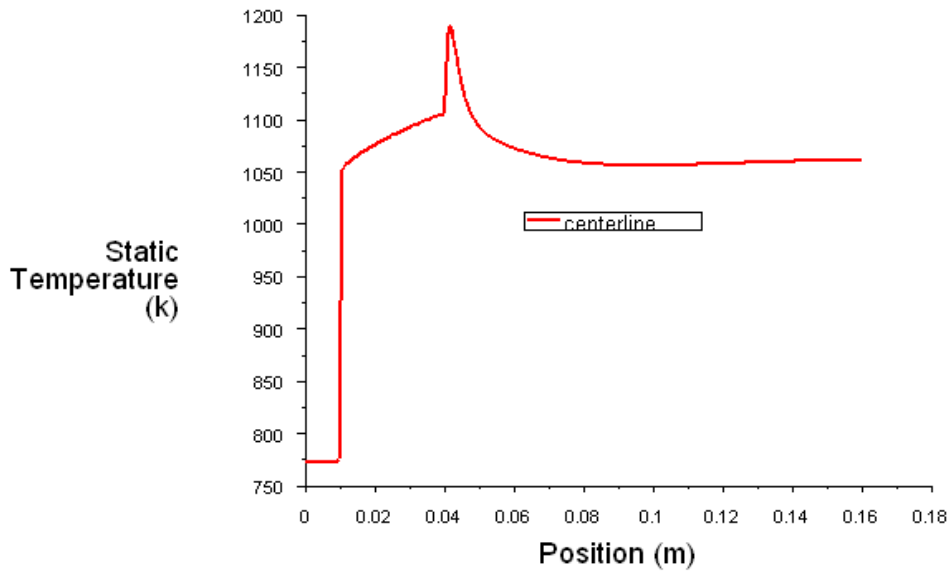


Figure 5.10: Temperature profile along the centreline of the reformer.

From these results, it can be seen that removal of inert porous region at the outlet of the catalyst bed has a positive effect on the performance of the reformer. Its removal helps to give a smooth temperature profile within the catalyst bed with the advantage that the size of the reactor can be reduced by 30mm along with a small increase in the hydrogen output. It was also found that with an increase of thermal conductivity of reformer wall material, the output of hydrogen could be further increased.

### 5.3 Numerical Simulations Using Shaw (2008) Experimental Operating Conditions (Phase-II)

The autothermal reformer with centerline thermocouple tube as used in experimental study completed by Shaw (2008) was simulated as shown in Figure 5.11 and numerical results were obtained using experiment operating conditions.

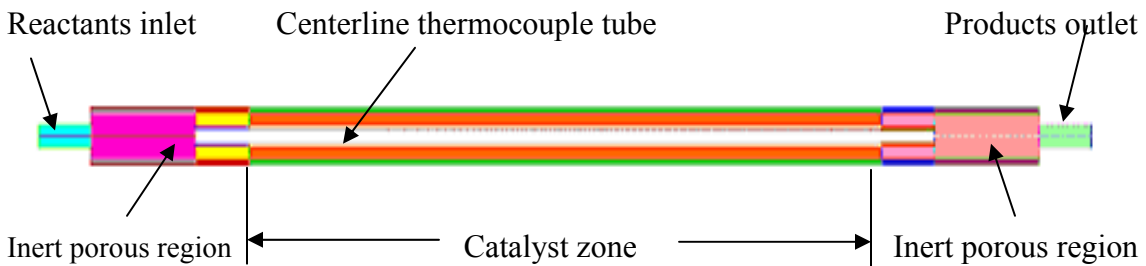


Figure 5.11: Reformer used in experimental study by Shaw (2008), length = 180 mm, outer radius = 4.75 mm, with hollow central tube of length =140mm and outer radius = 1.6mm and inner radius =1.05mm.

Two main output variables namely output reformate composition and temperature profiles were used to analyze the results. The temperature profiles are discussed along with the effect that the input variables had on the lowest and the peak temperatures. This is followed by an analysis of the reformate composition and the overall reactor performance. The results are given in the following subsections.

#### 5.3.1 Effect of effectiveness factor upon the performance of the reactor

To determine the influence of the effectiveness factor on the performance of the reactor, results were obtained for various values of the effectiveness factor ranging from 0.001 to 0.01 and compared with experimental data as shown in Table 5.3. It was found that an effectiveness factor value of 0.0032 gives numerical predictions close to the

experimental results as shown in Figure 5.12. Hence in subsequent simulations, a value of 0.0032 for the effectiveness factor was used in obtaining numerical solutions.

Table 5.3: Selected results from the model of the ATR at inlet temperature = 500°C, thermal conductivity (TC) of tube and wall = 17.5 ~31.5 W/m.K and GHSV =20000h<sup>-1</sup>

Effectiveness Factor	O/C Molar Ratio	H <sub>2</sub> O/C Molar Ratio	Experimental H <sub>2</sub> Molar Ratio%	Numerical H <sub>2</sub> Molar Ratio%
0	1	2	32.1	
0.001	1	2	32.1	29.1
0.003	1	2	32.1	31.2
0.006	1	2	32.1	34.5
0.01	1	2	32.1	36.2

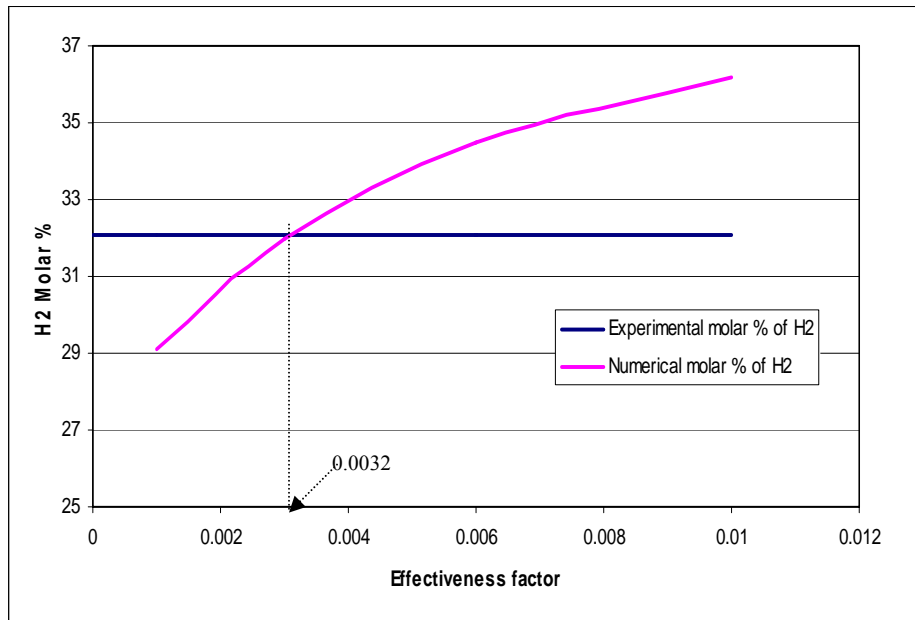


Figure 5.12: Comparison of numerical molar percentage of hydrogen at different values of effectiveness factors with experimental molar percentage of hydrogen determined by Shaw (2008).

### 5.3.2 Results Obtained with Using Experimental Conditions

A series of simulations were performed using the operating conditions used by Shaw (2008). A summary of the numerical results so obtained is given in Tables 5.4 and 5.5 and Figures 5.13 to 5.18.

Table 5.4: Numerical results from the model of the ATR at inlet temperature = 500°C, k of tube and wall = 17.5 ~31.5 W/m.K and GHSV =20000h<sup>-1</sup> and effectiveness factor = 0.0032

Comparable Experimental Number	O/C Ratio	H <sub>2</sub> O/C Ratio	H <sub>2</sub> Molar %	CO Molar %	CO <sub>2</sub> Molar %
1	0.7	1.0	27.8	12.0	4.28
2	0.7	2.0	27.8	12.6	3.58
3	0.7	3.0	28.4	12.0	3.48
4	1.0	1.0	30.2	14.5	4.88
5	1.0	2.0	32.6	14.8	4.22
6	1.0	3.0	31.3	13.6	3.79
7	1.3	1.0	29.0	14.2	5.31
8	1.3	2.0	32.0	14.8	4.74
9	1.3	3.0	29.5	13.0	4.20

Table 5.5: Peak and Lowest temperatures in the catalyst bed

Comparable Experimental Number	O/C Ratio	H <sub>2</sub> O/C Ratio	Peak Temperature (K)	Lowest Temperature (K)
1	0.7	1.0	1070	1010
2	0.7	2.0	1070	1010
3	0.7	3.0	1040	975
4	1.0	1.0	1080	1015
5	1.0	2.0	1070	1005
6	1.0	3.0	1060	995
7	1.3	1.0	1100	1025
8	1.3	2.0	1090	1015
9	1.3	3.0	1060	980

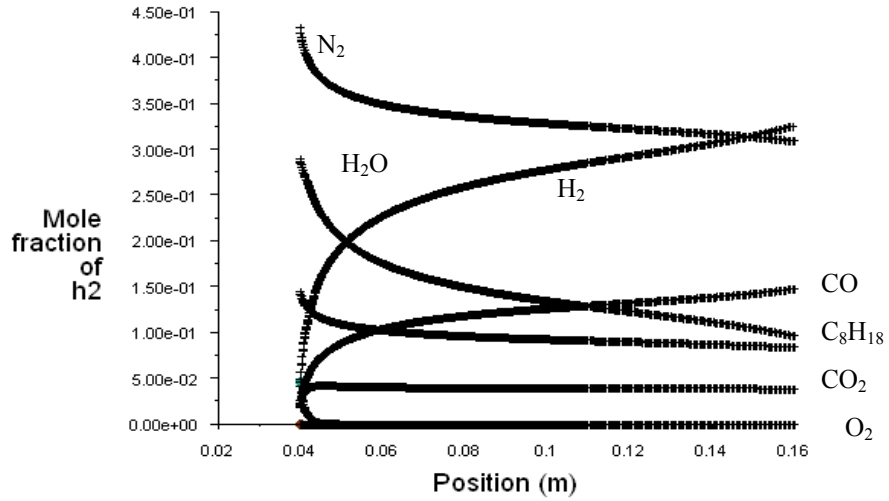


Figure 5.13: Profiles of mole fractions of reformate composition in the catalyst bed, at GHSV = 20,000 h<sup>-1</sup>, S:C=2, O:C=1, effectiveness factor = 0.0032

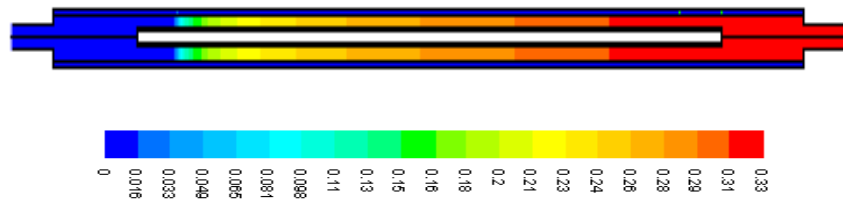


Figure 5.14: Mole fractions of hydrogen distribution in the catalyst bed of the reformer (GHSV=20,000 h<sup>-1</sup>, S:C = 2, O:C = 1).

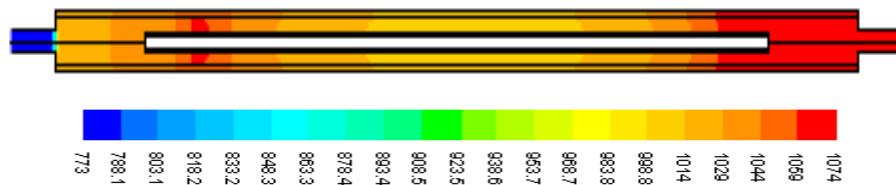


Figure 5.15: Temperature distribution along the axial length of the reformer (GHSV=20,000 h<sup>-1</sup>, S:C = 2, O:C = 1).

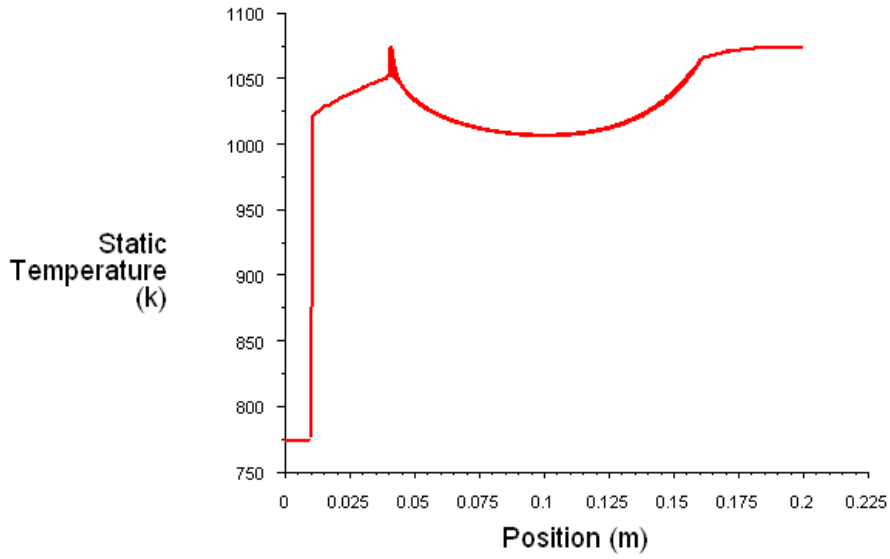


Figure 5.16: Temperature profile along the centreline of the reformer. (GHSV =20,000 h<sup>-1</sup>, S:C = 2, O:C = 1)

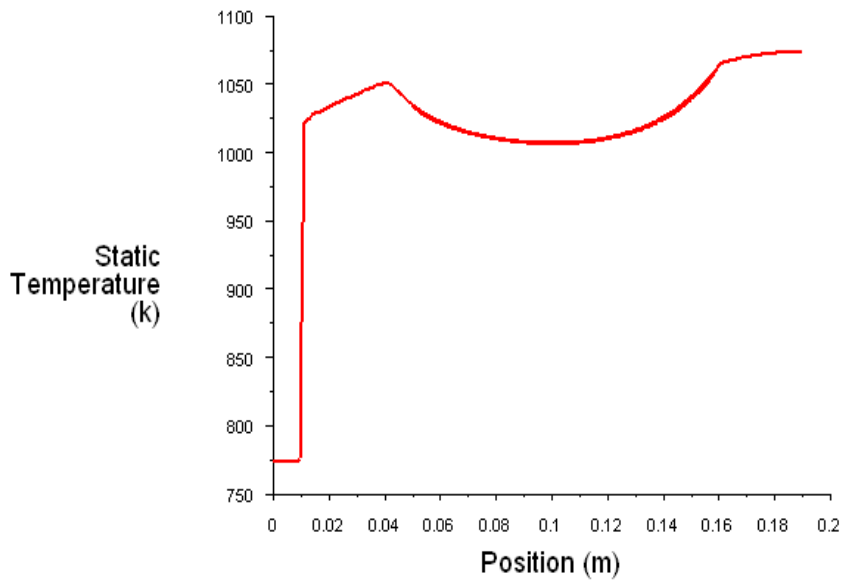


Figure 5.17: Temperature profile along the outer wall of the reformer (GHSV =20,000 h<sup>-1</sup>, S:C = 2, O:C = 1) .

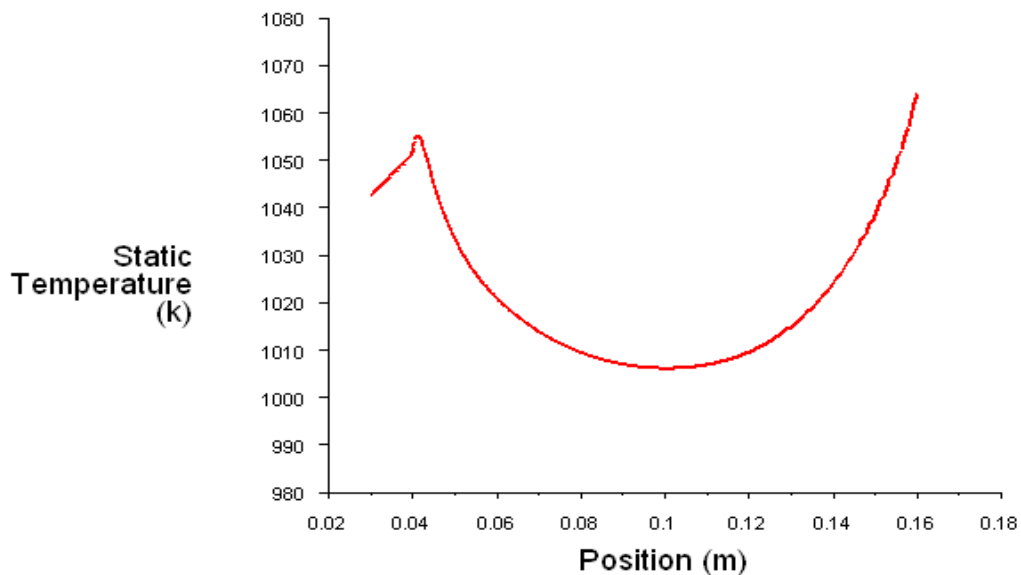


Figure 5.18: Temperatures profile along the thermocouple tube wall of the reformer (GHSV=20,000 h<sup>-1</sup>, S:C = 2, O:C = 1)

The results obtained in the present simulations shown in Tables 5.4 and 5.5 and Figures 5.13 to 5.18 are further discussed in the following sections.

### 5.3.3 Effect of Main Input Variables on Results

In this section, the effects of the main input variables on the dry outlet composition of the reformer are discussed. The results indicate that the composition of the products depends upon the O/C and H<sub>2</sub>O/C molar ratios of the reactants. Seven different gaseous species in the product stream were calculated, these being C<sub>8</sub>H<sub>18</sub> (unburned), H<sub>2</sub>O, H<sub>2</sub>, CO, CO<sub>2</sub>, O<sub>2</sub> and N<sub>2</sub>. The relationship between the dry outlet composition and the O/C ratio is shown in Figure 5.19, while its relationship to the H<sub>2</sub>O/C ratio is shown in Figure 5.20. Each O/C ratio was used with three different H<sub>2</sub>O/C

ratios. In order to show the effect of O/C ratio on the concentration of outlet species, the results for these three H<sub>2</sub>O/C ratios were averaged.

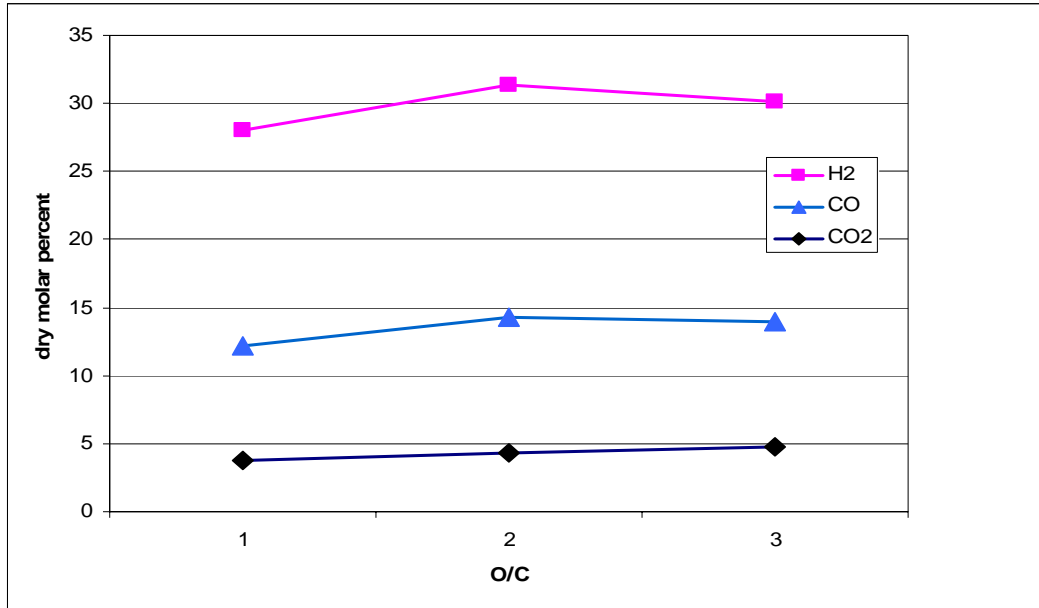


Figure 5.19: Average dry molar percentage of outlet gases vs. O/C obtained in present numerical results

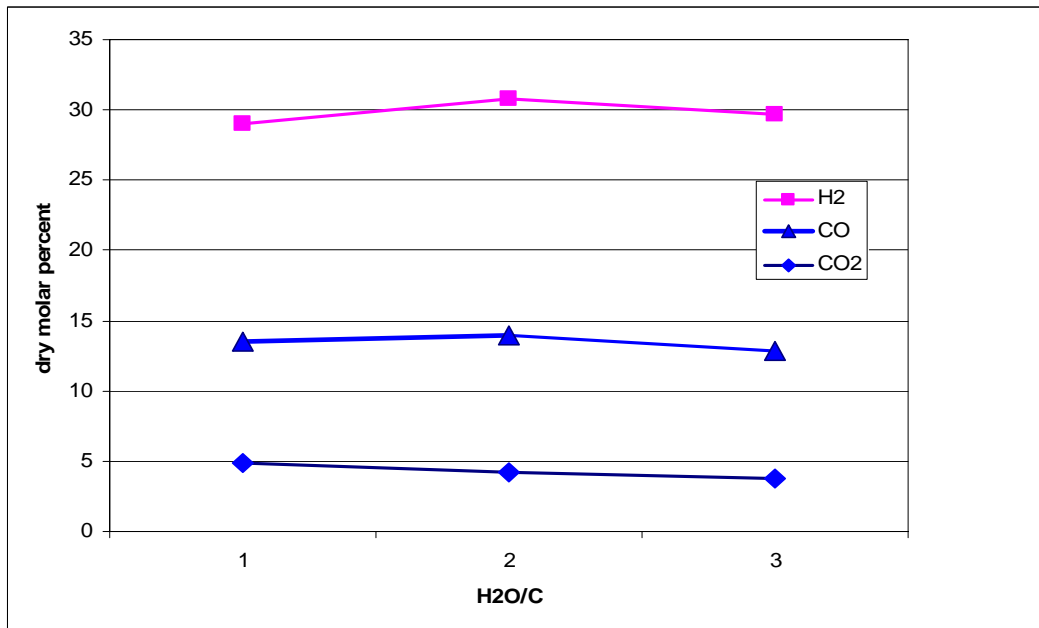


Figure 5.20: Average dry molar percentage of outlet gases vs. H<sub>2</sub>O/C obtained in present numerical results

It will be seen from Figure 5.19 that with an increase in the O/C molar ratio from 0.7 to 1, the hydrogen molar percentage increases from 27.8 to 30.2 at its peak and then decreases to 29 at an O/C ratio of 1 to 1.3. The reason is that at lower O/C ratio of 0.7, the partial oxidation reaction does not provide enough heat for the hydrogen efficient steam reforming reaction and at the higher O/C ratio of 1.3 most of the fuel is consumed by the less efficient partial oxidation reaction. The increase in the carbon monoxide and carbon dioxide amounts can be attributed to the increase in temperature associated with increasing the O/C ratio.

From Figure 5.20, it will be noted that with an increase of  $H_2O/C$ , there is a slight increase in the dry hydrogen molar percentage from 27.8 to 28.4. This trend is associated with temperature changes in the reformer which may promote further hydrogen production due to the water-gas-shift reaction. The same trends were reported by Shaw (2008) in his experimental work.

### **5.3.4 Temperatures Distributions**

In this section, the general forms of the temperature profiles along the axial length of the reformer and the affect of the main input variables on the temperature distribution are discussed. It has been reported in previous studies that the performance of the reformer is highly dependent upon the temperature at which the reactions take place, so it is useful to examine the temperature profiles along the catalyst bed. The temperature profiles along the catalyst bed were given in previous figures. When the reactants reach the catalyst bed, the temperature rises suddenly. As compared to the inlet temperatures, the temperature spike can be easily seen in the previous figures where the heat release

due to exothermic partial oxidation reaction creates a hot spot near the start of the catalyst bed. The inlet temperature for all trials was selected 773k because it causes vaporization of the inlet mixture of fuel and water. The inert porous regions of 30mm length at both ends of catalyst bed had considerable effect on the shape of temperature profile because of higher thermal conductivities of inert porous regions as compared to catalyst bed.

Changes in the O/C and H<sub>2</sub>O/C molar ratios of the inlet reactants also have significant effects on the shape of the temperature profiles and reformat compositions. With an increase in O/C ratio, the exothermic partial oxidation reaction rate increases. As a result, the peak and average bed temperatures increase as can be seen from Table 5.5. The H<sub>2</sub>O/C molar ratio also had a large effect on the overall temperatures in the reformer. It can be seen from table 5.5 that at O/C ratio of 1.3 and H<sub>2</sub>O/C ratio of 1, the peak temperature was highest that is 1100K and at O/C ratio of 0.7 and H<sub>2</sub>O/C ratio of 3, the peak temperature was lowest and is 1040K. The H<sub>2</sub>O/C ratio also plays an important role in determining the operating temperature of the reformer. As the flow rate of steam at inlet of the reformer increases, the temperature of the reformer decreases due to the endothermic nature of the steam reforming reaction. It is noted that at H<sub>2</sub>O/C ratio of 1 and O/C ratio of 1.3, the highest centerline temperature is 1100k and at H<sub>2</sub>O/C ratio of 3 and O/C ratio of 0.7, the average centerline temperature is lowest and is 975k as shown in Table 5.5.

## 5.4 Comparison of Modeling Predictions to Experimental Results

The numerical results obtained by present simulations that are comparable to the experimental data are shown in Table 5.6.

Table 5.6: Numerical and experimental results of the ATR obtained by present simulations and by Shaw (2008) at outlet of the reformer (inlet temperature equal to 500 °C, and GHSV =20000h<sup>-1</sup> )

Trial No	O/C Ratio	H <sub>2</sub> O/C Ratio	Numerical Results			Experimental Results		
			H <sub>2</sub> Molar %	CO Molar %	CO <sub>2</sub> Molar %	H <sub>2</sub> Molar %	CO <sub>2</sub> Molar %	CO Molar %
1	0.7	1.0	27.8	12.0	4.28	25.2	12.1	6.7
2	0.7	2.0	27.8	12.6	3.58	27.7	14.4	4.6
3	0.7	3.0	28.4	12.0	3.48	28.6	14.9	2.4
4	1.0	1.0	30.2	14.5	4.88	28.6	10.0	7.4
5	1.0	2.0	32.6	14.8	4.22	32.1	12.0	4.8
6	1.0	3.0	31.3	13.6	3.79	32.4	12.9	2.8
7	1.3	1.0	29.0	14.2	5.31	20.4	9.1	7.9
8	1.3	2.0	32.0	14.8	4.74	22.2	11.5	5.1
9	1.3	3.0	29.5	13.0	4.20	22.0	12.7	3.0

### 5.4.1 Comparison of the Outlet Composition

Numerical predictions of reformate composition at different O/C and H<sub>2</sub>O/C ratios at the outlet of the reformer were compared with the experimental results obtained by Shaw (2008) and are shown in Figures 5.21 and 5.22:

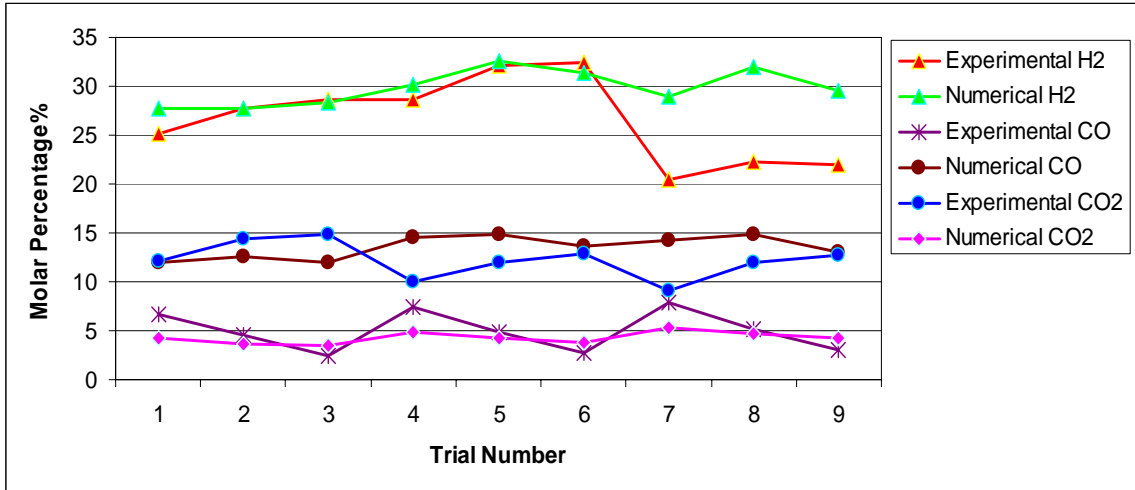


Figure 5.21: Profiles of numerical and experimental reformate composition at outlet of the reformer at different O/C and H<sub>2</sub>O/C molar ratios.

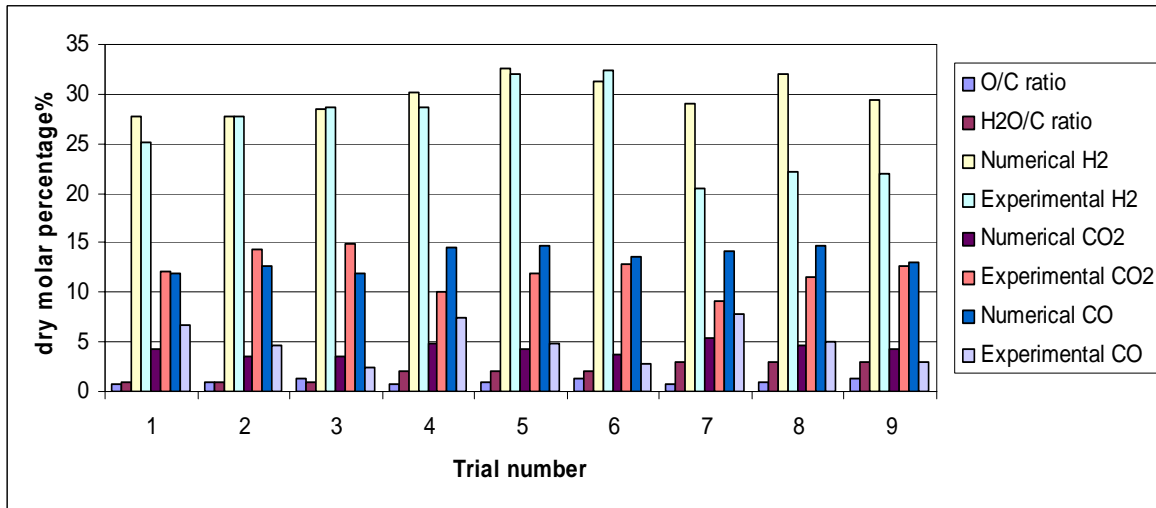


Figure 5.22: Comparison of numerical and experimental reformate composition at the outlet of the reformer at different O/C and H<sub>2</sub>O/C molar ratios.

Figures 5.21 and 5.22 illustrate the differences between the numerical results and the experimental data obtained by Shaw (2008). The predicted values of hydrogen molar percentage at outlet of the reformer match the experimental values for trials 1 to 6 quite

well but differ significantly from the experimental results for trials 7 to 9. This is the result of inadequacies in the reaction mechanism used. As seen in figures, the numerical CO and CO<sub>2</sub> molar concentrations are considerably different from the experimental values. The most likely reason for this difference is that in model it was assumed that there is no methane formation in the products while in experimental results methane was found to exist.

### 5.4.2 Comparison of Temperature Profiles

In this section the temperature profiles predicted by the model and obtained in experimental study by Shaw (2008) are discussed. Both the numerical and the experimental temperature profiles along the outer wall of the reformer and along the thermocouple tube walls have been shown earlier. The general trends displayed by the numerical and the experimental profiles agree except a few small dissimilarities. A comparison of the peak and the lowest temperatures observed within the reformer is shown in figure 5.23.

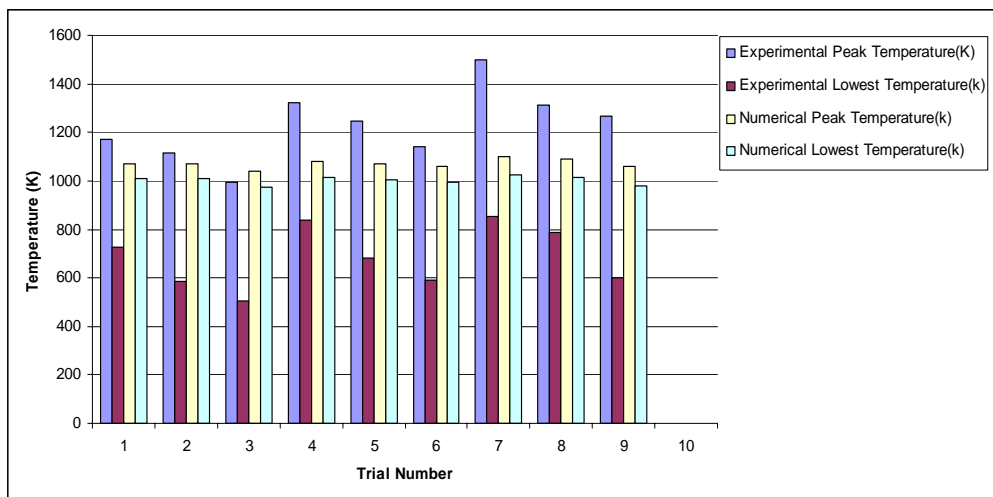


Figure 5.23: Comparison of numerical and experimental peak and lowest temperatures along the centerline of the reformer, GHSV = 20,000h<sup>-1</sup>, S:C = 2, O:C = 1.

From figure 5.23, it will be seen that there is a more difference between the lowest temperatures values and the peak temperatures values along the catalyst bed in the experimental results as compared to the difference between the numerical values for the lowest and the peak temperatures. This is probably due the fact that model assumes adiabatic walls, meaning there is no heat loss through the walls. In reality, significant heat losses were observed by Shaw (2008) during his experimental work, which can cause significant differences between peak and lowest temperature values.

## **5.5 Numerical Evaluation of possible improvements in the reformer design (Phase –III)**

In the third phase of the project, the concern was with improvements in the design of the reformer to reduce temperature gradients in the catalyst bed of the reformer and achieve the maximum hydrogen output. For this purpose, a series of simulations were performed by varying the dimensions of the reactor and the operating conditions. The results are discussed in the subsequent subsections.

### **5.5.1 Numerical Simulations with central solid rod and without the inert porous zone at the outlet of the reformer**

In this case, to reduce temperature gradients in the catalyst bed and increase hydrogen output, simulations were performed with central solid rods of different dimensions at different locations in the catalyst bed. From the simulation results, it was found that instead of using the hollow centerline thermocouple tube within the reformer for temperature measurements, use of a solid central rod of the same dimensions as that

of centerline thermocouple tube, shown in Figure 5.24, resulted in better performance of the reactor.

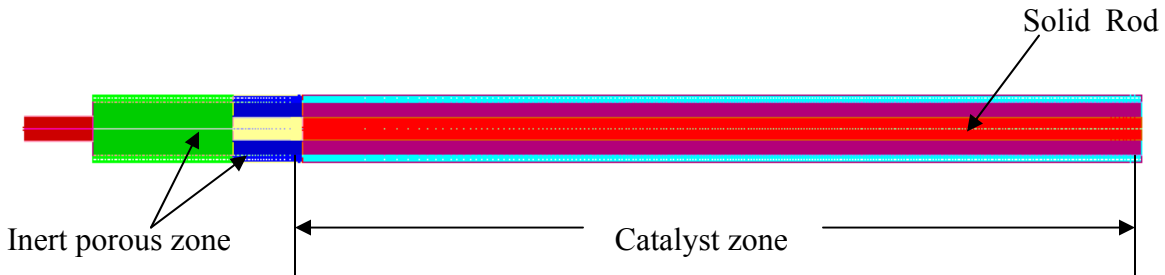


Figure: 5. 24: Reformer with central solid rod and without inert porous region at the outlet, Length =150 mm, Radius = 4.75 mm, with central rod of length =130 mm and radius = 1.6mm.

Simulations were undertaken for the experimental operating conditions as used by Shaw (2008). The summary of the numerical results obtained are shown in Table 5.7 and Figures 5.25 to 5.28.

Table 5.7: Selected results from the model of the ATR (inlet temperature = 500 °C, TC of rod and wall = 17.5 ~31.5 W/m.K and GHSV =20000h<sup>-1</sup> and effectiveness factor = 0.001)

Trial Number	O/C Ratio	H <sub>2</sub> O/C Ratio	H <sub>2</sub> Molar %	CO Molar %	CO <sub>2</sub> Molar %
1	0.7	1.0	30.0	14.0	4.27
2	0.7	2.0	28.0	12.7	3.58
3	0.7	3.0	29.2	13.1	3.12
4	1.0	1.0	31.0	14.8	4.91
5	1.0	2.0	29.1	13.4	4.27
6	1.0	3.0	30.3	13.7	3.78
7	1.3	1.0	28.4	13.6	5.35
8	1.3	2.0	28.8	13.3	4.74
9	1.3	3.0	24.6	11.10	4.24

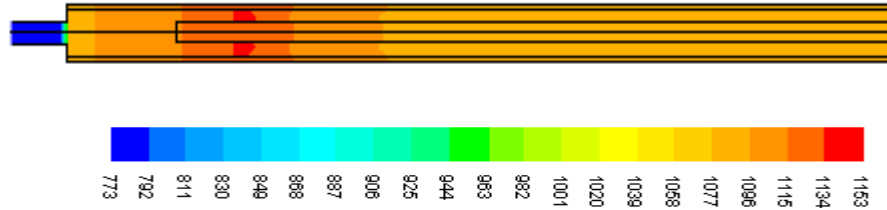


Figure 5.25: Reformer temperature distribution (GVSH = 20,000 h<sup>-1</sup>, H<sub>2</sub>O:C =2, O:C =1)

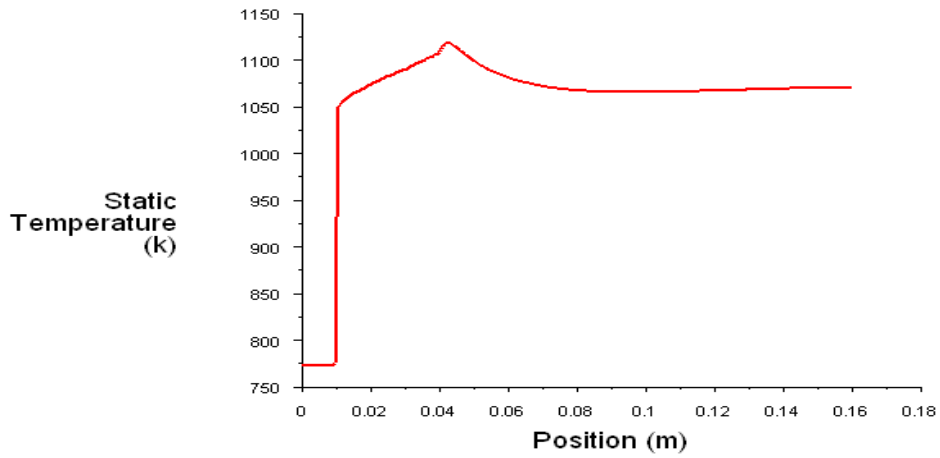


Figure 5.26: Temperature profile along the wall of the reformer, (GVSH=20,000 h<sup>-1</sup>, S:C=2, O:C=1)

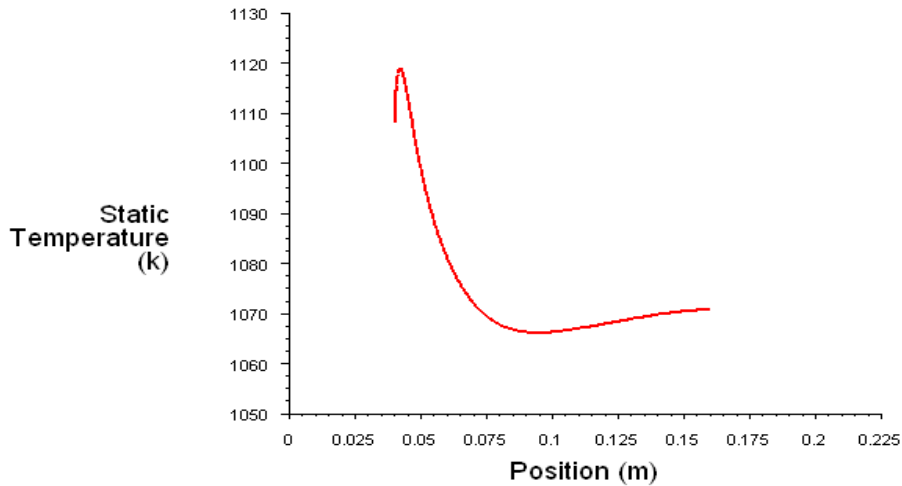


Figure 5.27: Temperature profile along the centerline of the reformer (GVSH=20,000 h<sup>-1</sup>, S:C=2, O:C=1)

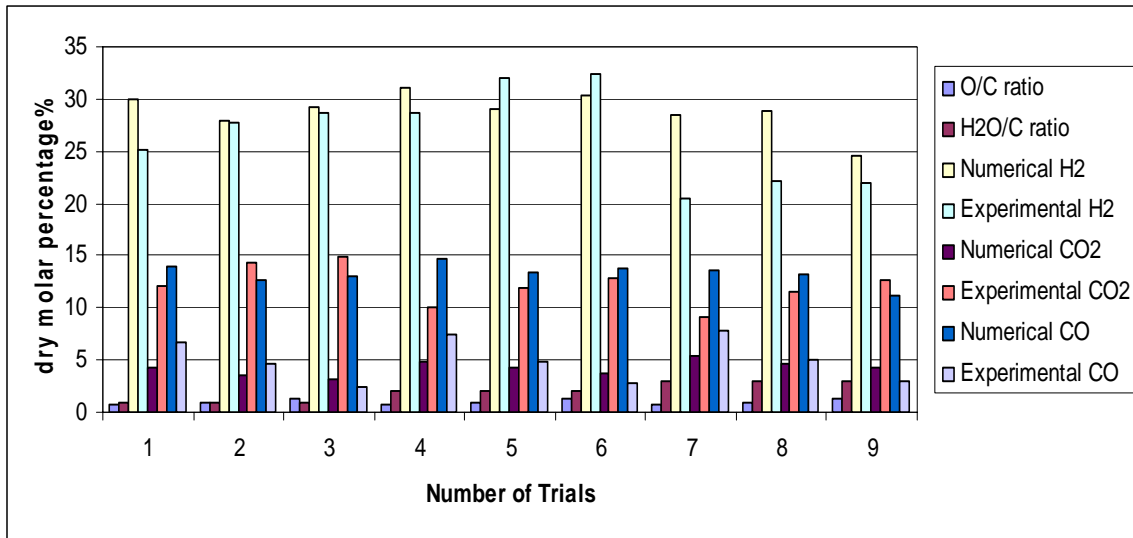


Figure 5.28: Comparison of numerical and experimental reformate composition at various O/C and H<sub>2</sub>O/C molar ratios and effectiveness factor = 0.001.

From these results, it will be seen that the replacement of centerline thermocouple tube with central solid rod and the removal of the inert porous region at outlet of the catalyst bed gives the outlet reformate composition much nearer to the experimental results obtained by Shaw (2008) even at lower effectiveness factor equal to 0.001. The size of the reactor was reduced by 30mm. Peak temperatures reached near the inlet to the catalyst bed because of exothermic partial oxidation reaction reduces from 1190 k to 1140 K due to more heat conduction in the central solid rod and temperature profile became smooth.

### 5.5.2. Final Design of the Autothermal Reformer Suggested

After the analysis and evaluation of all the results obtained from the simulations and the experimental work, certain improvements in the design of the reformer were incorporated these being as follows:

- The centerline thermocouple tube was replaced with solid centerline rod of length 130 mm and diameter 3.2 mm.
- A material with a higher thermal conductivity was selected for the solid rod, this rod having thermal conductivity value equal to 100W/m.K.
- The length of the inert porous region at outlet of the catalyst bed was reduced by 20mm.
- A material with a lower effective thermal conductivity was selected for the inert porous region at the outlet of the catalyst bed, a thermal conductivity value equal to 2W/m.K being used.

. Thus a new design was simulated with centerline solid rod of length 130 mm and diameter 3.2 mm made of material having thermal conductivity of 100W/m.K and 30mm inert porous region at the inlet made of silicon carbide and 10mm inert porous region at the outlet of the catalyst bed made of a material having thermal conductivity of 2 W/m.K as shown in Figure 5.29

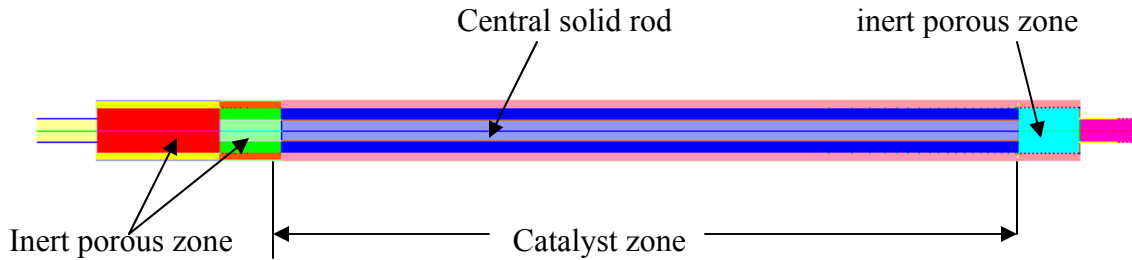


Figure: 5. 29: Reformer with central solid rod of length =130mm and radius = 1.6mm, inert porous region at inlet of length 30mm and inert porous region at outlet of the catalyst bed of length 10mm.

### 5.5.3 Numerical Simulations with new design

A series of simulation runs were undertaken by utilizing the experimental operating conditions. A summary of results obtained is shown in Tables 5.8 and 5.9 and in Figures 5.30 to 5.32

Table 5.8: Numerical results from the model of the ATR ( inlet temperature = 500°C, TC of rod =100 W/m.K, TC of wall =17.5 ~31.5 W/mk, GHSV =20000h<sup>-1</sup> and effectiveness factor = 0.0032)

Trial Number	O/C Ratio	H <sub>2</sub> O/C Ratio	H <sub>2</sub> Molar %	CO Molar %	CO <sub>2</sub> Molar %
1	0.7	1.0	37.7	18.7	4.19
2	0.7	2.0	43.6	20.4	3.52
3	0.7	3.0	45.1	20.4	3.05
4	1.0	1.0	34.7	17.7	4.83
5	1.0	2.0	40.8	19.4	4.2
6	1.0	3.0	42.5	19.5	4.12
7	1.3	1.0	32.4	17.0	5.27
8	1.3	2.0	38.2	18.5	4.66
9	1.3	3.0	40.2	18.7	4.20

Table 5.9: Peak and Lowest temperatures in the catalyst bed

Comparable Experimental Number	O/C Ratio	H <sub>2</sub> O/C Ratio	Peak Temperature (K)	Lowest Temperature (K)
1	0.7	1.0	1120	1090
2	0.7	2.0	1110	1080
3	0.7	3.0	1110	1080
4	1.0	1.0	1130	1100
5	1.0	2.0	1120	1090
6	1.0	3.0	1120	1090
7	1.3	1.0	1140	1110
8	1.3	2.0	1130	1100
9	1.3	3.0	1130	1100

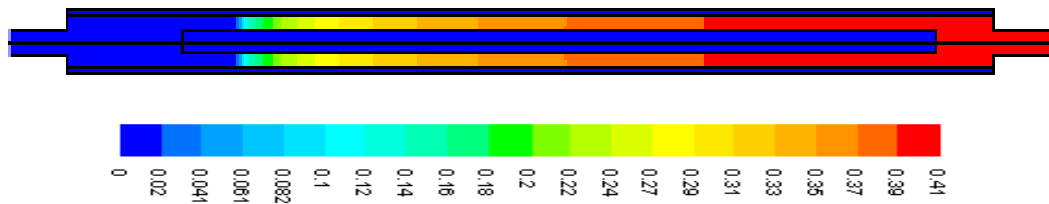


Figure 5.30: Reformer hydrogen distribution (GHSV=20,000 h<sup>-1</sup>, S:C = 2, O:C = 1)

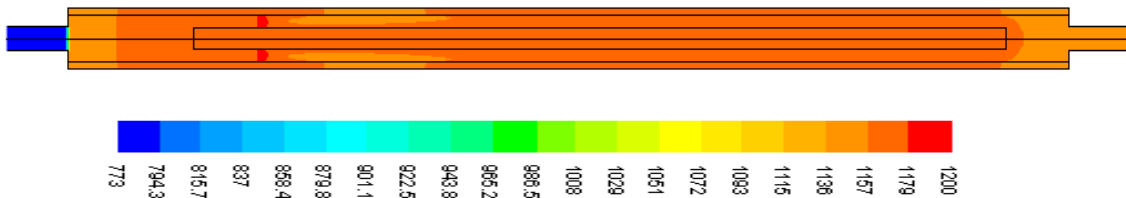


Figure 5.31: Reformer temperature distribution (GHSV=20,000 h<sup>-1</sup>, S:C = 2, O:C = 1)

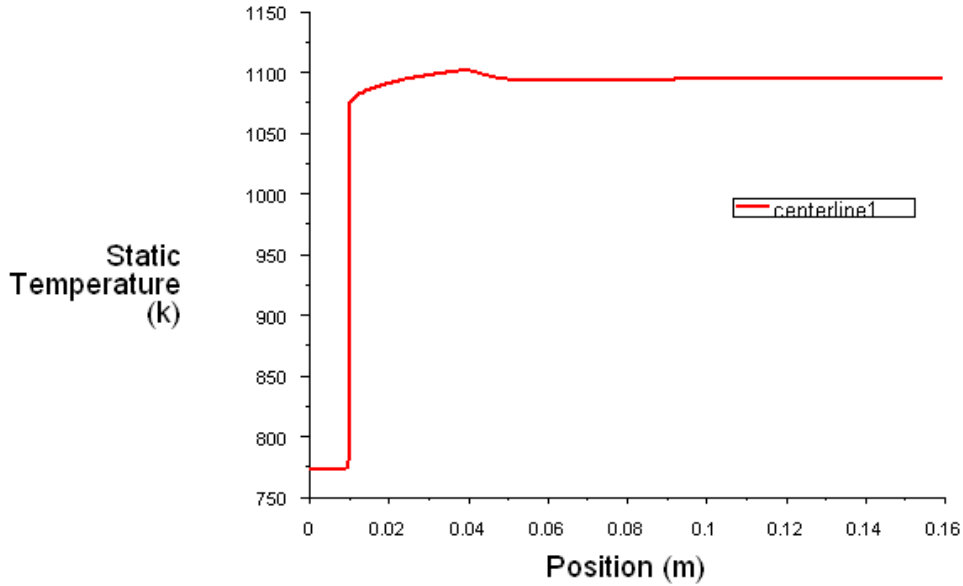


Figure 5.32: Temperature profile along the centerline of the reformer (GHSV=20,000 h<sup>-1</sup>, S:C = 2, O:C = 1)

When compared to the predicted and measured results of the original design, the increase in hydrogen output is evident as shown in Figures 5.33.

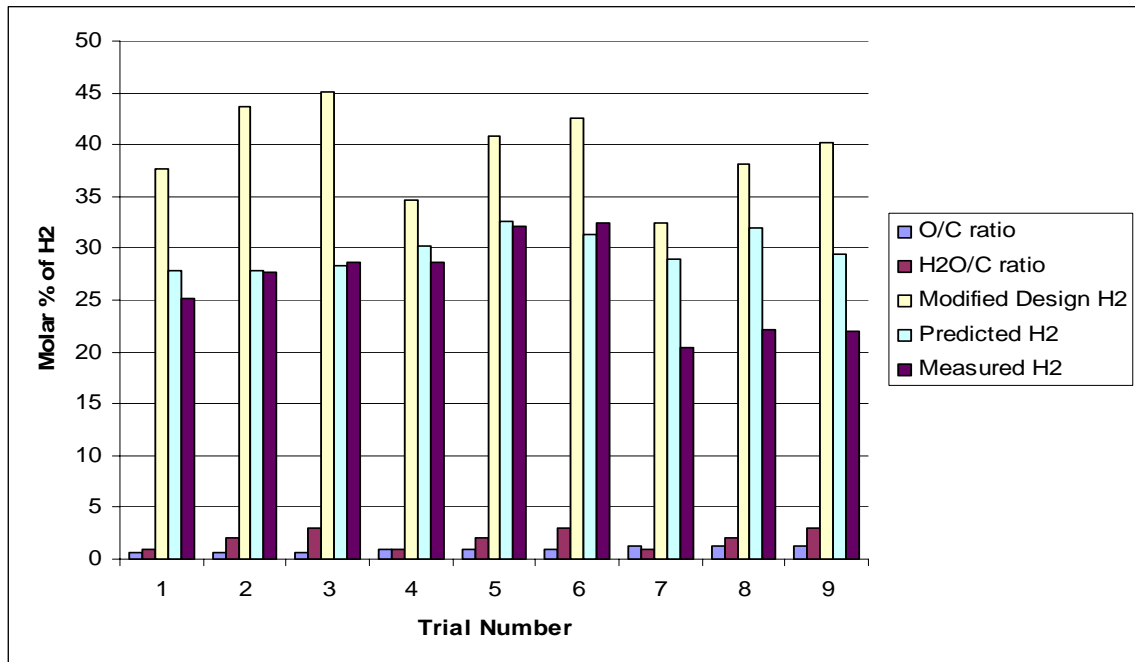


Figure 5.33: Comparison of numerical results of modified design with predicted and measured results of the original design at different O/C and H<sub>2</sub>O/C molar ratios, GHSV = 20,000h<sup>-1</sup>

It is evident from the numerical results for the new design that as a result of the incorporation of the design improvements, the output of the molar percentage of hydrogen can be increased by approximately 25% and length of the reformer can be reduced by 20mm. Moreover the temperature gradients are reduced and the temperature profiles become more even and the heat conduction along the catalyst bed is increased.

## Chapter 6

### Conclusions and Recommendations

#### 6.1 Conclusions

The design of a compact autothermal reformer using proprietary platinum on a zirconia-ceria base catalyst for the onboard production of hydrogen from iso-octane was analyzed and evaluated numerically to maximize hydrogen output by using a Computational Fluid Dynamics model prepared using the commercial software FLUENT. The present study was mainly undertaken to determine if by modifying the reformer design to reduce the temperature gradients and to increase the heat transfer rate in the catalyst bed the overall performance of the reformer could be improved. The main findings of present study are:

- Molar concentrations of product species and temperature profiles were found to follow the general trends associated with the autothermal reformer as reported in previous studies.
- The effect of varying the effectiveness factor on the molar concentrations of product species at exit was noted. A comparison of the numerical and the experimental results indicated that a value of effectiveness factor equal to 0.0032 gives the best agreement between the numerical and experimental results.
- For the simulations performed for the operating conditions used in the experimental study, the highest molar percent of hydrogen for a gas hourly space velocity of  $20000\text{h}^{-1}$  was found at an O/C ratio of 1.0 and a  $\text{H}_2\text{O}/\text{C}$  ratio of 2.0 and it was 32.6% .

- With the incorporation of design improvements for the operating conditions used in the experimental study, the molar percent of hydrogen at gas hourly velocity of  $20000\text{h}^{-1}$ , O/C ratio of 1.0 and  $\text{H}_2\text{O}/\text{C}$  ratio of 2.0 was found to be 40.8% i.e. an increase in the hydrogen output of approximately by 25% as compared to the original design.
- By the replacement of centerline thermocouple tube with a solid rod and increasing thermal conductivity of the rod, temperature gradients in the catalyst bed were reduced and a more evenly distributed temperature variation was achieved along the catalyst bed. Heat transfer takes place more evenly throughout the solid rod resulting in higher average reaction rates and higher hydrogen output.
- By reducing the thermal conductivity of the inert porous region at the outlet of the catalyst bed, a more evenly distributed temperature variation was obtained along the catalyst bed resulting in higher chemical reactivity and a better overall fuel conversion efficiency.
- By reducing the length of the inert porous region at the outlet of the catalyst bed by 20mm, the length of the reactor was decreased without affecting the overall performance of the reformer.
- An increase in the length and diameter of the reformer was found to have no any significant affect on the performance of the reformer.

- It was found that variations in the O/C molar ratios at inlet have a significant effect on the outlet concentrations of product species and also on the temperature profiles because the temperature increases at higher ratios and consumes more fuel through partial oxidation while at lower ratios, the temperature is reduced and the reaction rates become slower.

## 6.2 Recommendations for Future Work

The predictions made through present series of simulations and comparison with available experimental and numerical data provided much information to carry out some improvements in the design of the reformer, but still more steps are required to improve the numerical model so that even more accurate predictions of the reactor performance can be obtained. To improve the model, following steps are recommended for future work:

- More research is required into available catalysts that have higher thermal conductivity that can increase the chemical reaction rates in the catalyst bed.
- Inclusion of the formation of methane in the chemical reaction mechanism adopted will give more accurate predictions about the concentrations of carbon monoxide and carbon dioxide.
- By taking into account the diffusional effects in the model, improvements can be made in the selection of effectiveness factor for each reaction in the chemical mechanism.
- The present study is based on the steady state operation of the autothermal reformer. Further experimental work examining the transient state behaviour of the reformer could provide valuable information about the reformer performance during different operating conditions.
- Feeding different fuels to the reformer rather than the surrogate iso-octane, like (diesel or gasoline) would help obtain more practical information on the autothermal performance.

## References

Ahmed,S., Krumpelt, M., “ Hydrogen from hydrocarbon fuels for fuel cells” International Journal of hydrogen energy, Vol, 20. pp. 291-301 (2001)

Aicher T., Lenz B.,Gschnell F.,Groos U.,Federici F.,Caprile L.,Parodi L., “Fuel processors for fuel cell APU applications” Journal of Power Sources, Vol 154, pp.503-508

Arthur D. Little, Inc.,“Multi-fuel reformers for fuel cells used in transportation - assessment of hydrogen storage technologies” U.S. Department of Energy, DOE/CE/50343-1, 1994.

Argonne National Laboratories (ANL), [www.anl.gov](http://www.anl.gov), (2007a)

Berger R., Perez-Ramirez J, Kapteijn F, Moulijn J., “Catalyst performance testing: bed dilution revisited” Chemical Engineering Science, vol 57, pp. 4921-4932, (2002)

Brant A. Pepply, Patric Oosthuizen., “Reforming of Hydrocarbon (alcohol) fuels” NORDIC Hydrogen Seminar OSLD 6-8 February 2006

Canadian hydrogen, ”Current status & future prospectus” A Study conducted for natural resources Canada, August 2004

Caners, C.” The experimental evaluation of a compact autothermal gasoline reformer for fuel cell applications” MSc, Queen’s University (2005)

Chaitanya Sampara, Christopher Depcik and Dennis Assanis., “Framework for modeling components of a fuel processing system for fuel cell applications” Proceedings of IMECE’05: 2005 ASME Design Engineering Technical Conferences November 5-11 2005, Orlando, Florida, USA

Dixon, A.G., Nijemeisland, M., “CFD as a design tool for fixed-bed reactors” *Industrial Engineering Chemistry*, vol.40, pp. 5246-5254, (2001)

Dixon, A.G., Nijemeisland, M., “CFD study of fluid flow and wall heat transfer in a fixed bed of spheres” *AIChE Journal*, Vol. 50,pp. 906-921, (2004)

Ergun, S., “Fluid flow through packed columns” *Chemical Engineering Programming* Vol.48, pp. 89-94 (1952)

Ersoz, M., Olgun, H., Ozdogan, S., Gungor, C., Akgun, F., Tiris, M. “Autothermal reforming as a hydrocarbon fuel processing option for fuel cell” *Journal of Power Sources*, Vol.118,pp. 384-392, (2003)

Ferziger, J.H., “Estimation and reduction of numerical error” *ASME Winter Meeting*, CA, (1989)

Fluent User’s Guide, *Fluent Documentation 6.2*, Lebanon, NH (2005)

Fogler, S.,H., “ *Elements of Chemical Reaction Engineering*” Prentice-Hall, Inc., NJ (1999)

Gudlavalleti, S., Ros, T., Lieftink, D., “Thermal sintering studies of an autothermal reforming catalyst” *Applied Catalysis B: Environment*, Vol.74, Issue3-4, pp. 251-260, (2007)

H.K. Versteeg, W.malalasekera., “ *An introduction to Computational Fluid Dynamics, The Finite Volume Method*” Second Edition

Hoang, D.L., Chan, S.H., “Modeling of a catalyst autothermal methane reformer for fuel cell applications” *Applied Catalyst A: General*, Vol. 268, pp. 207-216. (2004)

Hagh B.F., “Stoichiometric analysis of autothermal fuel processing”, Journal of Power Sciences, Vol. 130, pp,85-94, (2004)

Ibrahim, H.H., Idem.,R.O., “ Kinetic studies of the partial oxidation of iso-octane for hydrogen production over a nickel- alumina catalyst” Chemical Engineering Science, Vol.61,pp 5912-5918, (2006)

Incropera, F.P., DeWitt, D.P. Bergman, T.L., Lavine, A.S., “Fundamentals of Heat and Mass Transfer 6<sup>th</sup> Edition” John Willy & Sons, NY, (2007)

Jin, W., Gu,X., Li,S.,Huang, p., Xu, N.,Shi, J., “Experimental and simulation study on a catalyst packed tubular dense membrane reactor for partial oxidation of methane to syngas” Chemical Engineering Science, Vol.55, pp.2617-2625, (2000)

Kaila, R.K., Krause, A.O.I, “ Autothermal reforming of simulated gasoline and diesel fuels” International Journal of Hydrogen Energy, Vol.31, pp. 1934-1941, (2006)

Kang,I.,Bae,J.,G.,” Performance comparison of autothermal reforming for liquid hydrocarbons, gasoline and diesel for fuel cell applications” Journal of power sources, Vol. 130, pp.85-94, (2004)

Krumpelt et al.” Fuel processing for fuel cell systems in transportation and portable power applications” Catalyst today, Vol 77, pp.3-16,(2002)

Larminie, J., Dicks, A., “Fuel Cell Systems Explained” John Willy & Sons, LTD., Chichester, England (2000)

Li, V.C., “Development of a basic numerical model of an iso-octane catalytic autothermal reformer for an automobile” MSc, Queen’s University, (2004)

Maestri, M., Beretta A., Groppi, G., Tronconi, E., Forzatti, P., “Modeling of fixed bed reactors for the catalytic partial oxidation of methane to syngas: a comparison among structured and packed bed reactors” Chemical Engineering Transactions, Vol.6, pp.13-18,(2005)

McIntyre,C., “Development of a numerical model of a compact autothermal reformer for the production of hydrogen from iso-octane” MSc, Queen’s University,(2005)

Midleton, C., “ Design and construction of an autothermal gasoline reformer” MSc, Royal Military College of Canada. (2004)

Moon D.J., et al.,” Studies on gasoline fuel processor system for fuel cell powered vehicle applications” Applied catalyst A: General, Vol 215, pp. 1-9, (2001)

Mónica Ospinal-Jiménez., “Hydrogen production study using autothermal reforming of biodiesel and other hydrocarbons for fuel cell Applications” MSc, University of Puerto Rico Mayaguez (2006)

Moran, M.J., Shapiro, H.N., “Fundamentals of Engineering Thermodynamics 5<sup>th</sup> Edition” John Willy & Sons, NY, (2005)

Murata, K., Satio, M., Takahara, I., “Hydrogen production by autothermal reforming of sulfur containing hydrocarbons over re-modified Ni.Sr/ZrO<sub>2</sub> catalysts” Applied Catalysts B: Environmental, Vol.70, pp. 509-514, (2007)

National Research Council Canada (NRC), “The State of Energy Efficiency in Canada”, (2006)

Pacheco et al.,” Reaction kinetics and reactor modeling for fuel processing of liquid hydrocarbons to produce hydrogen: iso-octane reforming” Applied Catalyst A; General, Vol 250 pp.161-175,(2003)

Rajesh B. Biniwale, Akira Mizuno, Masaru Ichikawa.,” Hydrogen production by reforming of iso-octane using spray-pulsed injection and effect of non-thermal plasma” Catalyst research center, Hokkaido University, Sapporo 001-0021 Japan (2004)

Rod Borup, W. Jerry Parkinson, Michael Inbody, Jose Tafoya, and Dennis R. Guidry.,”Diesel Reforming for Fuel Cell Auxiliary Power Units” SECA Core Technology Program Review *Los Alamos National Laboratory*

Roychoudhury, S. et al.,” Microlith catalytic reactors for reforming iso-octane based fuels into hydrogen” Journal of power sciences, Vol. 152, pp, 75-86,(2005)

Shaw, M. Adam.,”An experimental study of a compact autothermal gasoline reformer for the production of hydrogen” MSc, Queen’s University (2008)

Sylvestre, S.,”A Numerical study of an autothermal reformer for the production of hydrogen from iso-octane” MSc, Queen’s University (2007)

Villages.L. et al.,” A combined thermodynamic/experimental study for the optimization of hydrogen production by catalyst reforming of iso-octane” Applied catalyst, Vol. 281,pp. 75-83 92005)

Xianguo Li., “Principles of FUEL CELLS” John Willy & Sons, NY, (2006)

Xu, J., Froment, G.F., “Methane steam reforming: II. Diffusional limitations and reactor simulation” AIChE Journal, Vol.35, pp.97-103, (1989)

# Appendix A

## Fluent User Input

The summary given in Appendix A is an example of the user input necessary to define the CFD model. The summary describes the models selected, the relaxation factors, the discretization schemes, and the material properties. The reaction mechanism was input through a user-defined function and can be found in Appendix B.

### **FLUENT**

Version: axi, dp, segregated, spe, lam (axi, double precision, segregated, species, laminar)

Release: 6.2.16

### **Title:**

### **Models**

<b>Model</b>	<b>Settings</b>
Space	Axisymmetric
Time	Steady
Viscous	Laminar
Heat Transfer	Enabled
Solidification and Melting	Disabled
Species Transport	Reacting (7 species)
Coupled Dispersed Phase	Disabled
Pollutants	Disabled
Soot	Disabled

### **Solver Controls**

<b>Equation</b>	<b>Solved</b>
-----------------	---------------

---

Flow	yes
c <sub>8</sub> h <sub>18</sub>	yes
o <sub>2</sub>	yes
co <sub>2</sub>	yes
n <sub>2</sub>	yes
co	yes
h <sub>2</sub>	yes
Energy	yes

### **Relaxation**

<b>Variable</b>	<b>Relaxation Factor</b>
-----------------	--------------------------

---

Pressure	0.5
Density	0.6
Body Forces	0.6
Momentum	0.5
c <sub>8</sub> h <sub>18</sub>	0.4
o <sub>2</sub>	0.5
co <sub>2</sub>	0.5
n <sub>2</sub>	0.5
co	0.5
h <sub>2</sub>	0.5
Energy	0.4

### **Discretization Scheme**

<b>Variable</b>	<b>Scheme</b>
-----	
Pressure	PRESTO!
Momentum	Second Order Upwind
c <sub>8</sub> h <sub>18</sub>	Second Order Upwind
o <sub>2</sub>	Second Order Upwind
co <sub>2</sub>	Second Order Upwind
n <sub>2</sub>	Second Order Upwind
co	Second Order Upwind
h <sub>2</sub>	Second Order Upwind
Energy	Second Order Upwind

### **Solution Limits**

<b>Quantity</b>	<b>Limit</b>
-----	
Minimum Absolute Pressure	1
Maximum Absolute Pressure	5e+10
Minimum Temperature	1
Maximum Temperature	5000

### Material Properties

Material: **silicon-carbide** (solid)

Property	Units	Method	Value(s)
Density	kg/m <sup>3</sup>	constant	3220
Cp (Specific Heat)	J/kg-K	constant	650
Thermal Conductivity	W/m-K	constant	200

Material: **pt-catalyst** (solid)

Property	Units	Method	Value(s)
Density	kg/m <sup>3</sup>	constant	6500
Cp (Specific Heat)	J/kg-K	constant	500
Thermal Conductivity	W/m-K	constant	2

Material: **inconel-625** (solid)

Property	Units	Method	Value(s)
Density	kg/m <sup>3</sup>	constant	8440
Cp (Specific Heat)	J/kg-k	constant	410
Thermal Conductivity	W/m-K	polynomial	(811,17.5) (922,19) (1033,20.8)(1144,22.8) (1255 25.3) (1366,28.2) (1477,31.5)

Material: **(Hydrogen. n-octane-air) (fluid)**

Property	Units	Method	Value(s)
Cp (Specific Heat)	J/kg-K	polynomial	(500,14510) (750,14650) (1000,14980) (1100,15150) (1200,15340) (1400,15770)
Thermal Conductivity	W/m-K	constant	0.1672
Viscosity	kg/m-s	constant	8.411e-06
Molecular Weight	kg/kg-mol	constant	2.01594
Standard State Enthalpy	J/kg-mol	constant	-1881.377
Standard State Entropy	J/kg-mol-K	constant	130579.06
Reference Temperature	k	constant	298.14999
L-J Characteristic Length	angstrom	constant	2.92
L-J Energy Parameter	k	constant	38

Material: **(carbon-monoxide. n-octane-air) (fluid)**

Property	Units	Method	Value(s)
Cp (Specific Heat)	J/kg-K	polynomial	(300,1040)(600,1087) (1000,1185)(1500,1257) (2000,1294) (2500,1315)
Thermal Conductivity	W/m-K	constant	0.025
Viscosity	kg/m-s	constant	1.75e-05
Molecular Weight	kg/kg-mol	constant	28.01055
Standard State Enthalpy	J/kg-mol	constant	-1.1053956e+08
Standard State Entropy	J/kg-mol-k	constant	197531.64
Reference Temperature	k	constant	298.14999

Material: **(carbon-dioxide . n-octane-air)** (fluid)

Property	Units	Method	Value(s)
Cp (Specific Heat)	j/kg-k	polynomial	(300,846) (600,1075) (1000,1234) (1500,1326) (2000,1371) (2500,1397)
Thermal Conductivity	w/m-k c	constant	0.0145
Viscosity	kg/m-s	constant	1.37e-05
Molecular Weight	kg/kg-mol	constant	44.009949
Standard State Enthalpy	J/kg-mol	constant	-3.9353235e+08
Standard State Entropy	J/kg-mol-K	constant	213720.2
Reference Temperature	k	constant	298.14999

Material: **(n-octane-vapor . n-octane-air)** (fluid)

Property	Units	Method	Value(s)
Cp (Specific Heat)	J/kg-K	polynomial	(500,2513) (1000,3805) (1500,4428) (2000,4879)
Thermal Conductivity	W/m-K	constant	0.0178
Viscosity	kg/m-s	constant	6.75e-06
Molecular Weight	kg/kg-mol	constant	114.22
Standard State Enthalpy	J/kg-mol	constant	-2.09e+08
Standard State Entropy	J/kg-mol-K	constant	0
Reference Temperature	k	constant	298.14999

Material: **(nitrogen . n-octane-air)** (fluid)

Property	Units	Method	Value(s)
Cp (Specific Heat)	J/kg-K	polynomial	(300,1045) (600,1075) (1000,1164)(1500,1239) (2000,1283) (2500,1314)
Thermal Conductivity	W/m-K	constant	0.0242
Viscosity	kg/m-s	constant	1.663e-05
Molecular Weight	kg/kg-mol	constant	28.013399
Standard State Enthalpy	J/kg-mol	constant	0
Standard State Entropy	J/kg-mol-K	constant	191494.78
Reference Temperature	k	constant	298.14999

Material: **(oxygen . n-octane-air)** (fluid)

Property	Units	Method	Value(s)
Cp (Specific Heat)	J/kg-K	polynomial	(300,914) (600,1005) (1000,1084) (1500,1136) (2000,1175) (2500,1215)
Thermal Conductivity	W/m-k	constant	0.0246
Viscosity	kg/m-s	constant	1.919e-05
Molecular Weight	kg/kg-mol	constant	31.9988
Standard State Enthalpy	J/kg-mol	constant	0
Standard State Entropy	J/kgmol-K	constant	205026.86
Reference Temperature	k	constant	298.14999

Material: **(water-vapor . n-octane-air)** (fluid)

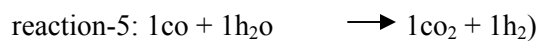
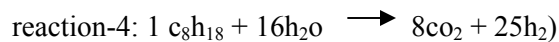
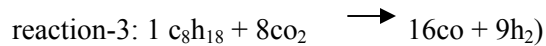
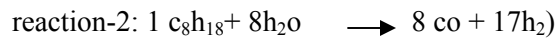
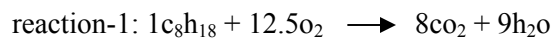
Property	Units	Method	Value(s)
Cp (Specific Heat)	J/kg-K	polynomial	(300,1858) (600,2020) (1000,2275)(1500,2601) (2000,2833) (2500,2996)
Thermal Conductivity	W/m-K	constant	0.0261
Viscosity	kg/m-s	constant	1.34e-05
Molecular Weight	kg/kg-mol	constant	18.015341
Standard State Enthalpy	J/kg-mol	constant	-2.418379e+08
Standard State Entropy	J/kg-mol-K	constant	188696.44
Reference Temperature	K	constant	298.14999

Material: **(n-octane-air (mixture))**

Property	Units	Method
----------	-------	--------

Mixture Species: (c<sub>8</sub>h<sub>18</sub>, o<sub>2</sub>, co<sub>2</sub>, n<sub>2</sub>, co, h<sub>2</sub>, h<sub>2</sub>o)

Reaction: finite-rate



Density	kg/m <sup>3</sup>	incompressible-ideal-gas
Cp (Specific Heat)	J/kg-K	mixing-law
Thermal Conductivity	W/m-K	mass-weighted-mixing-law

Viscosity	kg/m-s	mass-weighted-mixing-law
Mass Diffusivity	m <sup>2</sup> /s	user-defined (diffusivity::EF008)
Thermal Expansion Coefficient	1/k	constant

## Appendix B

### User-defined Function

The following code was written in C++ and incorporated into the Fluent software compiler to provide the user-defined functions describing the effective diffusivity and reaction rates in the Pacheco et al. (2003) chemical reaction model.

```
/******  
/* Reaction (1) Partial Oxidation */  
/* C8H18 + 12.5O2 -> 8CO2 + 9H2O*/  
/* Reaction (2) Steam Reforming Reaction i */  
/* C8H18+ 8H2O -> 8CO + 17H2 */  
/* Reaction (3) Carbon Reforming */ /* C8H18+ 8CO2 -> 16CO + 9H2 */  
/* Reaction (4) Steam Reforming Reaction ii */  
/* C8H18 + 16H2O -> 8CO2 + 25H2 */  
/* Reaction (5) Water-Gas Shift Reaction */ /* CO + H2O -> CO2 + H2 */  
/******  
  
#include "udf.h"  
  
/*This function defines the effective diffusivity term in equation 4.12*/  
  
DEFINE_DIFFUSIVITY (diffusivity, c, t,i)  
{  
  
#define d_inf 0.000001  
  
real D_eff;  
  
real u = C_U(c, t);  
  
real v = C_V(c, t);  
  
D_eff=.000625*sqrt(u*u+v*v);  
  
return D_eff;
```

```

}

/* This function defines the volumetric rate of reaction of the Pacheco et al. (2003) mechanism*/
DEFINE_VR_RATE(rate,c,t,r,wk,yk,rate,rr_t)
{
/*Pre-exponential factors and Activation energies. The pre-exponential factors are multiplied by
the density of the catalyst multiplied by the effectiveness factor*/

#define A1 2.58e8*1400*.0032
#define A2 2.61e9*1400*.0032
#define A3 2.78e-5*1400*.0032
#define A4 1.52e7*1400*.0032
#define A5 1.55e1*1400*.0032

#define E1 166e3
#define E2 240.1e3
#define E3 23.7e3
#define E4 243.9e3
#define E5 67.1e3

/*Heats of adsorption (J/kmol) - taken from Xu (1989)*/
#define HCO -70.65e3
#define HH2 -82.9e3
#define HC8 -38.28e3
#define HH2O 88.68e3

/*Universal Gas Constant (J/mol*K) */
#define UGC 8.314

/*Adsorption pre-exponential constants (bar-1) - taken from Xu (1989) except H2O, taken from
Pacheco et al. (2003)*/

```

```

#define ACO 8.23e-5

#define AH2 6.12e-9

#define AC8 6.65e-4

#define AH2O 1.57e4

/*Adsorption coefficient */

real KCO=ACO*exp(-HCO/(UGC*C_T(c,t)));

real KH2=AH2*exp(-HH2/(UGC*C_T(c,t)));

real KC8=AC8*exp(-HC8/(UGC*C_T(c,t)));

real KH2O=AH2O*exp(-HH2O/(UGC*C_T(c,t)));

/*Mass fractions*/

real mC8=C_YI(c,t,0);

real mO2=C_YI(c,t,1);

real mCO2=C_YI(c,t,2);

real mN2=C_YI(c,t,3);

real mCO=C_YI(c,t,4);

real mH2=C_YI(c,t,5);

real mH2O=C_YI(c,t,6);

/*Partial pressures*/

real pOp=1.01; /*operating pressure (bar)*/

real sum=(mC8/114+mO2/32+mCO2/44+mN2/28+mCO/28+mH2/2+mH2O/18);

real pC8=mC8/114/sum*pOp;

real pO2=mO2/32/sum*pOp;

real pCO2=mCO2/44/sum*pOp;

real pN2=mN2/28/sum*pOp;

real pCO=mCO/28/sum*pOp; 125

```

```

real pH2=mH2/2/sum*pOp;

real pH2O=mH2O/18/sum*pOp;

/*Denominator variable "DET" used in rate expressions*/

real DET=(1+KCO*pCO+KH2*pH2+KC8*pC8+KH2O*pH2O/(pH2));

/* Initialize equilibrium constants */

real K2;

real K3;

real K4;

real K5;

if (!strcmp(r->name, "reaction-2"))
{K2=5.75e12*exp(-11476/((C_T(c,t))));
*rate=A2*exp(-E2/(8.314*(C_T(c,t))))/pow((pH2),2.5)*(pC8*pH2O-
(pH2*pH2*pH2*pCO/K2))/(DET*DET);}

else if (!strcmp(r->name, "reaction-1"))
{*rate=A1*exp(-E1/(8.314*(C_T(c,t))))*pC8*pO2;}

else if (!strcmp(r->name, "reaction-3"))
{K3=exp(-30782/C_T(c,t)+38.9)/(100*100);
*rate=A3*exp(-E3/(8.314*(C_T(c,t))))*pC8*pCO2*(1-
(pCO*pCO*pH2*pH2)/(K3*(pC8*pCO2)));}

else if (!strcmp(r->name, "reaction-4"))
{K4=7.24e10*exp(-21646/((C_T(c,t))));
*rate=A4*exp(-E4/(8.314*(C_T(c,t))))/pow((pH2),3.5)*(pC8*pH2O*pH2O-
pH2*pH2*pH2*pH2*pCO2/K4)/(DET*DET);}

else if (!strcmp(r->name, "reaction-5"))
{K5=.009475*exp(4804/(C_T(c,t)));
*rate=A5*exp(-E5/(8.314*(C_T(c,t))))/pH2*(pCO*pH2O-pH2*pCO2/K5)/(DET*DET);}

```

```
if (*rate>10) /* stops reaction rate from becoming unreasonable high; facilitates convergence */
{*rate=10;}
else if (*rate<-10)
{*rate=-10;}
*rr_t=*rate;
}
```

## Appendix C

### Experimental Results Shaw (2008)

Run Number	GHSV (h-1)	O/C	H <sub>2</sub> O/C	Isooctane flow rate (mL/min)	Air flow rate (SLPM)	Water flow rate (mL/min)	Total pump flow (mL/min)
1	20000	0.7	1.0	0.52	1.02	0.45	0.98
2	20000	0.7	2.0	0.38	0.75	0.67	1.05
3	20000	0.7	3.0	0.30	0.60	0.79	1.10
4	20000	1.0	1.0	0.42	1.16	0.36	0.78
5	20000	1.0	2.0	0.32	0.90	0.56	0.89
6	20000	1.0	3.0	0.27	0.74	0.69	0.96
7	20000	1.3	1.0	0.35	1.26	0.30	0.65
8	20000	1.3	2.0	0.28	1.02	0.49	0.76
9	20000	1.3	3.0	0.23	0.85	0.61	0.84
9R1	20000	1.3	3.0	0.23	0.85	0.61	0.84
9R2	20000	1.3	3.0	0.23	0.85	0.61	0.84
9R3	20000	1.3	3.0	0.23	0.85	0.61	0.84

Run #	Dry Molar Percent					Output Flow rate (SLPM)				
	H <sub>2</sub>	N <sub>2</sub>	CO	CH <sub>4</sub>	CO <sub>2</sub>	H <sub>2</sub>	N <sub>2</sub>	CO	CH <sub>4</sub>	CO <sub>2</sub>
1	25.2	53.5	6.7	2.5	12.1	0.381	0.807	0.101	0.037	0.183
2	27.7	50.7	4.6	2.7	14.4	0.326	0.594	0.054	0.032	0.169
3	28.6	51.2	2.4	2.9	14.9	0.263	0.470	0.022	0.027	0.137
4	28.6	52.9	7.4	1	10	0.494	0.917	0.128	0.017	0.137
5	32.1	49.9	4.8	1.2	12	0.460	0.714	0.069	0.017	0.172
6	32.4	50.5	2.8	1.4	12.9	0.375	0.585	0.033	0.016	0.149
7	20.4	62.5	7.9	0.1	9.1	0.324	0.994	0.125	0.002	0.144
8	22.2	61.1	5.1	0.1	11.5	0.292	0.802	0.066	0.001	0.151
9	22	62.0	3	0.3	12.7	0.231	0.673	0.032	0.004	0.137
9R1	21	62.4	2.8	0.2	13.1	0.231	0.673	0.030	0.002	0.142
9R2	22	62.8	2.7	0.1	13.0	0.237	0.673	0.029	0.001	0.139
9R3	21	62.7	2.5	0.0	12.9	0.234	0.673	0.027	0.000	0.139

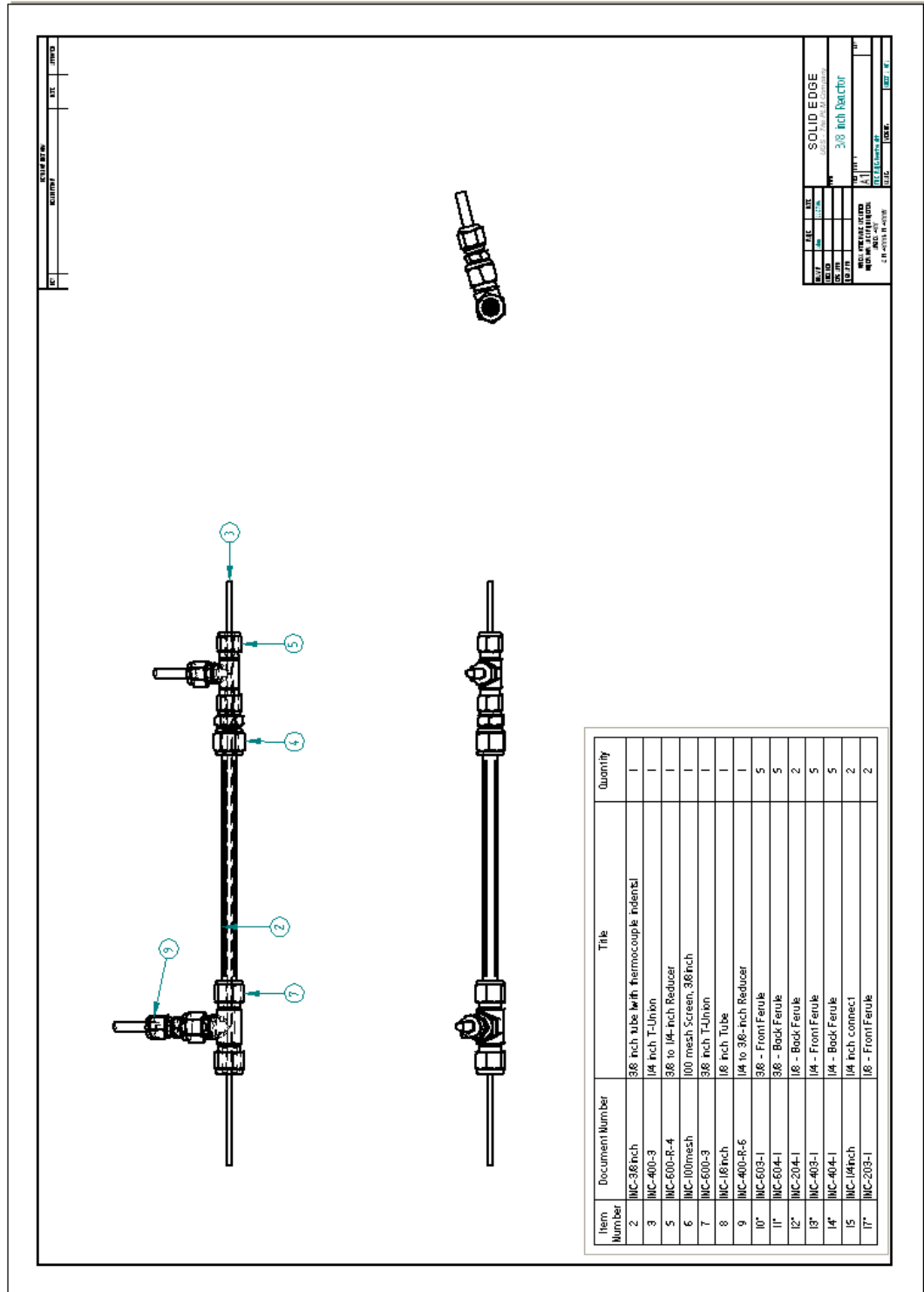
			Wall Temperatures(°C) [locations,x,in cm]						
	Fuel injection (oC)	Reformer inlet (oC)	Run#	CH5 (x=3.0)	CH6 (x=3.6)	CH8 (x=4.9)	CH9 (x=5.5)	CH10 (x=6.2)	CH11 (x=6.8)
1	540	288	459	563	656	787	788	780	758
2	550	293	333	395	464	689	729	750	736
3	539	282	240	281	336	551	596	632	637
4	540	288	564	691	775	889	889	877	849
5	563	346	431	523	619	833	860	865	837
6	546	250	327	397	478	719	765	797	789
7	540	142	574	711	831	1055	1084	1089	1060
8	564	362	522	643	755	949	966	961	928
9	555	332	352	436	535	807	852	878	864
9R1	549	210	403	494	590	832	868	885	864
9R2	559	350	407	508	623	819	860	875	852
9R3	560	348	392	488	585	818	860	877	855

Wall Temperatures(°C) [locations, x, in cm]										
Run #	CH12 (x=8.1)	CH13 (x=8.7)	CH14 (x=9.4)	CH21 (x=10.0)	CH24 (x=11.3)	CH25 (x=11.9)	CH26 (x=12.5)	CH28 (x=13.2)	CH29 (x=13.8)	CH30 (x=14)
1	725	708	688	668	630	623	600	580	573	561
2	707	689	670	648	608	600	577	559	550	538
3	637	622	605	587	554	548	527	512	501	491
4	798	777	754	730	690	682	656	645	636	625
5	773	749	724	700	657	649	625	614	603	590
6	741	717	690	665	615	606	581	579	568	556
7	999	970	937	904	836	822	788	774	763	755
8	866	842	814	787	733	722	694	680	668	659
9	818	793	767	739	684	672	643	631	618	610
9R1	807	782	755	728	675	665	637	628	612	598
9R2	803	780	754	728	676	666	639	622	610	600
9R3	808	781	758	729	676	664	637	624	611	600

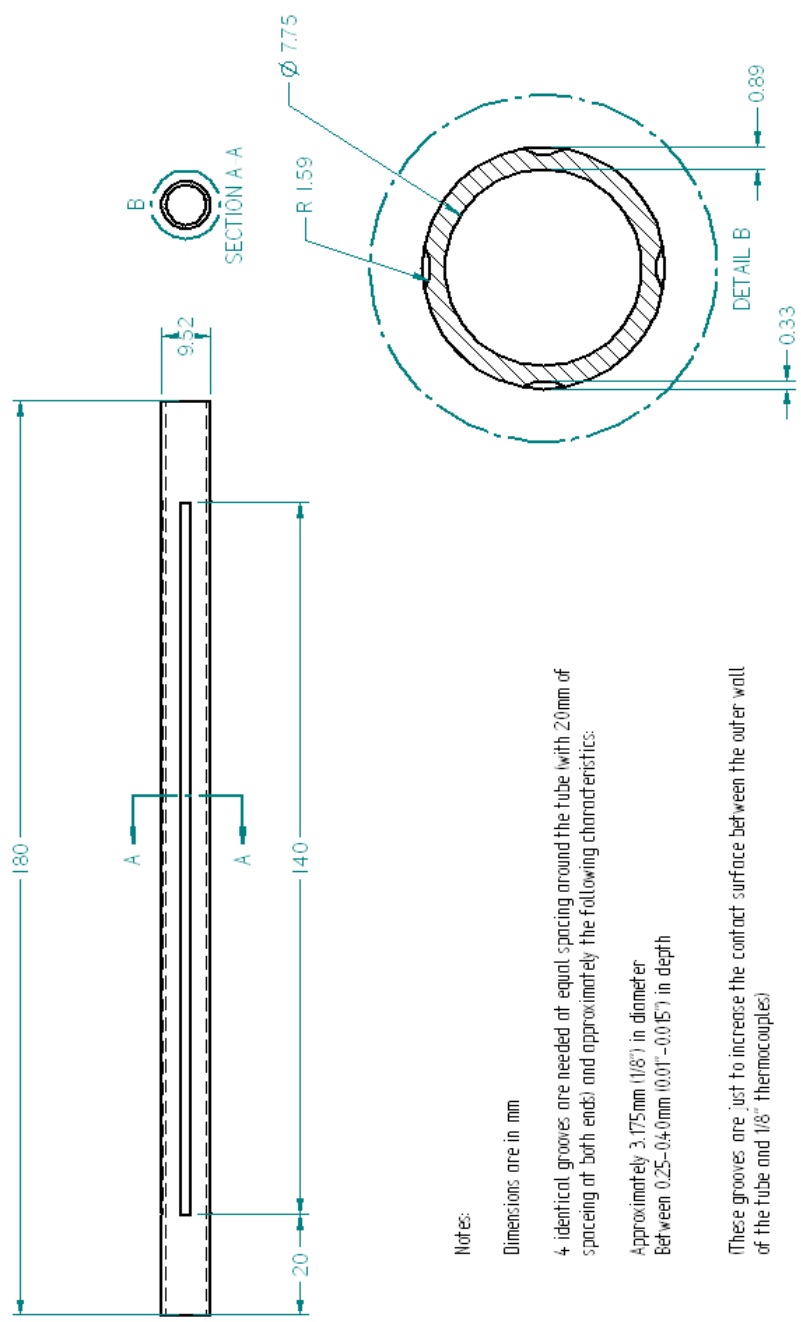
Centerline Temperature (°C) [locations, x, in cm]												
Run#	x=1.7	x=2.4	x=3.0	x=3.6	x=4.3	x=4.9	=5.5	x=6.2	x=6.8	x=7.4	x=8.1	x=8.7
1	454	511	633	775	819	870	896	845	812	781	767	752
2	310	337	398	495	596	772	842	836	805	770	754	737
3	230	244	273	333	405	569	680	723	723	693	675	660
4	567	646	795	884	946	1010	1050	961	912	875	852	829
5	410	464	584	719	819	930	976	950	902	866	840	813
6	319	354	429	523	633	819	867	886	855	808	781	755
7	581	661	805	931	1013	1166	1226	1208	1164	1143	1105	1066
8	515	590	715	863	947	1051	1039	1012	971	921	895	873
9	330	370	462	592	700	898	992	995	954	912	884	857
9R1	396	450	551	677	784	932	1001	991	946	899	873	847
9R2	404	464	579	707	823	927	975	962	922	882	860	837
9R3	381	435	537	665	768	918	984	980	938	895	872	845

Centerline Temperature (°C) [locations,x,in cm]												
Run#	x=9.3	x=10.0	x=10.6	x=11.3	x=11.9	x=12.5	x=13.2	x=13.9	x=14.4	15.1	x=15.7	x=16.3
1	737	454	511	633	775	819	870	896	845	812	781	767
2	717	310	337	398	495	596	772	842	836	805	770	754
3	653	230	244	273	333	405	569	680	723	723	693	675
4	800	567	646	795	884	946	1010	1050	961	912	875	852
5	770	410	464	584	719	819	930	976	950	902	866	840
6	727	319	354	429	523	633	819	867	886	855	808	781
7	1022	581	661	805	931	1013	1166	1226	1208	1164	1143	1105
8	861	515	590	715	863	947	1051	1039	1012	971	921	895
9	830	330	370	462	592	700	898	992	995	954	912	884
9R1	823	396	450	551	677	784	932	1001	991	946	899	873
9R2	808	404	464	579	707	823	927	975	962	922	882	860
9R3	817	381	435	537	665	768	918	984	980	938	895	872

# Appendix D: Reactor Drawings Shaw(2007)



REV	DESCRIPTION	DATE	APPROVED



Notes:

Dimensions are in mm

4 identical grooves are needed at equal spacing around the tube with 20mm of spacing at both ends) and approximately the following characteristics:

Approximately 3.175mm (1/8") in diameter  
 Between 0.25-04.0mm (0.01"-0.015") in depth

These grooves are just to increase the contact surface between the outer wall of the tube and 1/8" thermocouples)

DATE	DATE	DATE	DATE
1/24/02	1/24/02	1/24/02	1/24/02
DESIGNED	DRAWN	CHECKED	APPROVED
<b>SOLID EDGE</b>			
V.02.0 - The P.L.M. Company			
38° King St. Irvine, CA 92614			
TEL: 949.440.8600 FAX: 949.440.8601			
WWW.SOLIDEDGE.COM			
SCALE: 1:1 SHEET NO. 1			